Fall 2019

Experimental Investigations of Levee Breach Flows

Ibrahim Adil Ibrahim

Experimental Investigations of Levee Breach Flows

By

Ibrahim Adil Ibrahim

Bachelor of Science
University of Mosul, 1998

Master of Science
University of Mosul, 2005

Master of Science
University of South Carolina, 2019

Submitted in Partial Fulfillment of the Requirements

for the Degree of Doctor of Philosophy in

Civil Engineering

College of Engineering and Computing

University of South Carolina

2019

Accepted by:

Jasim Imran, Major Professor

M. Hanif Chaudhry, Committee Member

Enrica Viparelli, Committee Member

Jamil Khan, Committee Member

Cheryl L. Addy, Vice Provost and Dean of the Graduate School

DEDICATION

To “Almighty ALLAH” who gave me the opportunity, determination, strength, and patient to finish my research.

ACKNOWLEDGMENTS

I would like to thank my advisor, Prof. *Jasim Imran* for his support and advice during my study. Great thanks are extended to my dissertation committee members: Prof. M. *Hanif Chaudhry* and Dr. *Enrica Viparelli* for their valuable advice and help. Also, thanks are extended to my dissertation committee member Professor *Jamil Khan* for the time that he devoted to reviewing my proposal.

All appreciation and big thanks to the Iraqi Ministry of Higher Education and Scientific Research for the moral and financial support during my study. In addition to that, great thanks to Iraqi Cultural office in Washinton D.C. for all the facilities that provide to make my study move smoothly and continuously.

Great thanks to University of Mosul and Dam and Water Resource Research Center for all the supports and efforts that helped me to move forward to complete my Ph.D.

Great thanks and deep gratitude to my parents, *Dr. Adil Al-Hafidh*, my mother, *Mrs. Rajaa Al-Shabkhoon*.

Great thanks and sincere appreciation to my wife, sweetheart, and best friend, *Farah*. She gives me love, hope, and continuous help and support to move forward in my life. Big love to my kids *Lina*, *Radhwan*, *Yaman*, and *Juman*. The shining faces and big smiles of my kids support me during difficult times. I love you, my family.

Thanks, are extended to my colleagues in the water resources group, Dr. *Melih Calamak*, Dr. *Ezzat Elalfy*, Dr. *Hassan Ismail*, and Dr. *Lindsey LaRocque*, for their help in my experimental works. Great thanks to Professor John Dickerson, one of the kindest people that I meet in USC for his help and support in technical issues and also for the technicians in the Civil and Environmental Department at the University of South Carolina, Brian Hull, Paul, and Russel Inglett.

Big thanks to Ms. *Julia Ferill* from International Student Services, University of South Carolina for all her help, effort and support that make my life move easier in USA

Great thanks to my brother, *Dr. Omar Al-Hafidh* and sisters *Alhaan* and *Anwar* for their unconditional love and support. I hope they will be proud of me.

ABSTRACT

Two individual but related problems involving levee breach flow are studied. The first one involves experimental and dynamic modeling of steady flow through a levee breach, and the second one involves experimental investigation of flood management by an engineered levee breach. Both studies are conducted in the Hydraulics Laboratory, the University of South Carolina.

In the first problem, an idealized levee breach on a trapezoidal embankment was studied. Flow data including water depths, surface velocities, and flow discharges were collected from 28 experiments considering different cases of breach width and downstream water depth. Ultrasonic sensors were used to record the water depth in the channel and the breach. The water surface velocity was measured using a particle tracking velocity method. A one-dimensional theoretical model was developed to predict levee breach flow. This model is based on the conservation of mass and momentum in two control volumes. For known upstream flow discharge, water depth, and the downstream stage, the model predicts the breach discharge and the average flow depth along the breach. Two model coefficients were calibrated by using the experimental data, namely, the interfacial shear force coefficient between the two control volumes and the separation shear force coefficient in the channel downstream of the breach. The proposed model shows satisfactory performance against an additional set of experimental data.

In the second problem, flood management using engineered levee breach was studied. Laboratory experiments were conducted to investigate the effects of the inflow hydrograph characteristics, breach opening, tailwater depth, and floodplain storage volume on flood attenuation. The inflow hydrograph was controlled by a computer-controlled valve allowing for various peak discharges, hydrograph shapes and flood durations in the channel. Two approaches were used to generate the hydrograph. In the first approach three different inflow hydrographs having the same volume of water, but different durations were released. In the second approach, three different inflow hydrographs that had different volumes of water, but different durations were released. Three different breach widths - 0.2, 0.4, and 0.8 m - were considered by instantaneously opening a gate. Three different areas of flood basin (9, 6 m^2, and open floodplain) were tested for each hydrograph and breach width. Both active and passive flood management scenarios were considered. In the active flood management scenario, the breach was created instantaneously as the flood wave approached breach location. In the passive management scenario, the floodgate was already open, and the floodplain had the same water depth as the main channel prior to the arrival of the flood wave. The engineered levee breach provided a reduction of flood stage both upstream and downstream of the breach by modifying the flood wave. Dimensional analysis has been done to express the reduction of flood stage as a function of the breach width, channel width, distance of the target location from the breach centerline, hydrograph characteristics, and area of the basin.

TABLE OF CONTENTS

DEDICATION ii

ACKNOWLEDGMENTS iii

ABSTRACT v

LIST OF TABLES ix

LIST OF FIGURES x

LIST OF SYMBOLS xiv

CHAPTER 1 INTRODUCTION 1

1.1. Motivation 1

1.2. Literature Review 4

1.3. Research Objective 12

CHAPTER 2 EXPERIMENTAL SETUP AND PROCEDURE 17

2.1. Steady Flow Through a Levee Breach 17

2.2. Engineered Levee Breach 20

CHAPTER 3 EXPERIMENTAL INVESTIGATION AND 1D DYNAMIC MODELING OF STEADY FLOW THROUGH A LEVEE BREACH 37

3.1. Overview 37

3.2. Flow Characteristics 39

3.3. Water Depth 40

3.4. Velocity Magnitudes 40

3.5. Analytical Model and Theoretical Approach 42

3.6. Calibration of The Model Coefficients 48

3.7. Model Validation 49

3.8. Summary 50

CHAPTER 4 EXPERIMENTAL INVESTIGATION OF FLOOD MANAGEMENT BY AN ENGINEERED LEVEE BREACH 74

4.1. Overview 74

4.2. Results and Discussion 76

4.3. Dimensional Analysis 80

4.4. Multivariate Regression Analysis 82

4.5. Summary 86

CHAPTER 5 CONCLUSION 120

BIBLIOGRAPHY 125

LIST OF TABLES

Table 3.1 Dimensional and non-dimensional experimental data for this study.....52

Table 3.2 Data for validation experiments.....53

Table 4.1 The plan of experiments 89

Table 4.2 Data of experiments.....92

Table 4.3 P-value for the independent variables in first part of regression analysis 95

Table 4.4 P-value for the independent variables in the second part of regression analysis.....96

Table 4.5 Percentage volume of water pass to the floodplain basin.....96

LIST OF FIGURES

Figure 1.1 17th Street Canal, New Orleans, Louisiana before Hurricane Katrina (Alchetron 2005) 14

Figure 1.2 17th Street Canal, New Orleans, Louisiana after Hurricane Katrina (Sharp, n.d.) 14

Figure 1.3 New Orleans, Louisiana 2005 (Britannica 2019) 15

Figure 1.4 New Orleans, Louisiana 2005 one day after hurricane Katrina (Britannica 2019) 15

Figure 1.5 Yolo Bypass flooding in March 2011 (California Water n.d.) 16

Figure 1.6 Bird Point-New Madrid Floodway before and after the flood (USGS 2011) ..16

Figure 2.1 Aerial view of the experimental setup for steady levee breach flow 25

Figure 2.2 Schematic of the experimental model for steady flow through a levee breach (not to scale, all dimensions in meter) 26

Figure 2.3 A Baumer probe (UNAM 18U6903) 27

Figure 2.4 Water depth across the channel at section (a) 1, (b) 8, (c) 10, (d) 12, (e) 15 ..27

Figure 2.5 Movement of buyant black particles in water used to measure the velocity components. (Image by author) 30

Figure 2.6 The head tank system with pipes (Image by author) 30

Figure 2.7 The Digital Manometer (Image by author) 31

Figure 2.8 Valve system (Image by author) 31

Figure 2.9 Schematic of the experimental set-up for flood reduction by engineered levee breach (not to scale), (a) Vertical cross section of the experimental setup (b) plan of the channel and floodplain basin 32

Figure 2.10 First set of input hydrographs 33

Figure 2.11 Water depth hydrographs at target location 3 without the breach.....33

Figure 2.12 Second set of input hydrographs 34

Figure 2.13 Second set of water depth hydrographs at target location 3 without the breach 34

Figure 2.14 Repeatability tests of Hydrograph 1 35

Figure 2.15 Repeatability tests of Hydrograph 2 35

Figure 2.16 Repeatability tests of Hydrograph 3 36

Figure 2.17 Photograph of the Channel and the flood basin.....36

Figure 3.1 The length of the interface, breach = 0.7 m and weir height =0.08 m (image by authors) 54

Figure 3.2 The length of the separation zone, breach width = 0.7 m and weir height = 0.12m (image by author).....54

Figure 3.3 Illustration of separation zone for Breach with of 0.5 m; (a) Weir height = 0.08 m; (b) Weir height = 0.1 m; (c) Weir height = 0.12 m; (d) Weir height = 0.14 m. (image by author).....55

Figure 3.4 Water depth at section Y3: (a) Breach width = 0.4 m; (b) Breach width = 0.5 m; (c) Breach width = 0.6 m; (d) Breach width = 0.7 m 56

Figure 3.5 Water depth at section Y5: (a) Breach width = 0.4 m; (b) Breach width = 0.5 m; (c) Breach width = 0.6 m; (d) Breach width = 0.7 m 58

Figure 3.6 Streamwise velocity for breach width 0.7 m for different D.S weir heights at: (a) Y1; (b) Y2; (c) Y3; (d) Y4; (e) Y5; (f) Y6; (g) Y7; (h) Y8; (i) Y9; (j) Y10 60

Figure 3.7 Transverse velocity for breach width 0.7 m for different D.S. weir heights at: (a) Y1; (b) Y2; (c) Y3; (d) Y4; (e) Y5; (f) Y6; (g) Y7; (h) Y8; (i) Y9; (j) Y10 65

Figure 3.8 Conversion of the cross sectional area for the channel width and water surface profile.....70

Figure 3.9 Open channel and breach with two control volumes and notation.....70

Figure 3.10 the interfacial shear coefficient K_i, versus $\xi=Q_2/Q_1$ 71

Figure 3.11 the separation zone shear coefficient, K_s, versus $\xi=Q_2/Q_1$ 71

Figure 3.12 K_i versus downstream water depth/Breach Width 72

Figure 3.13 K_s versus downstream water depth/Breach Width 72

Figure 3.14 Comparison between Predicted and measured breach discharge 73

Figure 3.15 Y_2 Comparison between predicted and measured breach water depth.....73

Figure 4.1 Flood stage due to inflow hydrograph (1,2,3) at the target location (a) upstream of the beach (b) downstream of the breach, in case of the empty flood basin ...97

Figure 4.2 Flood stage due to inflow hydrographs (1,2,3) in case of initial tailwater depth in the floodplain basin at the target location (a) upstream of the beach (b) downstream of the breach 98

Figure 4.3 Nondimensional water depth upstream of the breach target location when there is no tailwater depth in the floodplain (a) Area 6 m^2, (b) Area 9 m^2, (c) Open Area 99

Figure 4.4 Nondimensional water depth at the downstream target location when there is no tailwater depth in floodplain basin (a) Area 6 m^2, (b) Area 9 m^2, (c) Open Area 100

Figure 4.5 Nondimensional water depth at the upstream target location when there is initial tailwater depth in floodplain basin (a) Area 6 m^2, (b) Area 9 m^2.....102

Figure 4.6 Nondimensional water depth at the downstream target location when there is initial tailwater depth in floodplain basin (a)Area 6 m^2, (b) Area 9 m^2.....103

Figure 4.7 The percent of water depth reduction at the upstream target location when there is no tailwater depth in the floodplain (a) Area 6 m^2, (b) Area 9 m^2, (c) Open Area.....104

Figure 4.8 The percent water depth reduction at the downstream target location when there is no tailwater depth in the floodplain (a) Area 6 m^2, (b) Area 9 m^2, (c) Open Area.....105

Figure 4.9 The percent water depth reduction at the upstream target location when there is initial tailwater depth in the floodplain (a) Area 6 m^2, (b) Area 9 m^2.....107

Figure 4.10 The percent water depth reduction at the downstream target location when there is initial tailwater depth in the floodplain (a) Area 6 m^2, (b) Area 9 m^2.....108

Figure 4.11 Depth due to the release of Hydrograph 1 in case of empty floodplain basin at the target location (a) upstream of the beach (b) downstream of the breach 109

Figure 4.12 Depth due to the releases of Hydrograph 1 in case of initial tailwater depth floodplain basin at the target location (a) upstream of the beach (b) downstream of the breach 110

Figure 4.13 Non-dimensional water depth due to Hydrograph 1 at target location (a) upstream breach (b) downstream breach, in case of empty floodplain basin 111

Figure 4.14 The effect of floodplain area on the water depth at the upstream target location when there is no tailwater depth in the floodplain (a) Hydrograph 1, (b) Hydrograph 2, (c) Hydrograph 3 112

Figure 4.15 The effect of floodplain area on the water depth at the downstream target location when there is no tailwater depth in the floodplain (a) Hydrograph 1, (b) Hydrograph 2, (c) Hydrograph 3 113

Figure 4.16 Inflow Hydrograph 1 and outflow hydrographs 115

Figure 4.17 Inflow Hydrograph 2 and outflow hydrographs 115

Figure 4.18 Inflow Hydrograph 3 and outflow hydrographs 116

Figure 4.19 Reduction in volume of flood water at channel downstream for different inflow hydrographs 116

Figure 4.20 Percentage of increasing the volume of flood water passed to the floodplain basin fro different inflow hydrographs 117

Figure 4.21 Predicted and measured $\Delta Y_t/W_b$ (active flood management tests).....118

Figure 4.22 Predicted and measured $\Delta Y_t/W_b$ (fixed flood basin area) 118

Figure 4.23 Predicted and measured $\Delta Y_t/W_b$ (flood basin with an outlet) 119

Figure 4.24 Predicted and measured $\Delta Y_t/W_b$ (passive flood management tests) 119

LIST OF SYMBOLS

A	Cross-section area (m^2).
B	Component of pressure force due to the channel of control volume width (m).
b	Channel bottom width (m).
b_{eq}	Equivalent channel width which represents the average width between the channel bottom width and water surface width at the same section (m).
C_f	Friction coefficient.
C_*	Chezy coefficient.
F	Froude number.
F_b	Friction force acting on the control volume bounders.
F_s	The shear force due to the separation zone that acting on the control volume two.
G	Acceleration of gravity (ms^{-2}).
K_i	Interfacial shear coefficient.
K_s	Separation zone shear coefficient.
k	Karman constant (0.41).
L_i	Interface length (m).
L_1	Length of control volume one (m).
L_2	Length of control volume two (m).
Q	Discharge (m3s-1).

P	Hydrostatic pressure force.
S	Interface shear force between two control volumes.
Z	Side slope of the channel.
Z	The vertical distance from the bed to the measurement velocity point.
Y	The depth of water (m).
V	Mean velocity (ms^{-1}).
u	Reynolds average streamwise velocity (ms^{-1}).
u_*	Shear Velocity.
ξ	The ratio of breach discharge to total discharge.
ρ	Water density (Kg/m^3).
γ	Water specific weight (N/m^3).
η	Water depth ration.
w	Ratio of width
Y_d	Water depth at the target point, dependent variable (L).
V_{ol}	The volume of the water under the hydrograph (L^3).
A_b	Area of the basin (L^2).
W_b	Width of the breach (L).
W_c	Width of the channel (L)
ρ	The density of water ($M\ L^{-3}$).
T	Base time (total time of the flood) (T).
T_p	Time to peak (T).
g	Gravity ($L\ T^{-2}$).

N	Manning Coefficient ($TL^{-1/3}$).
Xt	Distance to target (L).
Q_p	Peak discharge ($L^3\ T^{-1}$).
Q_i	Initial discharge ($L^3\ T^{-1}$).
Y_i	Initial water depth (L).

CHAPTER 1

INTRODUCTION

1.1. Motivation

A flood may occur in an area that is normally dry due to high precipitation rate, melting ice and snow in a mountain, storm surge, a dam failure or a levee breach. Extensive damage and loss in property and lives often accompany floods. Many historic floods have occurred recently in the USA and around the world. On the basis of population density and GDP per capita, Jongman et al. (2012) estimated a total global exposure to river and coastal flooding of 46 trillion USD in 2010. By 2050, these numbers are projected to increase to 158 trillion USD. In the United States, for instance, Hurricane Harvey, 2017 in Houston, Texas caused 68 fatalities, displaced 30000 people, destroyed 200000 homes and businesses with estimated damage of 126.3 billion dollars.

Levees and flood walls are constructed to protect major cities from design floods. However, these protection structures may fail during historic floods due to storms and snow melt and cause fatalities and extensive property damages. A few examples of such floods are the 1927 and 1993 Mississippi floods that affected vast areas in the Midwest, the 2010 flood in Pakistan (LaRocque et al. 2013). Many levees in the USA were constructed more than a hundred years ago by non-engineers to stop the flood of water from the rivers. The levees need regular maintenance to keep them safe especially in the vicinity of urban areas to protect people and infrastructure from flood damage.

Climate change appears to have led to an increase in the frequency and intensity of extreme weather events such as hurricanes, storms, and tornadoes. In Aug. 29, 2005, Hurricane Katrina hit the city of New Orleans, Louisiana and several levees that protect the city failed causing an unprecedented disaster as about 80% of the city flooded (Kunreuther 2006). 300,000 homes were destroyed completely. The flood damage in New Orleans was about 104 billion dollars and over1800 people perished (ToDAY, n.d.). Figure 1.1 (Alchetron 2005) and Figure 1.2 (Sharp, n.d.) show part of New Orleans, Louisiana before and after August 29, 2005. Figure 1.3 New Orleans, Louisiana 2005 (Britannica 2019) shows an aerial view of down town New Orleans before Hurrican Katrina and Figure 1.4, shows the same one day after the flooding caused by levee breach (Encyclopædia Britannica 2019). Other recent examples of historic floods in recent years include those caused by Hurricane Sandy in 2012 that hit New York and New Jersey, Hurricane Joaquin in 2015 that caused historic rain and flood in South Carolina, and Hurricane Florence in 2018 in Carolinas.

The degree of damage in floods caused by levee breach depends strongly on the amount of breach discharge and the water depth within the breach area. It is necessary to correctly estimate the breach discharge and water depth at the breach in order to effectively and efficiently close the breach and manage the flood in the adjacent floodplains.

When a large population center or an important infrastructure is threatened by the high water level in a river, part of the levee is breached intentionally to attenuate the flood at target locations. An example of such an engineered levee breach is the Birds Point- New Madrid Floodway. The performance of an intentional levee breach may depend on the size

of the breach, area of floodplain basin, the volume of water that is diverted, and duration of the flood.

Managing inland and coastal flooding has been a long-standing challenge. Traditionally, reservoirs have been used to provide the storage necessary to mitigate floods in urban systems, but for many reasons, this may not be a favourable solution in this day and age. An alternative is to set aside portions of the floodplain that can be filled with water during floods (Jaffe and Sanders 2001a). In addition, to help attenuate floods, temporary storage in floodways offer benefits to fisheries, wetlands, wildlife, and agriculture (Sommer et al. 2001). Floodways are parts of the floodplain that can be activated during an extreme event to store and convey flood water. Examples include the Yolo and Sutter Bypass near Sacramento, California, the Red River Floodway near Winnipeg, Canada, the Morganza Floodway near Morganza, Louisiana, and the Birds Point-New Madrid Floodway (NMF) near Cairo, Illinois. The Yolo Bypass is used for agricultural purposes most of the year, but during the flood season, it is used for storage and conveyance (Jaffe and Sanders 2001a).

Figure 1.5 (California Water n.d.) shows Yolo Bypass's location during flood March 2011. The Birds Point-New Madrid floodway is designed to prevent the Mississippi River and Tributary (MR&T) project design flood from exceeding the design elevation on the Mississippi River levees in the vicinity of the confluence of the Mississippi and Ohio rivers. The floodway not only protects Cairo, Illinois but also 2.5 million acres of land in Missouri, Arkansas, Kentucky and Tennessee (Engineers and Mississippi Valley Division 2019). Figure 1.6 (USGS 2011) shows the floodplain area before and after the flood. Despite the

potential of flood mitigation by controlled levee breach, there is a lack of systematic study of the problem under controlled conditions.

1.2. Literature Review

This section presents a review of the literature on levee breach flow under steady flow conditions, flow convergence and division at an open channel junction, and flood attenuation by intentional levee breaches.

1.2.1. Steady flow through a levee breach

The catastrophic New Orleans Flood in 2005 during Hurricane Katrina was due to the failure of several levees that could not withstand the highwater level in the surrounding water bodies, mainly Lake Pontchartrain. A 122 m wide levee failure occurred at the east side of the 17th Street Canal, near the Hammond Highway Bridge. This particular breach of the levee and I-wall disproportionately contributed to the overall flooding of the Metropolitan Orleans East Bank protected basin; more than half of the loss of life, and a similar fraction of the overall damages occurred in this heavily populated basin. Floodwaters continued to stream through this breach for two and a half days (Seed et al. 2008), (LaRocque et al. 2013). Sattar, Kassem, and Chaudhry (2008) identified the reasons for failure to close the breach over an extended period and studied various breach closure procedures for the 17th Street levee breach site using a 1:50 scale physical model. LaRocque, Imran, and Chaudhry (2013) used the scale physical model to study the detailed flow field in the breach section and the flooded basin. Others (e.g., USACE 2017) have extensively studied the failure mechanism of the New Orleans levee system by a combination of field-based forensic study and centrifuge modelling.

Several experimental studies on levee/earthen-embankment failure have been reported (e.g., Coleman, Andrews, and Webby (2002); Franca and Almeida (2002); Chinnarasri et al. (2003); Rozov (2003), Feliciano Cestero, Imran, and Chaudhry (2015), Asghari et al. (2017), Elalfy, Tabrizi, and Chaudhry (2017)). ASCE (2011) summarizes over 700 test runs on embankment dams, levees, and sea-dikes breaching conducted since the 1960s. A majority of these tests involved small-scale, non-cohesive and homogeneous embankments with overtopping as the failure mechanism. The number of studies on levee breach (main flow direction parallel to the embankment crest) is far fewer compared to dam breach (main flow direction perpendicular to the embankment crest). Recently, Kakinuma and Shimizu (2014) conducted four large-scale experiments on riverine levee breach with a variation of inflow rate, levee material, and levee shape. (Elalfy, Tabrizi, and Chaudhry 2017) conducted numerical and experimental modelling of levee breach including slumping failure of the breach sides. Riahi-Nezhad (2013) conducted experiments and developed an analytical model for predicting breach discharge and water depth at the breach for a channel with vertical sidewalls. The analytical model of Riahi-Nezhad (2013) was based on the model of Shabayek, Steffler, and Hicks (1999) for dividing open channel flow.

Elalfy (2015) studied a general case of levee breach in a rectangular channel. He developed a numerical model to solve shallow-water equations by applying a finite-difference scheme. A comparison between numerical and experimental results was done. In addition, a comparison between one-dimensional and two-dimensional approaches has also been done. Elalfy et al. (2018) studied two cases of levee breach with constant rectangular and trapezoidal channel cross sections. The 2D shallow-water model equations

and spatially varied flow equations are used in the numerical model. Elalfy et al. (2018) simulated different cases with a variation of breach width, downstream breach crest, and discharges in the main channel. The 2D shallow water model gave better prediction compared to the 1D spatially varied model.

Because of the similarity between lateral flow in a levee breach and that in a dividing channel junction, the literature on the latter is reviewed here as well. Experimental and analytical modelling of dividing open channel flow at a junction date back to the work of (Taylor 1944). The work focused on the depth ratio between the upstream branch and the downstream channel. A graphical solution for the specific case of right-angle junctions was proposed by Taylor (1944) based on experimental observation. Webber and Greated (1966) studied the general characteristics of flow in an open-channel junction. They used the conformal mapping method to analyse the flow pattern through the region of channel junction. Webber and Greated (1966) were able to theoretically predict the location of the stagnation point at the upstream corner of the channel junction and the zone of separation. They also developed a method for estimating the relative loss of energy across the channel junction. Best and Reid (1984) presented results from an experimental study on the separation zone in open channel junctions. Four junction angles, 15^o, 45^o, 70^o, and 90^o were studied. They observed that the separation zone width and length increase with an increase in the discharge ratio. Ramamurthy, Carballada, and Tran (1988) applied separate momentum equations of flow in the branch and lateral channels. The flow was considered critical in the downstream branch. The lateral momentum contribution increased when the lateral discharge ratio increased. Furthermore, the coefficient of momentum correction was found to be about 1.20, independent of the Froude number and lateral discharge ratio.

Ramamurthy, Tran, and Carballada (1990) developed a model of flow division at a right-angle junction in rectangular open channels. The momentum transfer in the main channel, downstream depth in the main channel and discharge ratio were estimated as functions of the Froude number in the upstream main channel and downstream of the junction. Gurram, Karki, and Hager (1997) conducted experiments to study the flow pattern in channel junctions for subcritical and transitional flows. Three angles of the junction were considered in their work: 30^o, 60^o and 90^o, and the Froude number of tailwater were 0.25, 0.5, 0.75, and 1.0. In addition, five discharge ratios were used: 0, 0.25, 0.5, 0.75, and 1.0. They performed a momentum analysis, which provided an equation for the prediction of water depth increase across the junction. Barkdoll, Hagen, and Odgaard (1998) presented a comparison between velocity and water surface elevation in free surface open channel flow and in symmetry-plane in duct flow in T-Junction. They found that up to 2.1% of super elevation of the water surface was caused by the centrifugal force. Hsu, Wu, and Lee (1998a) describe a one-dimensional approach to find upstream water depth at the right-angle junction of subcritical open channel flow. In their study, the experimental results and one-dimensional prediction of the momentum and energy correction coefficients correlated well. Hsu, Lee, and Cheng (1998b) developed a model to predict flows in a channel with junction angles of 30^o, 40^o and 50^o. Weber, Schumate, and Mawer (2001) conducted a comprehensive experimental study and provided a data set for three velocity components, water surface profile, and turbulence stress for combining flow at a 90^o open channel intersection.

Shabayek, Steffler, and Hicks (1999) developed an analytical model of dividing junction flow based on the conservation of mass and momentum principles applied to two

control volumes. Shabayek, Steffler, and Hicks (2002) followed up with an analytical model of combining channel flow based on the same principles. They considered hydrostatic pressure force, interfacial shear force, separation drag, and bed drag in the momentum conservation equations in a 1D framework. Shabayek, Steffler, and Hicks (2002) derived empirical equations for interfacial shear coefficient (K*) and separation zone coefficient (K) based on experimental results available in the literature.

Jianchun, Weber, and Lai (2002) reported a three-dimensional numerical modeling study of combining flow in open-channel junctions. The model was validated using data from (Weber, Schumate, and Mawer 2001). Ramamurthy, QU, and Vo (2007) presented a three-dimensional model of turbulent flow to investigate the flow characteristics in a dividing open channel flow. The results show that the separation zone length and width in the branch channel decrease when the discharge ratio (branch discharge over upstream discharge) increases. Near the bottom of the channel, the separation zone is smaller than that near the surface. Ramamurthy, QU, and Vo (2007) also stated that separation zone may appear downstream of the junction and the length and width of the separation zone increase with an increase in discharge ratio.

Pirzadeh and Shamloo (2007) applied a CFD package, FLUENT, software to simulate 2D and 3D lateral intake flow. They compared their numerical results with experimental measurements in a lateral intake. Both 2D and 3D simulations gave a good agreement with the data. Yu et al. (2009) provided a two-dimensional numerical simulation of the flood propagation at the levee breach under complex boundary conditions and unsteady process of flood in a river and in a dry floodplain. Yang et al. (2009) studied the separation zone characteristics in a river confluence. This study showed that the size of the

separation zone changes with the discharge ratio and water depth. Savant et al. (2011) presented an implicit finite-element model of the dam and levee breach flow by applying a pseudo-transient continuation (PTC) flow model concept. Verification of this model was done against real-world test cases and an analytical model. Van Emelen et al. (2012) presented a finite-volume numerical model of two-dimensional depth-averaged equations of open channel flow. They simulated flood in a scale physical model of an urban area and found that the transient part of the flood is very short compared with the long flood duration.

1.2.2. Engineered Levee Breach

The floodplain storage is one of the effective ways to hold part of the volume of flood water during the flood period, thus reducing the peak discharge (De Paola and Marini 2011). Moreover, the detention floodplain basins have become a primary tool for environmental and stormwater management at the watershed scale (Del Giudice et al. 2014). Major examples of floodwater diversion in the USA include the Yolo bypass in in Sacramento Valley and the Birds Point-New Madrid Floodway (BP-NMF) in Missouri, and the Atchafalaya Basin Floodway in Louisiana. The Yolo bypass in California's Sacramento Valley, not only protects the state's capital of Sacramento and other nearby cities from flood, but also provides important habitat for the native flora and fauna (e.g., Feyrer, Sommer, and Harrell (2006), Hydrobiologia 573, Sommer et al. (2001), Fisheries 26 (8)). The routine operation of Yolo Bypass provides a favourable condition for the wildlife habitat and the cropland. The BP-NMF, on the other hand, has been operated only twice during the last 80 years. In 2011, the BP-NMF was activated through the explosive detonation of the 'fuse plug portion of its levees, resulting in elevated property and

economic damages, crop losses, and litigation. The operation was disruptive to the cropland, the natural environment, and the wildlife habitat (Walker 2016). Controlled data and practical tools on floodway operations are limited.

De Martino and De Paola (2010) conducted experimental research on off-stream floodplain storage for two cases of rectangular side weir as flood relief mechanism: with and without the floodplain being submerged. In the case of submerged rectangular side weir, the flood wave moved from the storage basin back to the channel. McEnroe (1992) studied the relationship between the sizing of detention reservoirs and the reduction of peak flood discharge using reservoir routing analysis. The analysis showed that the required storage to flood volume is determined primarily by the ratio of peak outflow to peak inflow, the outlet type, and the inflow hydrograph shape. McEnroe (1992) found that the overflow outlet is less effective than a submerged outlet in that less detention storage is needed to achieve the same reduction in peak flood discharge for the same inflow hydrograph. Guo (1999) mentioned that retention and detention basins are used as a storage facility to control the quality and quantity of storm water. Guo (2012) observed that the required off-stream detention volume is maximized by the rainfall event longer than the time of concentration of the tributary area. In comparison, the off-stream detention volume can be significantly less than an in-stream, depending on the flow-through capacity in the downstream channel (Guo 2012). A design procedure to maximize the off-stream detention volume, to size the flow-diversion weir, and to set the floodgate operation on the equalizer conduit was also presented by (Guo 2012). Topa, Giugni, and De Paola (2015) studied the effect of an off-stream floodplain storage volume on peak flood reduction. They conducted experimental measurements by varying the geometric characteristics of the weir and compared results

with those inferred from a one-dimensional numerical model. Rifai et al. (2018) conducted laboratory experiments to study overtopping induced levee breaching. They investigated the effects of floodplain tailwater on the breach expansion and the outflow discharge. Using the recorded data, they proposed a simplified regression model relating the breach stabilization time and the final breach width to the floodplain confinement and inflow Froude number in the main channel.

Sanders and Katopodes (1999 a,b) used adjoint sensitivity methods founded on 1D and 2D shallow water equations in a series of computational experiments and demonstrated that active mitigation of unimodal flood waves can be achieved by selective boundary flow withdrawal. Jaffe and Sanders (2001b) studied flood mitigation by engineered levee breach. Their hypothesis was that the rapid filling of the floodplain creates a dynamic wave action that can be tactically controlled to reduce peak flood stage in key areas. They combined a least-square-type objective function with the shallow water equations to examine the roles of flood plain storage, breach size, flood discharge, flood duration, and breach timing in the optimal design of engineered levee breaches. The functional relationship between the object functions and the variables of interest was expressed as $J = F\ (Q_f, T_f, A_s, L_b, n, S_o, W_c, t_b)$ where J = objective function; Q_f = flood discharge; T_f = flood wave period; A_s = floodplain storage basin area; n = Manning coefficient; S_o= bed slope; t_b = time of the breach, and T_f and W_c are the characteristic time and length scales. The results from their simulations showed that substantial flood stage reduction can be achieved with an engineered breach. Shome and Steffler (2006) developed a theoretical model to estimate the velocity of flood wave and lateral flow volume that leave the main

channel going to the floodplain. The considerable promise of engineered levee breach notwithstanding, there is a lack.

1.3. Research Objective

The present work focuses on two individual problems. The first problem involves an experimental and analytical model of steady flow through a levee breach. Although this area of research has received considerable attention, there is a lack of data and only a few models were developed to predict levee breach flow. The main objective and goal of the first study are to obtain a data set on levee breach flow and adapt a one-dimensional dynamic model of flow division in a branching channel to predict breach discharge and depth of water in the breach.

An idealized physical model was constructed in the Hydraulics Laboratory, the University of South Carolina with a half-trapezoidal cross section. Tests were conducted with one discharge, four different breach openings, and seven different downstream stages. A comprehensive set of data was collected from 28 experiments. The data include the water depth in the upstream, downstream, and the breach, and surface velocity. An analytical model for dividing flows in open channel junctions is adapted to predict flow division at a breached levee. The model considers the conservation of mass and momentum in two control volumes. The 1D approach ignores the junction angle but considers width change, separation zone shear force, drag forces, interfacial shear force, and hydrostatic pressure forces. The experimental data are utilized to calibrate model coefficients. The calibrated model is then validated against a separate set of data.

The second study focuses on collecting and analyzing an extensive set of data on engineered levee breach flow by conductive controlled laboratory experiments. An 11 m long 0.4 m wide rectangular channel with an attached flood basin was constructed for this study. A head tank with a volume of 8 m^3 was used to feed water to the channel using two pipes. The 6-inch-diameter pipe was used to maintain a steady flow rate of 0.004 m^3/s and the 8-inch-diameter pipe was used to generate an unsteady flood hydrograph using a computer-controlled valve. Calibrated digital manometers attached to each pipe provided the flow rate reading in each pipe. Water depth was measured at four different target points located along the channel. A set of ultrasonic distance profilers were installed at the target locations to measure the water depth. An additional profiler was installed near the downstream calibrated weir to continuously monitor the channel outflow discharge. Six different inflow hydrographs, three different breach width, active and passive flood management, and three different storage volumes including an infinite flood basin area are considered. Using dimensional analysis and a multi-variate regression method, non-dimensional water depth at target locations is expressed as a function of inflow hydrograph characteristics, breach width, the distance of the target location and floodplain storage area. Separate relations are developed for the open and close floodplain.

Figure 1.1 17th Street Canal, New Orleans, Louisiana before Hurricane Katrina
(Alchetron 2005)

Figure 1.2 17th Street Canal, New Orleans, Louisiana after Hurricane Katrina
(Sharp, n.d.)

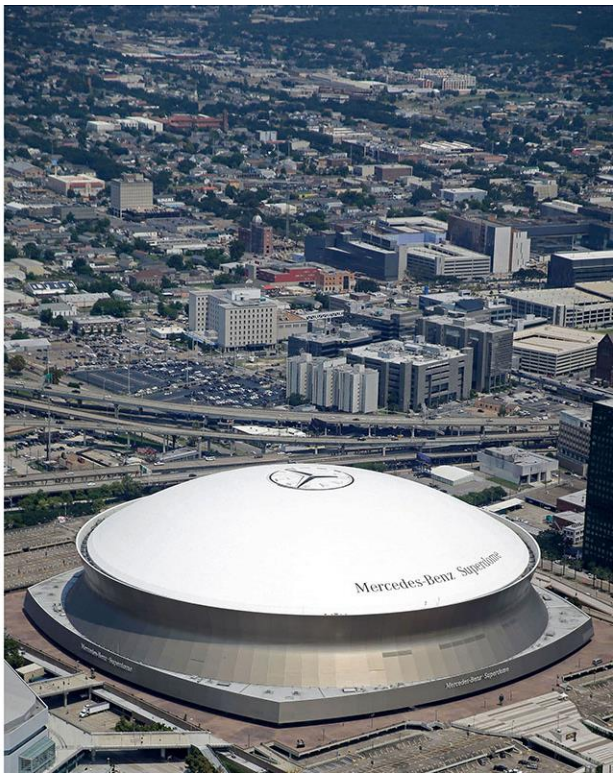

Figure 1.3 New Orleans, Louisiana 2005 (Britannica 2019)

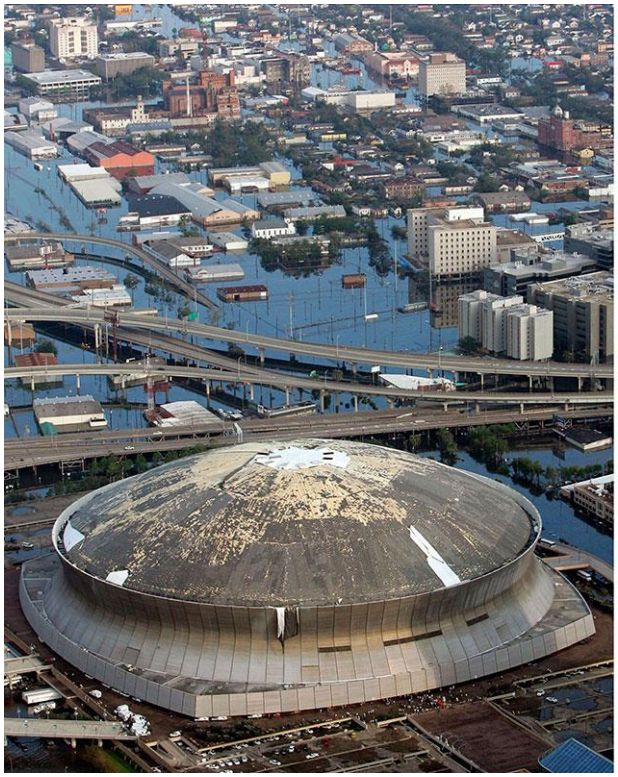

Figure 1.4 New Orleans, Louisiana 2005 one day after hurricane Katrina (Britannica 2019)

Figure 1.5 Yolo Bypass flooding in March 2011 (California Water n.d.)

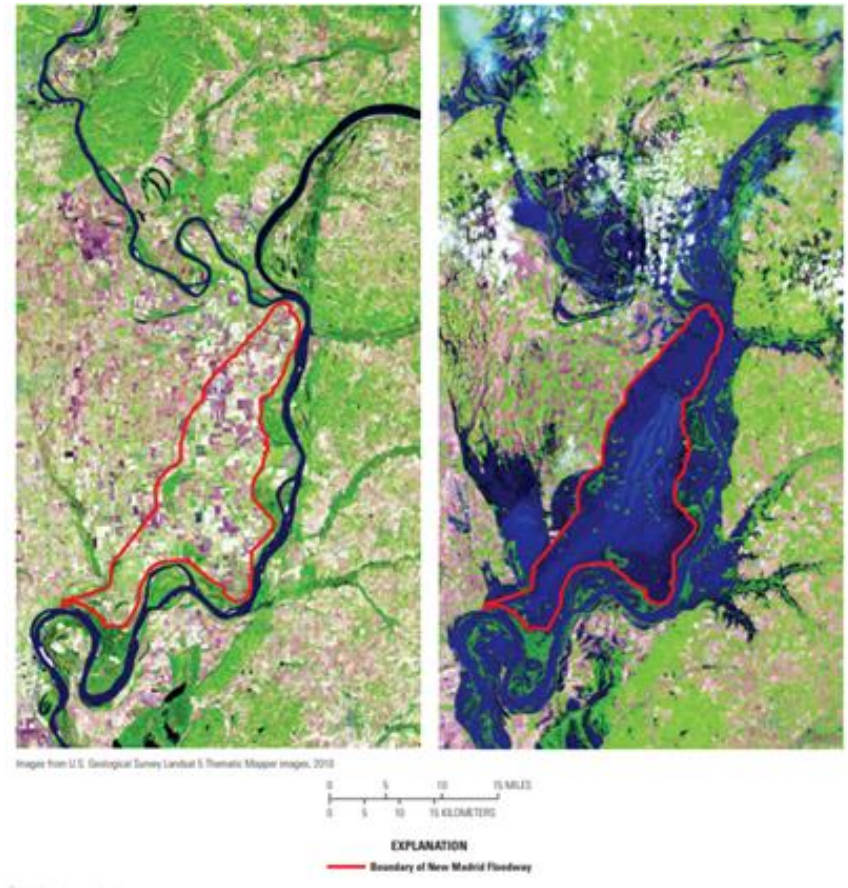

Figure 1.6 Bird Point-New Madrid Floodway before and after the flood (USGS 2011)

CHAPTER 2

EXPERIMENTAL SETUP AND PROCEDURE

The experimental setup and procedure are described in this chapter. The experiments were conducted in the Hydraulics Laboratory, the University of South Carolina. The setup for the steady flow through levee breach experiments was used previously by Elalfy, Tabrizi, and Chaudhry (2017) to study the evolution of a levee breach. In the present case, the breach was considered to be already developed, did not contain any erodible material, and was fully open for the duration of the experiment. The setup for the engineered levee breach experiments was built for the present experiment. The idealized models in both experiments were constructed using plywood. The bed was made rough by spreading sand on the freshly painted surface.

2.1. Steady Flow Through a Levee Breach

2.1.1. Experimental Setup

The experimental model had three main parts. First, the main channel consisting of a half trapezoidal section. The right side of the channel (looking downstream) was a vertical wall while the left side was a levee-shaped wall with a side slope of 2:1 (H: V) 0.2 m height and 0.10 m crest width. The total length of the channel was 11.9 m, and the bed width was 0.8 m. The downstream water depth was adjusted using a calibrated sharp-crested weir. Seven different heights of the sharp-crested weir were used to control downstream water depth (0.08, 0.09, 0.1, 0.11, 0.12, 0.13 and 0.14 m). Second, the breach was implemented

on the left side of the channel at a distance of 7.4 m from the main channel inlet. Four breach widths were used in these experiments (0.7, 0.6, 0.5, and 0.4) m. Third, the floodplain which is open on three sides and receives water from the breach. All those parts were constructed on a 0.3 m high raised platform from the laboratory floor to allow a free fall from the floodplain. Figure 2.1 shows the plan view of the experimental model. Water was supplied to the main channel by an axial flow pump. Constant discharge of 0.075 m^3/s was used for all the experiments. The discharge was monitored using an in-line electromagnetic flow meter. A honeycomb made of short pipe sections, and flow straighteners were used are used at the inlet of the main channel to reduce turbulence. A wave suppressor was used to reduce the water surface fluctuation. The downstream discharge was measured by using the sharp crested weir equation after making a calibration to find the discharge coefficient. The breach discharge was calculated by using the mass balance equation.

The bed of the model was marked as a square grid with a spacing of 0.152 m in longitudinal and transverse directions. The water depth and flow velocity were measured from Y1 to Y5 inside the channel, Y6 to Y10 inside the breach, and 1 m upstream of the breach to 1 m downstream of the breach in the main channel as shown a schematic experimental model setup in Figure 2.2.

2.1.2. Water Depth Measurement

A Baumer ultrasonic distance measuring sensor shown in Figure 2.3, was used to measure the depth of the water with scanning range between 60 to 400 mm and repeat accuracy <0.5 mm. The sensor has been extensively used in other experiments in the Hydraulics Laboratory, the University of South Carolina to study steady and unsteady free

surface flow (Larocque 2012, Riahi-Nezhad 2013, Abdo 2014). In the present work the measurements included the area between 1m upstream of the breach and repeated every 0.152 m and ended at 1 m, 1.1 m, 1.2 m, 1.3 m downstream of the breach (width = 0.7 m, 0.6 m, 0.5 m, 0.4 m), respectively. The Baumer probe was mounted on a movable bridge as shown in Figure 2.1. The probe was moved at a constant speed above the water surface in using a motorized cart; the measurement track started at the vertical right wall of the main channel and ended at the edge of the floodplain.

Prior to the beginning of the tests, calibration was done at a specific spot on the floodplain to ensure that the position of the Baumer does not change. Next, the elevation of the dry bed for all the target sections was measured. During the experiment, the water surface profile was measured and recorded along the same transects. The water depth is calculated as the difference between the dry bed and water surface elevation. Measurements were made along 10 sections for each experiment; five in the main channel and five sections at the breach as shown in Figure 2.2. Figure 2.4 shows water depth measurements from a randomly selected experimental run. As shown in Figure 2.4 (b) in section 8 in the breach the ultrasonic probe captures the fluctuation that occurred as a result of the vortex appearing on the left side of the breach.

2.1.3. Velocity Magnitudes

The water surface velocity is calculated from recorded images of floating tracers using the PIVLab Matlab tool (Thielicke and Stamhuis 2014). A large number of small floating black particles was dropped manually at the upstream end of the main channel, and they moved with the flow through the breach and to the downstream part of the main channel. Figure 2.5 shows the movement of the particles through the model. A large

separation zone in the main channel opposite to the breach is clearly recognized. The flow also detached from the upstream edge of the breach creating an asymmetric flow to the floodplain. A High definition video camera was installed above the floodplain to record the movement of the black particles. The PIVLab Matlab tool was utilized to analyze the sequential images of each video and to draw the streamline position, specify the separation zone and interfacial zone, and for calculating water surface velocity.

The reference point for measurements was specified one meter upstream of the breach at the right wall. The streamwise and transverse components of the surface velocity were extracted at an interval of 0.152 m from the reference point for a distance of 2.7 m in the downstream and 1.5 m in the transverse direction.

2.2. Engineered Levee Breach

2.2.1. Experimental Setup

Conducting a laboratory study on the effects of an engineered breach on the water depth at target locations upstream and downstream of an intentional levee breach is the main purpose of this work. An analogue model was constructed in the Hydraulics Laboratory, at the University of South Carolina to represent a channel and off stream floodplain storage. An existing 8 m^3 head tank and two PVC pipes - 6- and 8-inches in diameter were utilized for delivering water from the tank to a 10.87 m long channel and a floodplain storage basin. Figure 2.6 shows the head tank and pipe system used in this study. The tank is elevated 6 m above the channel bed. A 25 HP pump is used to pump water from the sump to the head tank. Bypass valve connected with the pump is used to control the flowrate and a half-pipe overflow weir is used to control the water level in the tank by returning back part of the water to the sump. Calibrated digital manometers shown in

Figure 2.7 are attached to each pipe to measure the flow discharge in the pipes during the experiments. The manometer readings were converted into volume flow rate from inches of water column using calibration curves. Multiple butterfly valves installed in each pipe were used to control the flowrate. The valve in the smaller pipe was controlled manually, whereas a computer program was used to control the valve in the larger pipe as shown in Figure 2.8. The operation of this valve allowed the release of different water volumes with different peak discharges and various flood durations, thus representing a wide variety of hydrographs. The rectangular channel was 0.4 m wide and 0.5 m high. At the end of the channel, a 0.1 m high sharp crested weir was installed to measure downstream discharge. The relationship between the manometer reading and discharge was used to estimate the discharge coefficient (C_d) of the weir, which was found to be 0.76. Equation (2.1) is used to evaluate the downstream discharge.

$$Q_{out} = \frac{2}{3} C_d \sqrt{2g}\, L\, H^{3/2} \tag{2.1}$$

where, Q_{out} = downstream discharge, C_d = discharge coefficient, L = width of the weir, H = water head above the weir.

A side gate, that represents the engineered breach, was installed on the right side of the channel along the flow direction. The centreline of the gate was located at 5.5 m from the downstream end of the channel. The gate was part of a mechanical system that used a counterweight to lift the gate. The centerline of the gate was located 5.5 m from the downstream end of the channel. The gate was lifted by using a guillotine-type mechanism (Miller and Chaudhry 1989); (LaRocque, Imran, and Chaudhry 2013). The gate was opened to release the flow into the floodplain basin. Three different breach widths were

tested: 0.2 m which is half of the channel width, 0.4 m which is equal to the channel width, and 0.8 m, twice the channel width. The gate was used to emulate two approaches to flood management: active and passive. In the first one, the gate remained closed with steady flow in the channel. It was opened suddenly to allow a part of the flow to divert to rectangular the floodplain basin. The basin had the same elevation as the channel bottom. The floodplain was dry and with no initial water. In the second case, the breach was open completely and the initial tailwater depth in the floodplain basin was the same as the water depth during the steady state flow condition. Three different floodplain basin areas were used: 9 m^2, 6 m^2 and infinite area (floodplain with an outlet). The flood basin had 0.5 m high of the side walls. Several Baumer probes, commercially available ultrasonic distance measuring sensors, with a scanning range between 60 to 400 mm and a repeat accuracy of less than 0.5 mm, were used to measure the instantaneous water depth. Eight sensors were distributed in the experimental setup to monitor and record the elevation of water; six in the channel and two corners of the flood basin. Three sensors were located upstream of the breach and three downstream of the breach. Figure 2.9 (a) shows the vertical section of the experimental setup including the tank and system pipe that supplied the water to the channel. Figure 2.9 (b) shows the plan view of the experimental model with Baumer locations.

2.2.2. Experimental procedure

The experiments were initiated by releasing 0.006725 m^3/s constant discharge from the 6-inch pipe to the channel for an extended period. This represented the initial pre-flood flow in the channel. Baumer readings at location 4 were used to check if the flow reached a steady state condition or not. When the flow reached a steady-state condition, the flood

hydrograph was released from the 8-inch pipe using the computer-controlled valve. To control the water level in the head tank during the release of the flood wave, the bypass valve of the pump was closed completely as soon as the computer-controlled valve was opened to maintain the head tank water level. A video camera was used to record the water level in the tank to ensure that the water level does not drop too much. In addition to that, another video camera was used to record the manometer readings during the experiments to check the fluctuations in the readings. The observation of the first manometer that was connected to the 6-inch pipe showed that the readings were stable with a slight fluctuation when the bypass valve was closed during the experiment. The readings of the second manometer that was connected to the 8-inch pipe were used to obtain the inflow hydrographs. By trial and error, the maximum volume of water that could be released from the head tank as a flood wave without effecting the steady-state flow condition in the 6-inch pipe was determined to be 3.5 m^3. Two approaches were followed to generate five different hydrographs. In the base case scenario, a hydrograph was generated over a period of 51 seconds that supplied a water volume of 3.46 m^3 to the channel. In the first approach, along with the reference hydrograph, two other discharge hydrographs having the same volume, but different duration, i.e., 63 s and 98 s, and smaller peak discharges were considered. These hydrographs are shown in Figure 2.10. Figure 2.11 shows the reference water depth hydrographs (channel not connected to the floodplain storage) for the first approach at one of the target locations along the channel. In the second approach, along with the base case hydrograph, two hydrographs having the same duration, i.e., 51 s, but different peak discharges and water volumes, i.e., 2.46 m^3 and 1.47 m^3, were considered as can be seen in Figure 2.12.

Figure 2.13, shows the reference water depth hydrographs for the second approach at the same target location as in Figure 2.11. Figure 2.14, Figure 2.15, and Figure 2.16 show the input hydrographs from repeated test runs showing excellent repeatability.

Baumer sensors at locations 1, 2, 3, 4, 5, and 6 provided a measurement of the water depth in the channel, while Baumer sensors at locations 7 and 8 provided the record of the water depth in the floodplain basin. Three breach widths with three different floodplain basin areas were tested for each hydrograph for both active and passive flood management scenarios. This yielded 80 experimental runs which are listed in Table 4.1 The plan of experiments. The experimental campaign started with a 0.2 m breach width and a floodplain basin area of 9 m^2. In the first case (active management) the breach was initially closed, and the flood basin was empty. The flood gate was lifted as the flow approached the breach location. In the second case (passive management), the breach was already open before the flood wave was released and the floodplain basin had the initial water depth of 0.13 m, which is the same as the steady state water depth in the channel. These steps are repeated for the 6 m^2 basin area. As the third floodplain option, the wall of the basin located directly in front of the breach was removed and the floodplain basin was turned into an unlimited size open area. To investigate the effects of the breach width on flood attenuation, the breach width was increased to 0.4 m and 0.8 m and all these scenarios were repeated. The configuration of the physical model is shown in Figure 2.14.

The Baumer probe at location 3 was used to monitor the water depth at the downstream end of the channel close to the weir. The data at this location are used to measure the out-flow discharge and find the volume of water that goes to the floodplain basin during the passage of the flood wave.

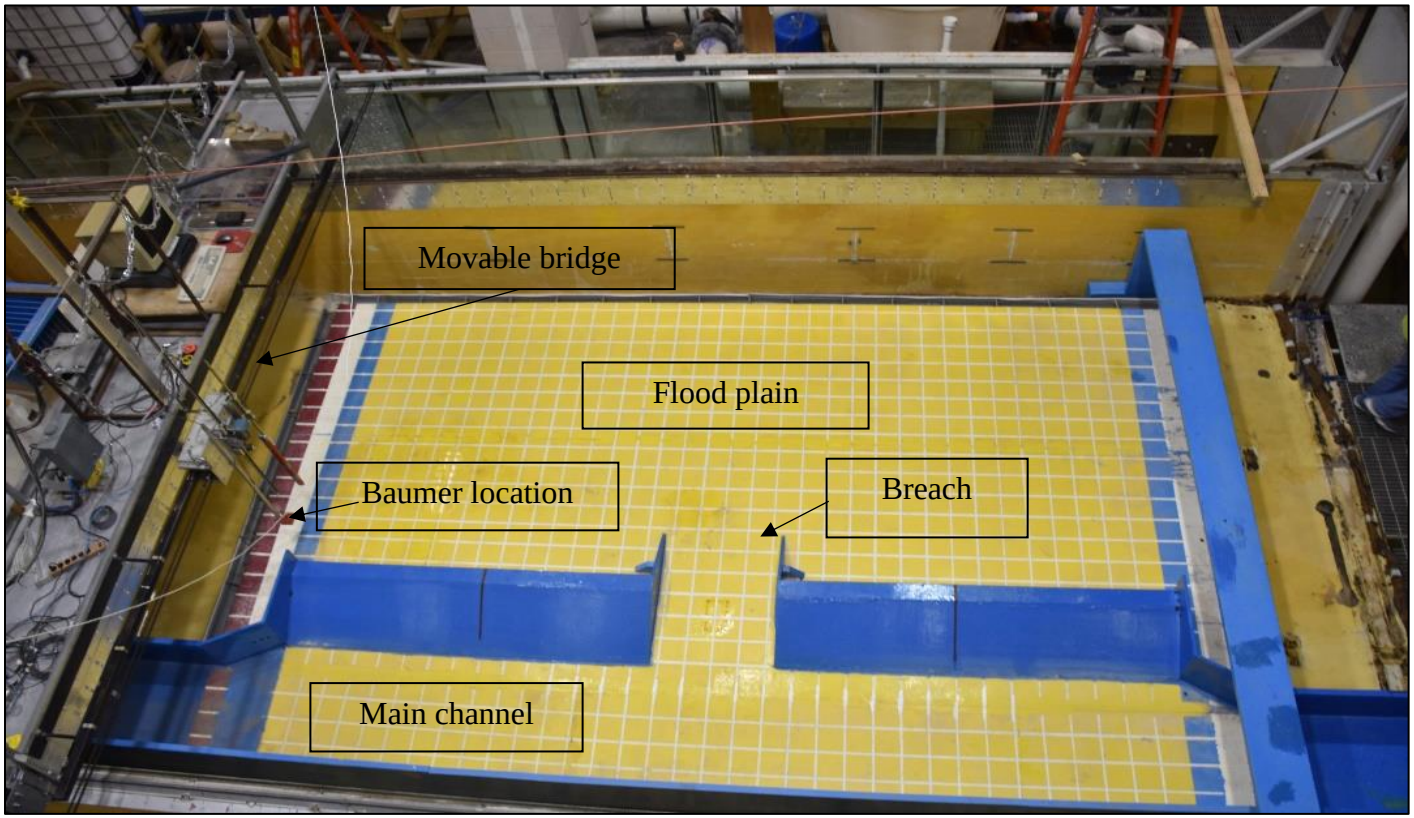

Figure 2.1 Aerial view of the experimental setup for steady levee breach flow

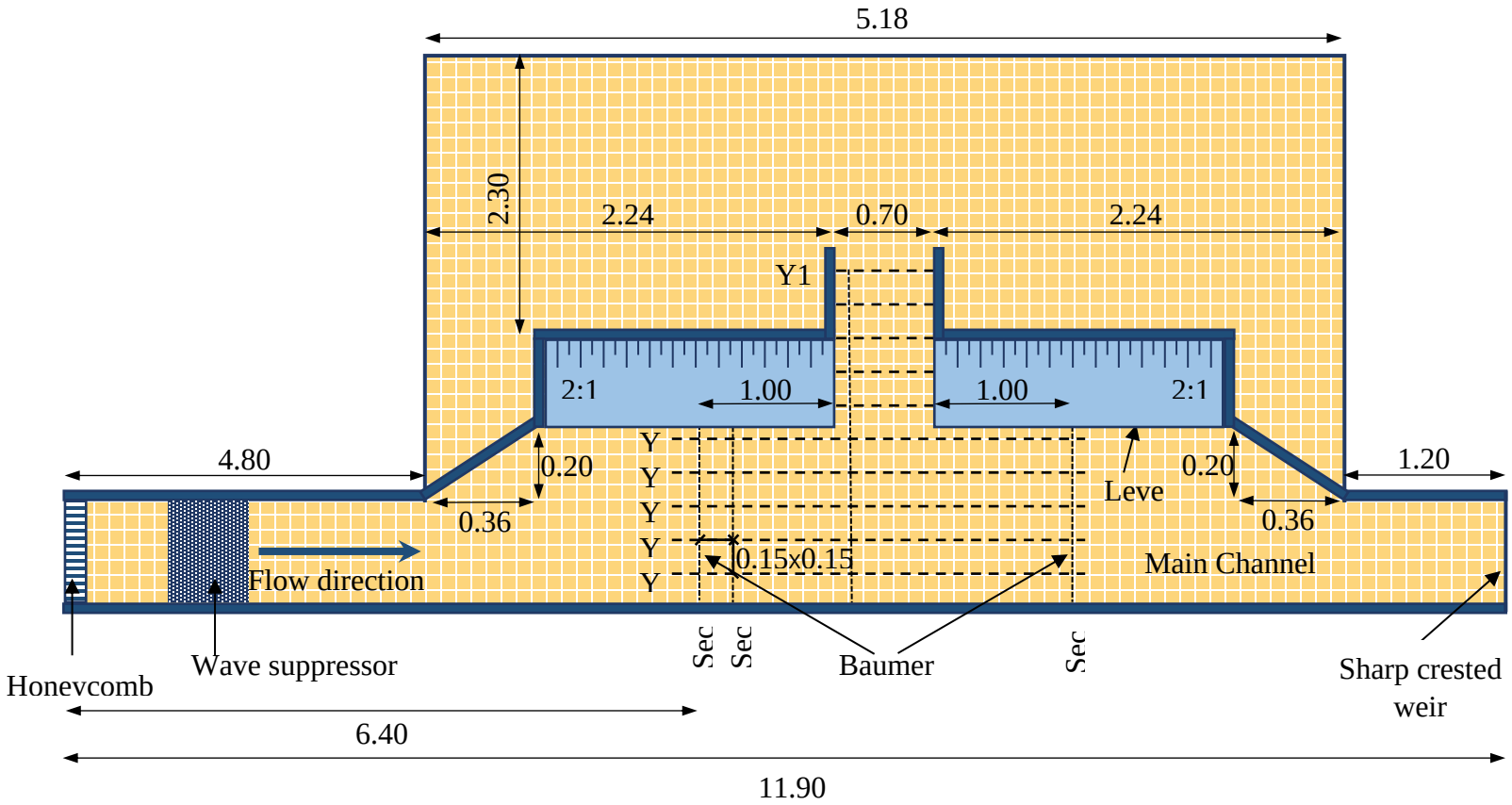

Figure 2.2 Schematic of the experimental model for steady flow through a levee breach (not to scale, all dimensions in meter)

Figure 2.3 A Baumer probe (UNAM 18U6903)

(a)

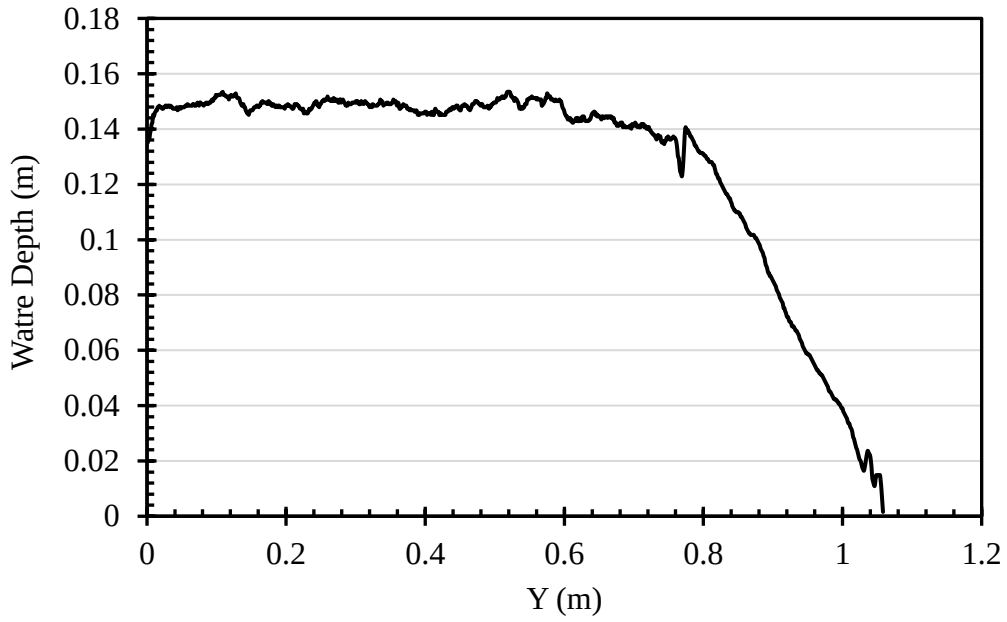

Figure 2.4 Water depth across the channel at section (a) 1, (b) 8, (c) 10, (d) 12, (e) 15

(b)

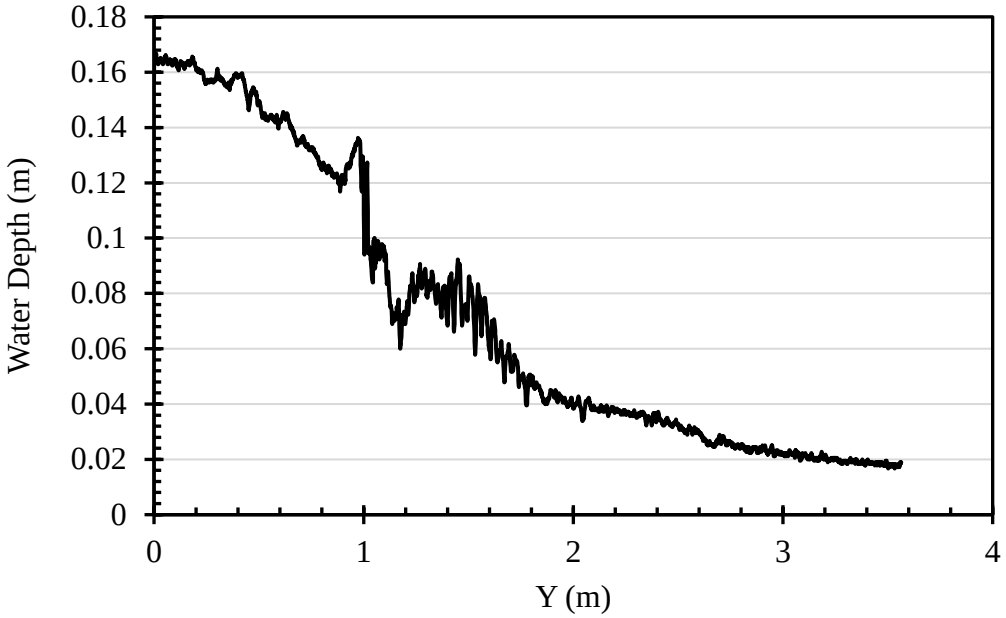

(c)

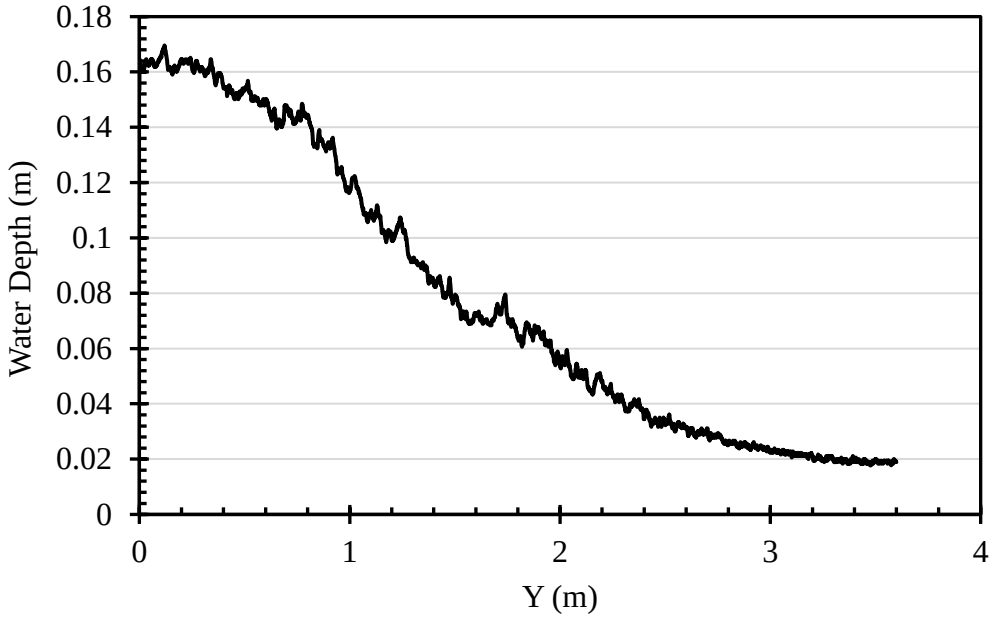

Fig. 2.4 Cont'd

(d)

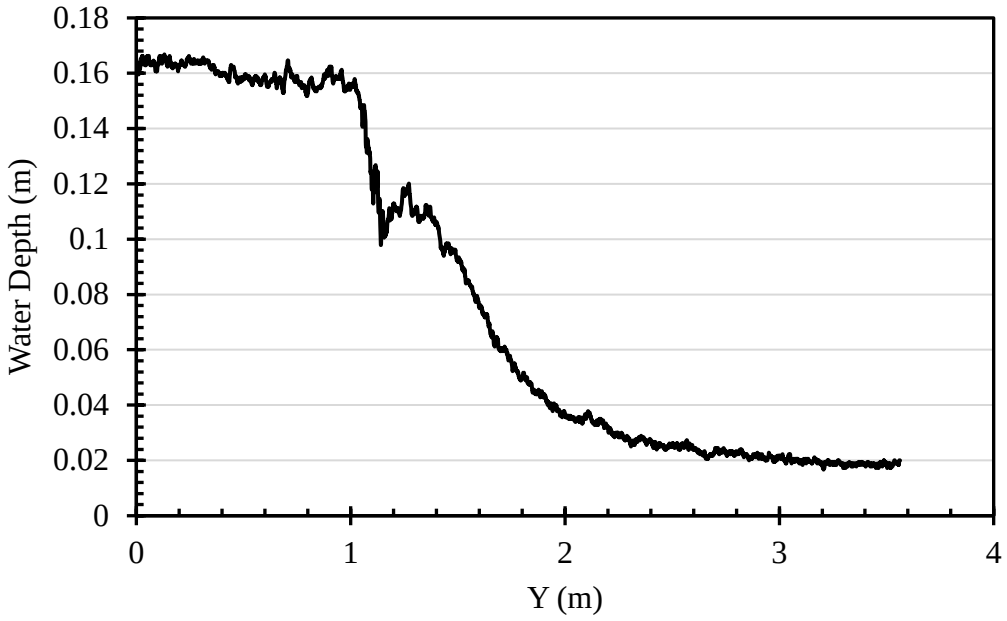

(e)

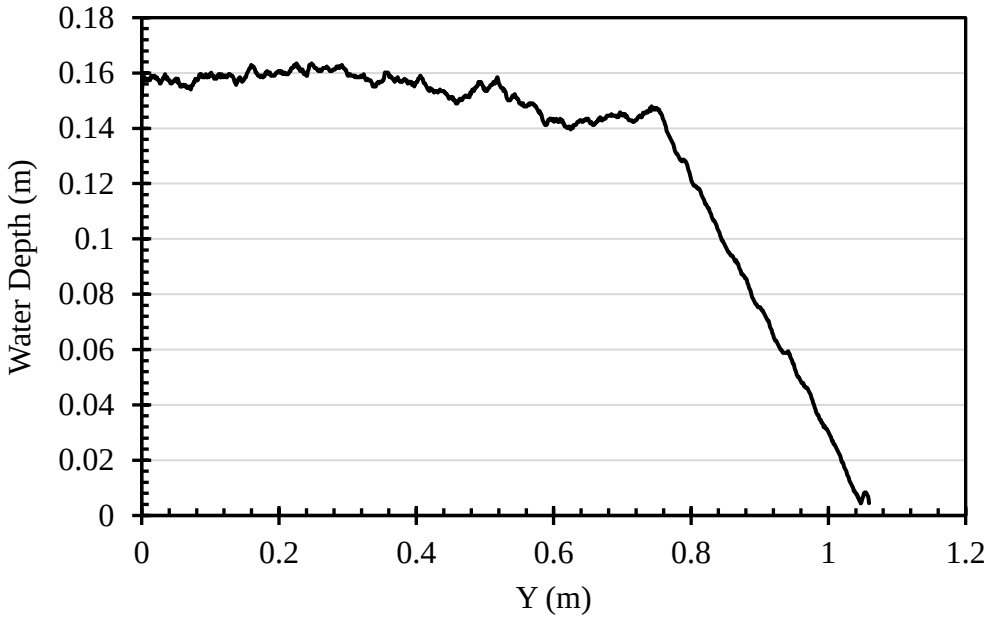

Fig. 2.4 Cont'd

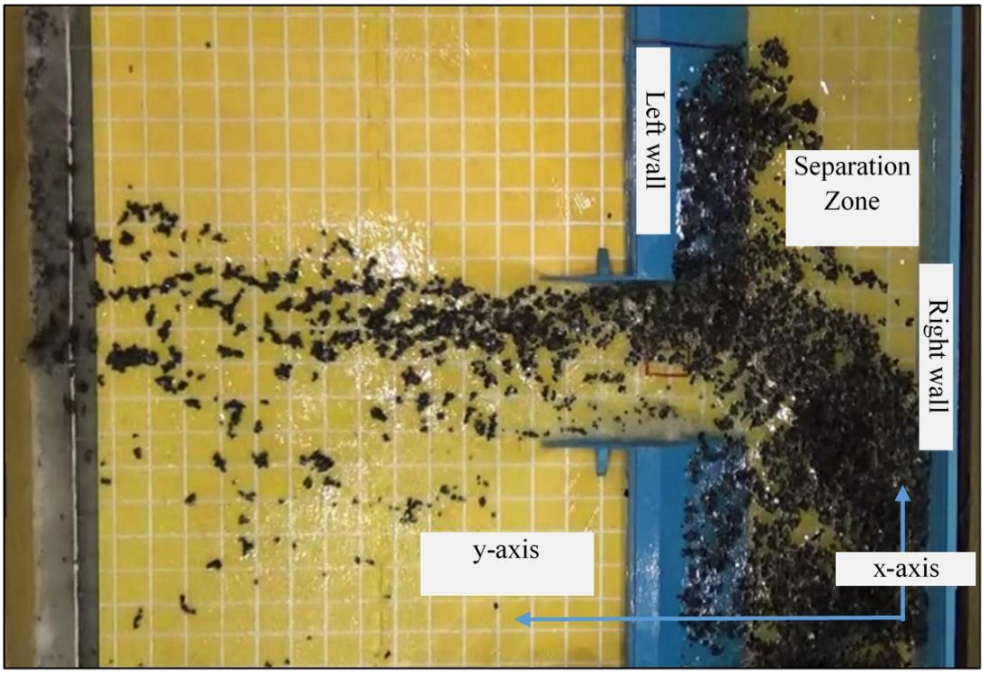

Figure 2.5 Movement of buyant black particles in water used to measure the velocity components. (Image by author)

Figure 2.6 The head tank system with pipes (Image by author)

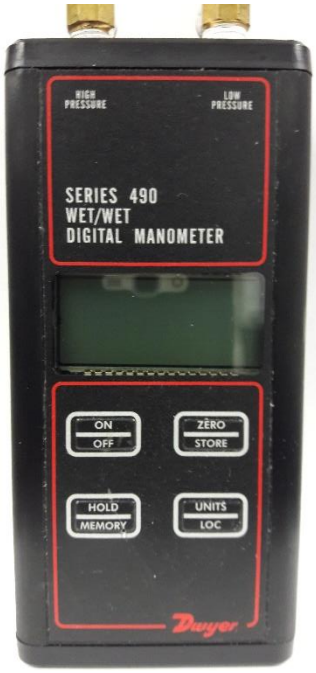

Figure 2.7 The Digital Manometer (Image by author)

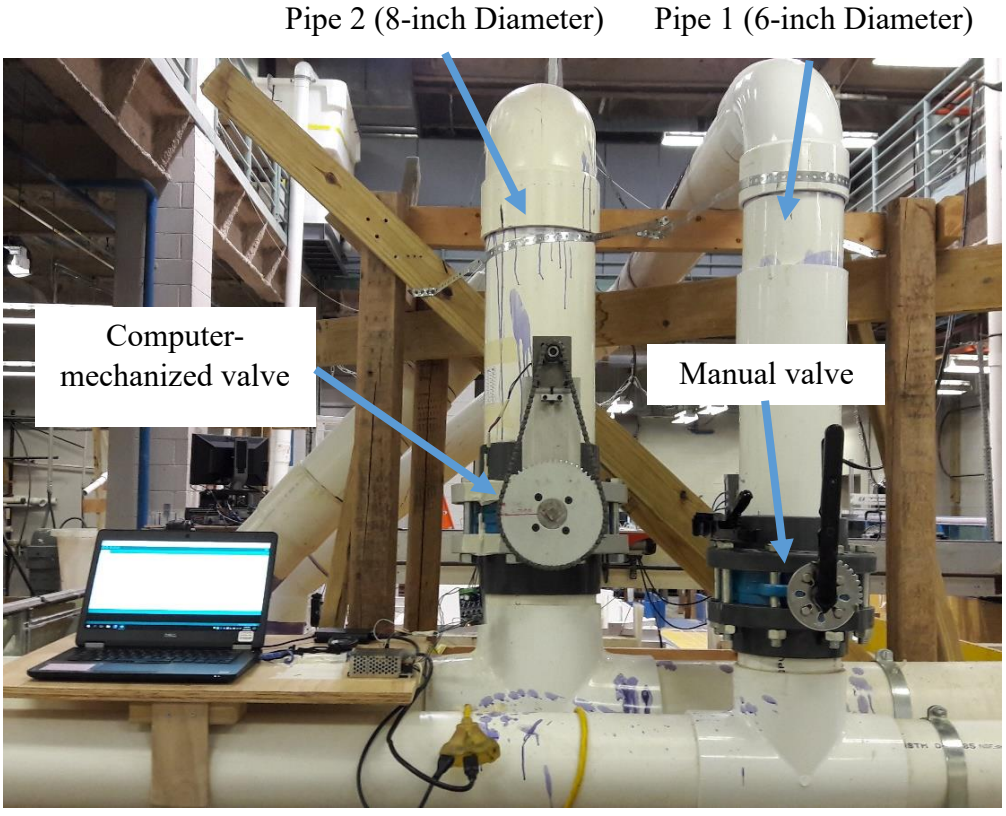

Figure 2.8 Valve system (Image by author)

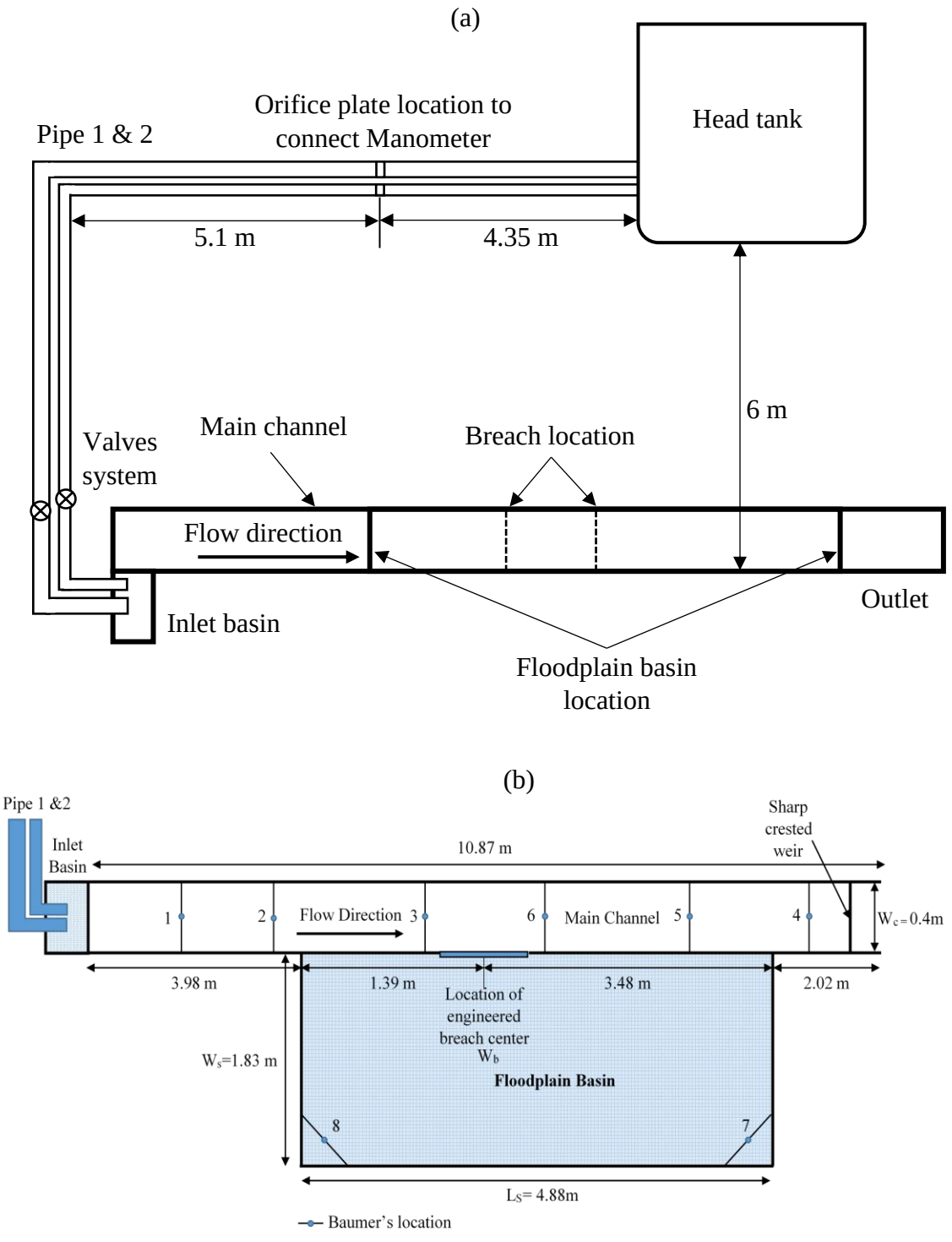

Figure 2.9 Schematic of the experimental set-up for flood reduction by engineered levee breach (not to scale), (a) Vertical cross section of the experimental setup (b) plan of the channel and floodplain basin

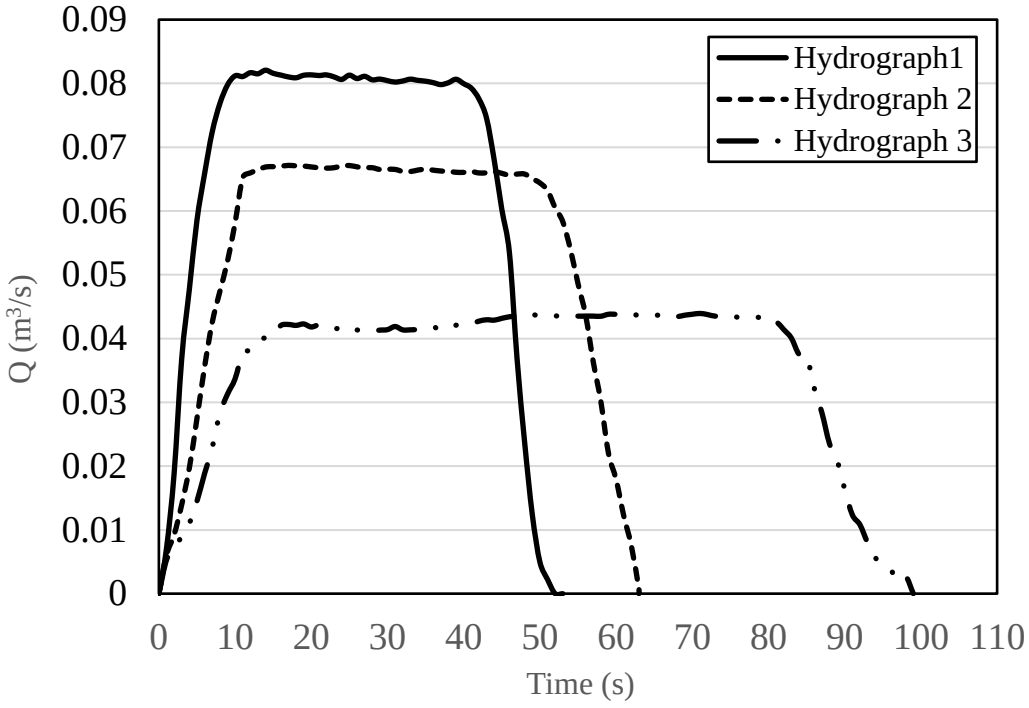

Figure 2.10 First set of input hydrographs

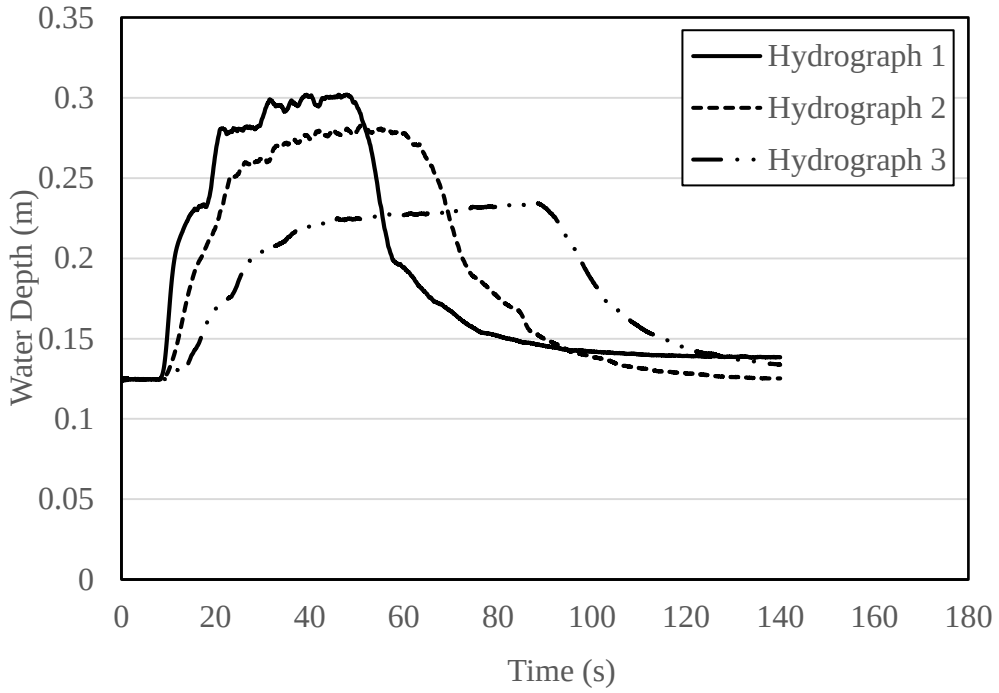

Figure 2.11 Water depth hydrographs at target location 3 without the breach

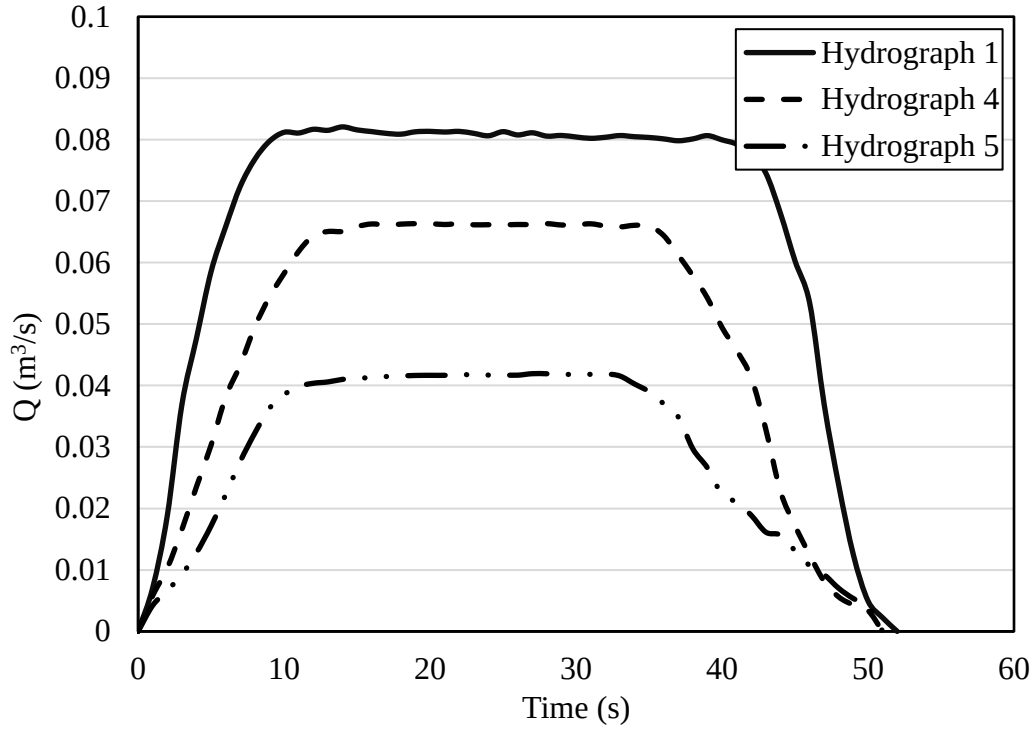

Figure 2.12 Second set of input hydrographs

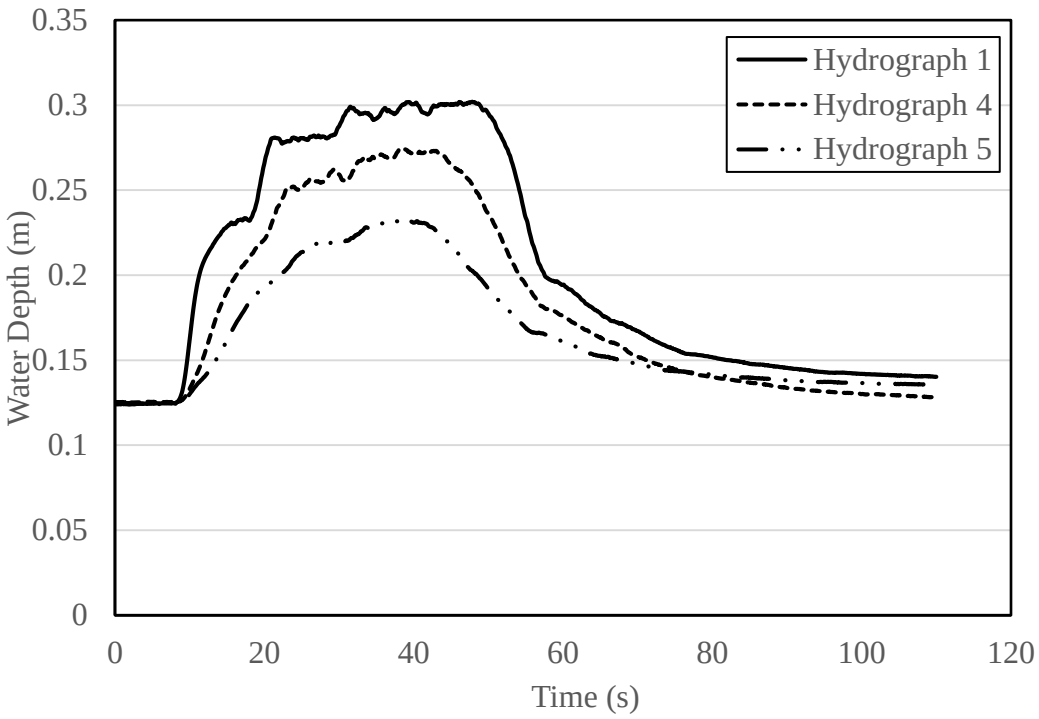

Figure 2.13 Second set of water depth hydrographs at target location 3 without the breach

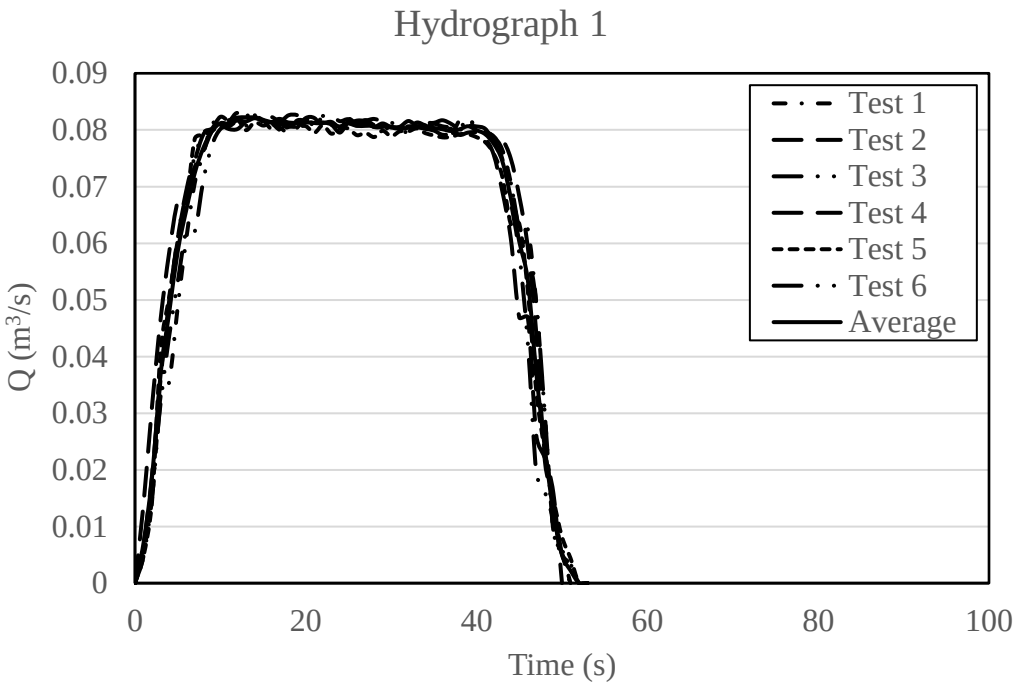

Figure 2.14 Repeatability tests of Hydrograph 1

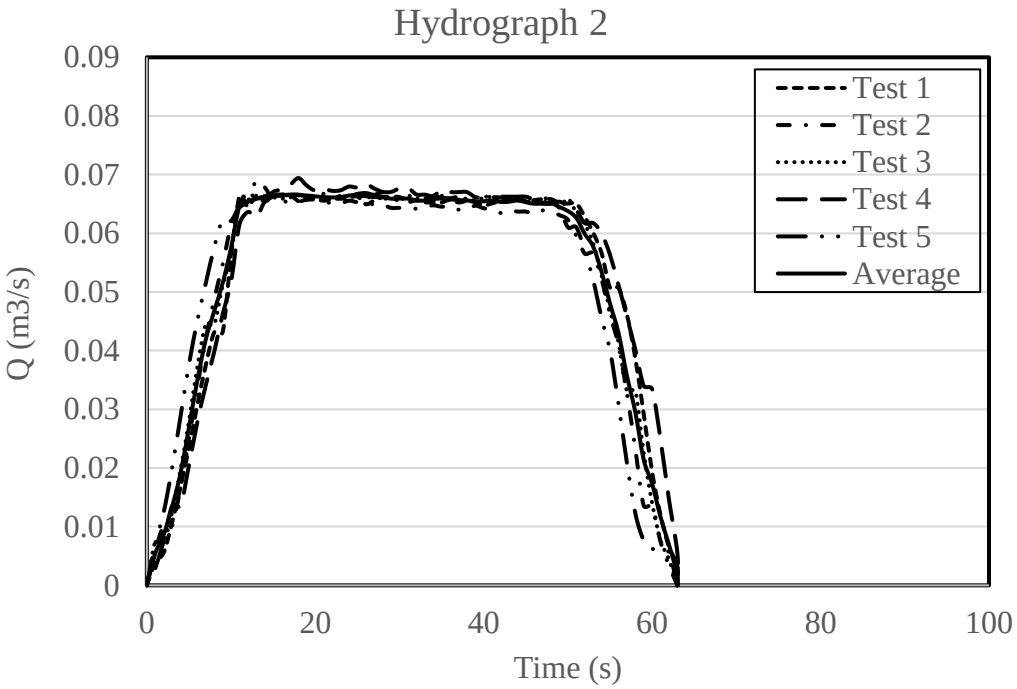

Figure 2.15 Repeatability tests of Hydrograph 2

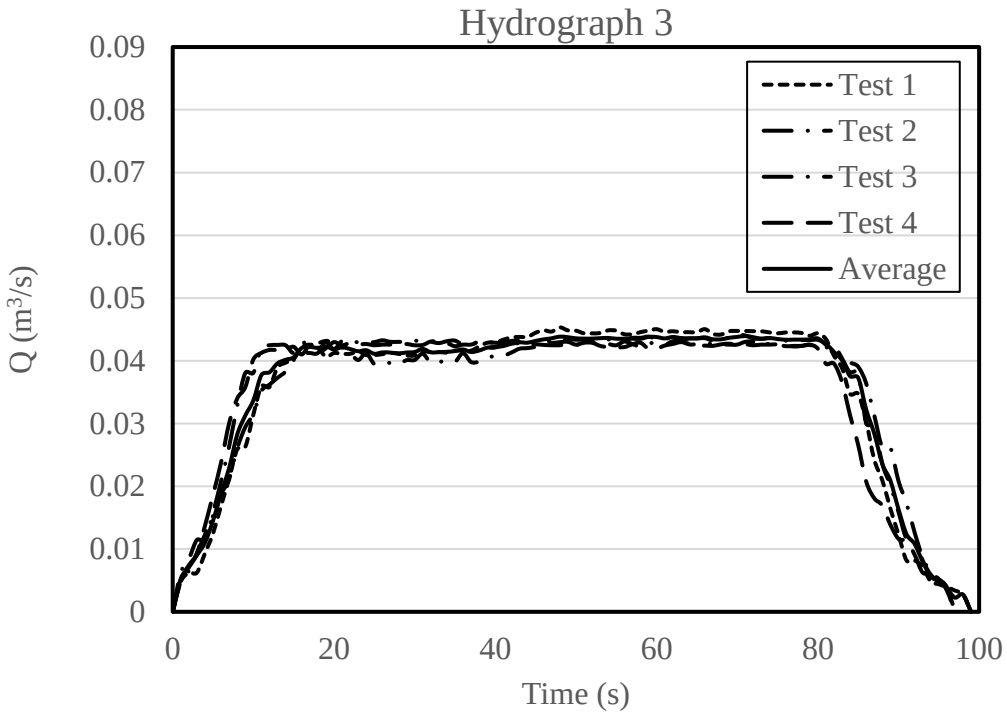

Figure 2.16 Repeatability tests of Hydrograph 3

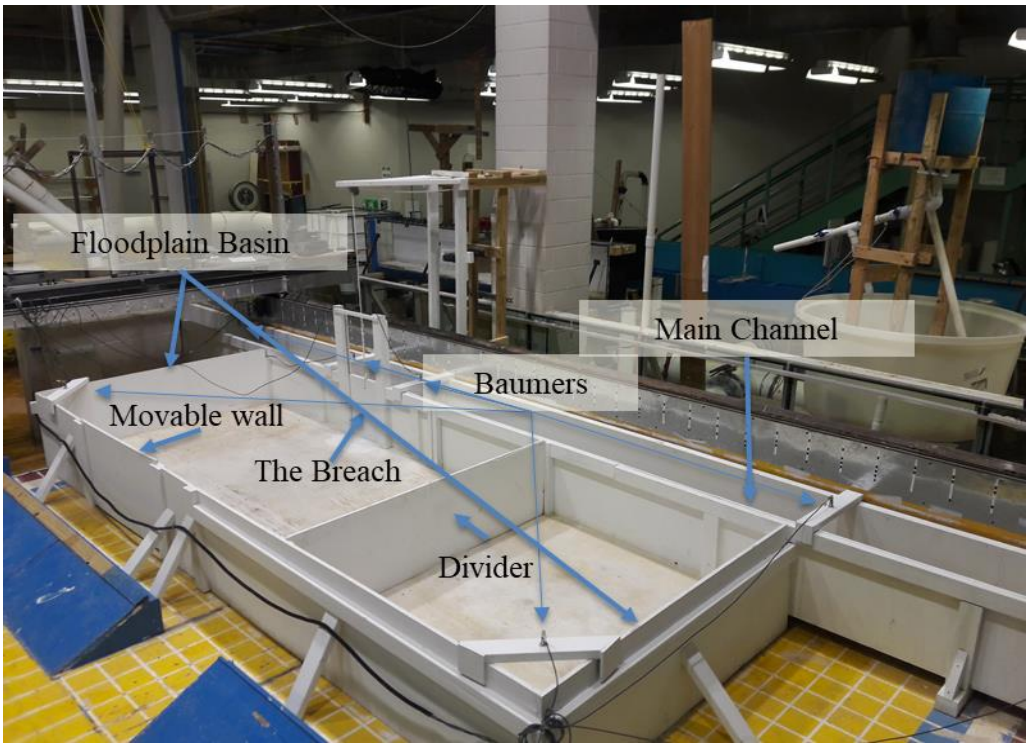

Figure 2.17 Photograph of the Channel and the flood basin

CHAPTER 3

EXPERIMENTAL INVESTIGATION AND 1D DYNAMIC MODELING OF STEADY FLOW THROUGH A LEVEE BREACH

3.1. Overview

Levees are constructed primarily to prevent flooding of populated areas and to protect important infrastructure. The National Committee on Levee Safety has estimated that there are more than 100,000 miles of levees nationwide in the USA. Levee-breach floods are commonplace around the world. Several large storms including hurricanes Katrina in 2005, Sandy in 2007, Joaquin in 2015, Harvey in 2017, and Florence in 2018, caused extensive flooding in the USA in recent years. The flood damage during the passage of these hurricanes was exacerbated by levee and embankment breaches. In particular, the primary cause for the devastating New Orleans flood was several breached levees. Experiments have been conducted during the past decades to study embankment breach processes. ASCE (2011) summarized over 700 tests on embankment dams, levees, and sea-dikes breaching. The majority of these studies involved breaching of small-scale, non-cohesive and homogeneous embankments placed across the flow thus emulating a dam-break flow. In a dam breaching event, the breach size and outflow are usually limited by reservoir characteristics rather than downstream tailwater conditions. In a levee or dike failure along a large lake, the water level either does not drop or drops minimally. In the case of a riverine levee breach, the flow is parallel to the embankment, whereas, in a dam breach, the flow is

perpendicular to the embankment. A difference between dam and river levee breaching is expected due to the direction of the momentum flux (ASCE 2011).

Systematic studies of flow through a levee breach are few and far between. Analytical models of flow division have been mainly done on channel junctions as mentioned in Chapter One.

All previous works reported above in the literature review were on experiments involving rectangular channel cross sections, case studies, or analytical models of channel junction flows. In the present study, experiments were conducted on a steady flow in a half trapezoidal channel. A levee breach with a constant width was created on the sloping side of the channel. A total of 28 experiments were run. Measurements include the water depth at the breach and upstream and downstream of the breach. In addition, the water discharge entering the channel and at the end of the channel was recorded, and the balance of the two was calculated as the breach discharge.

A one-dimensional analytical model of dividing channel flow based on the conservation of mass and momentum is adapted to estimate breach outflow. Two control volumes are considered. The first one starts upstream of the breach area and extends through the breach, and the second one starts upstream of the breach and extends downstream of the breach in the main channel. Conservation of momentum is used between control volume one and two in the streamwise direction. The interfacial shear force between the two control volumes, separation zone shear force on the right side of control volume that extends downstream of the breach, and the boundary friction force between the water and the bed surface are all included in the model formulation. The interfacial shear force coefficient and separation shear force coefficient are calibrated using the

experimental data. Using the analytical model, the breach discharge and the average water depth within the breach may be predicted using the upstream main channel discharge, water depth, and main channel downstream water depth. The model is validated against data from a set of eight experiments that are separate from the 28 experiments used for calibration of model coefficients.

3.2. Flow Characteristics

All the experiments have been run with a single discharge of 0.075 m^3/s. Flow variation among different experiments was achieved by varying the downstream weir level and the width of the breach. In this study, the flow was subcritical with a Froude number 0.27–0.61 upstream of the breach in the main channel. Subcritical with a high Froude number to critical at the breach with a Froude number of 0.9-1.0, subcritical at the channel downstream reach with a Froude number of 0.032-0.158. The flow was fully turbulent with a range of Reynolds number 46621 - 56184 upstream of the breach, 55439 - 92439 at the breach, and 4499 - 23043 downstream of the breach.

The flow had two separation zones: one on the left side of the breach wall and one in the downstream of the breach adjacent to the right bank (looking downstream in the channel direction Figure 2.5, Figure 3.1, Figure 3.2, and Figure 3.3. A large separation zone in the main channel opposite to the breach is clearly recognized in these figures. The flow detached from the upstream edge of the breach creating an asymmetric flow to the floodplain. The size of the separation zones in the breach and the main channel depended on both the breach opening and the downstream water level. In general, the separation zone is smaller in the levee breach than in the main channel. For a given breach width, the size of the main channel separation zone increased with an increase of downstream water level.

The level of flow asymmetry in the floodplain depended on the level of flow detachment from the upstream edge of the breached levee. Due to the strong lateral momentum guided by the breach walls, the flow retained the shape of a channel flow for some distance before spreading in a fan shape Figure 3.1.

3.3. Water Depth

Figure 3.4, shows the water depth at section Y3, 0.456 m from the right channel wall in the middle of the main channel for breach width (0.4, 0.5, 0.6, 0.7) m respectively and for four downstream weir heights. These figures show a systematic change in the water depth with different weir heights downstream of the main channel and different breach widths. As the weir height increased, the water surface elevation also increased. A wider breach leads to a shallower depth. The flow depth decreased upstream due to the backwater effects. The water surface was more undulated in the case of lower weir height due to increased flow velocity in the channel. Figure 3.5 shows the corresponding plots in section Y5, adjacent to the breach entrance. The water surface is significantly perturbed along this section. A dip in the water surface occurs along the breach opening which is more pronounced in case of large breach openings i.e. breach width of 0.6 m and 0.7 m.

3.4. Velocity Magnitudes

The PIVLab Matlab tool was used to calculate the surface velocity in both directions. Figure 3.6 shows the streamwise velocity for 0.7 m breach width and different weir heights (0.08, 0.1, 0.12, 0.14) m. The plots of Figure 3.5 demonstrate that the streamwise velocity decreased in the main channel flow direction due to the effect of breach discharge. As the downstream weir height increased the streamwise velocity decreased. Also, the figure

shows that the streamwise velocity decreased moving from section Y1 toward the breach area and tended to be zero within the breach section (Y7 through Y10) highlighting the predominantly lateral direction of the breach flow. The breach flow, in this case, acts like a divided channel junction flow due to the shape of the levee on the landside. In the experiment of Riahi-Nezhad (2013) the breached levee was a vertical wall. As a result, the flow out of the channel followed mainly the pre-breach direction coming out of the breach at a smaller angle with the adjacent downstream levee wall.

As shown in Figure 3.6, the streamwise velocity downstream of the breach, at sections Y9 and Y10 is close to zero due to the predominantly lateral direction of the flow (Figure 3.1 and Figure 3.2).

Figure 3.7 shows the transverse velocity from sections Y1 to Y10. The transverse velocity is almost zero at sections Y1 and Y2 and increases due to breach discharge moving from section Y3 downstream until it reaches its maximum value in section Y10 (Figure 3.7j).

To develop the analytical model the half trapezoidal channel cross-section upstream and downstream of the breach was converted to a rectangular area by averaging the bed channel width with the water surface width to get (b_{1eq} and b_{3eq}), (Figure 3.8 a, b). In addition, the water depth at the breach was also averaged as shown in Figure 3.8 c.

Table 3.1 shows the experimental data and parameters, namely, b_{1equ}, b_{3equ}, ξ, η_2, η_3, W_2, W_3, a, and F_{r1}^2, respectively representing equivalent width of the channel upstream of the breach, equivalent width of the channel downstream of the breach, discharge ratio

(Q_2/Q_1), water depth ratio at the breach, downstream water depth ratio, breach width ratio, downstream width ratio, ratio of (b_{1eq}/y_1), and the Froude number.

3.5. Analytical Model and Theoretical Approach

An analytical model is for levee breach flow is developed by adapting the model of Shabayek, Steffler, and Hicks (1999, 2002) for a channel junction, as shown in Figure 3.9. The model considers two control volumes. The first one (CV1) starts in the main channel upstream of the breach and continues to the breach. The second one (CV2) starts to parallel to the first one and continues in the main channel downstream of the breach area. The control volumes can be discerned from the velocity field shown in Figure 3.1. An interfacial zone between the two control volumes and the separation zone in CV2 clearly appeared during all the experiments. The contribution of the small separation zone in CV1 is neglected.

The mass conservation equation is:

$$Q_1 = Q_2 + Q_3 \tag{3.1}$$

The conservation of momentum in the streamwise direction for control volume One, CV1, is:

$$\rho\, Q_2\, V_2 - \rho\, Q_2\, V_1 = P_{12} - P_2 + B_1 - S + F_{b1} \tag{3.2}$$

and the conservation of momentum for control volume Two, CV2, is:

$$\rho\, Q_3\, V_3 - \rho\, Q_3\, V_1 = P_{13} - P_3 + B_2 + S - F_{b2} - F_s \tag{3.3}$$

where Q_1 = inlet discharge, Q_2= breach discharge, Q_3 = downstream discharge, ρ = density of water, V = velocity, P = hydrostatic pressure force acting on the control surface, B = Component of pressure force due to change of control volume width, S = Interface

shear force between two control volumes, F_b = friction force acting on the control volume boundaries, F_s = Shear force due to separation zone acting on CV2.

The hydrostatic pressure forces upstream, at the breach, and downstream of two control volumes are P_{12}, P_{13}, P_2, and P_3 are generalized for the trapezoidal cross section in the main channel as:

$$P_{12} = \frac{1}{2}\,\gamma\, y_1^2\, b_{1eq}\,\xi \tag{3.4}$$

$$P_{13} = \frac{1}{2}\,\gamma\, y_1^2\, b_{1eq}\,(1-\xi) \tag{3.5}$$

where $b_{1eq} = b_1 + Zy_1$, Z being the channel side slope Figure 3.8 Equation (3.4) and (3.5) are used for a trapezoidal cross section. And in our case, half trapezoidal cross section, the same equations will be used just by multiplying the length ($Z\ y_1$) by 0.5 because the side slope channel is 1V:2H.

$$P_2 = \frac{1}{2}\,\gamma\ \ y_2^2\, b_2 \tag{3.6}$$

$$P_3 = \frac{1}{2}\,\gamma\ \ y_3^2\, b_{3eq} \tag{3.7}$$

where, y = water depth; γ = specific weight of water; b_1 =width of the bottom channel, Z = side slope of the channel, y_1 = upstream water depth, y_2 = breach water depth, b_2 = width of the breach, y_3 = downstream water depth, $b_{1eq} = b_1 + Zy_1$, $b_{3eq} = b_3 + z\ y_3$ are equivalent main channel cross section upstream and downstream of the breach for a trapezoidal cross section. In the present case of half trapezoidal cross section, Z is multiplied by a coefficient of 0.5 Figure 3.8.

The force components, B_1 and B_2, appear due to change in control volume width and act in the longitudinal direction on the lateral boundaries of each control volume:

$$B_1 = \frac{1}{2}\,\gamma\, y_1^2\,[b_2 - b_{1eq}\,\xi] \tag{3.8}$$

and

$$B_2 = \frac{1}{2}\,\gamma\, y_1^2\,[b_{3eq} - b_{1eq}\,(1-\xi)] \tag{3.9}$$

The interfacial shear force, S, is parallel to the interface between the two control volumes but acts in an opposite direction. To estimate this force, the area of the interface is multiplied by the average shear stress:

$$S = C_f \frac{\rho\,(V_2^2 - V_3^2)}{2}\left(\frac{y_2 + y_3}{2}\right) L_i \tag{3.10}$$

Where C_f = friction coefficient, V_2 = velocity at the breach, V_3 = downstream velocity, and L_i = the interface length. Several trials were made to estimate the length as observed in the experiments. First, L_i was assumed to be equal to the harmonic mean of the upstream width of two control volumes (Shabayek, Steffler, and Hicks 2002), i.e., $L_i = 2(b_1+0.5\,Z\,y_1)[\xi\,(1-\xi)]$ which gave a range of values between 0.0812 – 0.248 m which is too small compared to the bottom width of the channel (0.81 m) and observations made in the experiments. Figure 3.2, shows the length of the interface between two control volumes for one of the experiments. From this picture and observation from videos of all experiments, the length of the interface between two control volumes can be approximated as the circumference of a quarter circle, $L_i = 0.5\,\pi\,b_{1eq}\,\xi$. This gives a reasonable value of Li in the range of 0.807 – 1.362 m.

By combining all coefficients and constants in a single parameter, K_i, the shear force is written in the following form:

$$S = K_i \rho (V_2^2 - V_3^2)(y_2 + y_3)(0.5 \pi b_{1eq} \xi) \quad (3.11)$$

The friction force F_{b1} and F_{b2} that act on CV1 and CV2 due to walls and bed of the channel are:

$$F_{b1} = \rho \left(\frac{V_1}{C_*}\right)^2 \left[(b_{1eq} L_1 \xi - \xi b_{1eq} b_2) + (L_1 y_1 - b_2 y_1) \right] + \left[\rho \left(\frac{V_2}{C_*}\right)^2 \left(\frac{1}{2} b_2 b_{1eq} \xi \right) \right] \quad (3.12)$$

and

$$F_{b2} = \rho \left(\frac{V_1}{C_*}\right)^2 \left[\frac{b_{1eq}(1-\xi) + b_{3eq}}{2} L_1 + y_1 L_1 \right] + \rho \left(\frac{V_3}{C_*}\right)^2 \left[b_{3eq} (L_2 - L_1) + 2 y_3 (L_2 - L_1) \right] \quad (3.13)$$

The non-dimensional Chezy coefficient C_* appears in these equations and an individual experiment was run by completely closing the breach opening and making the water move straight from upstream to downstream for a flow rate of 0.08725 m^3/s. Velocity profiles at different sections along the channel were obtained using an Acoustic Doppler Velocimeter (ADV). The nondimensional Chezy coefficient can be expressed as:

$$\sqrt{C}_* = \frac{U}{u_*} \quad (3.14)$$

where U = depth-averaged velocity (m/s), and u_* = shear velocity (m/s). The shear velocity was estimated using the law of the wall:

$$u = \left(\frac{u_*}{k}\right) \ln\left(\frac{z}{z_o}\right) \tag{3.15}$$

where u = Reynolds average streamwise velocity at a distance z from the bed, k = von kàrmàn constant = 0.41 z_o = the y-intercept of the fitted line through the data. The average non-dimensional Chezy coefficient for the channel was found to be 18.03.

The separation zone shear force F_s acts on CV2 as a result of recirculating flow after the flow divides into two parts. This force is computed as:

$$F_s = K_s \rho V_3^2 y_3 L_s \tag{3.16}$$

where K_s = Separation zone shear coefficient, and L_s = length of the separation zone. As shown in Figure 3.2, the length of separation can be represented as the circumference of half of the circle which appeared clearly from the observation of all the experiments. Therefore, this length is calculated as $Ls = \pi\, b_{3eq}.\xi$. By combining all the coefficients into a single one, the separation zone shear coefficient, K_s, the equation of separation zone shear force can be written as:

$$F_s = k_S \rho V_3^2 y_3 \pi b_{3eq} \xi. \tag{3.17}$$

by substituting the forces into the momentum equations (3.2) and (3.3), the following relations are obtained for momentum balance in CV1 and CV2:

$$\rho\, Q_2\, V_2 - \rho\, Q_1\, V_1 = \frac{1}{2}\,\gamma\, y_1^2\, b_{1eq}\,\xi - \frac{1}{2}\,\gamma\, y_2^2\, b_2 + \frac{1}{2}\,\gamma\, y_1^2\,(b_2 + b_{1eq}\xi) - K_i\,\rho\,(V_2^2 - V_3^2)\,(y_2 + y_3)(0.5\,\pi\, b_{1eq}\,\xi) - \rho\left(\frac{V_1}{C_*}\right)^2\left[(b_{1eq}\,L_1\,\xi - b_{1eq}b_2\,\xi) + (y_1\,L_1 - y_1 b_2)\right] - \rho\left(\frac{V_2}{C_*}\right)^2\left[\frac{1}{2}\,b_2 b_{1eq}\xi\right] \quad (3.18)$$

and,

$$\rho\, Q_3\, V_3 - \rho\, Q_3\, V_1 = \frac{1}{2}\,\gamma\, y_1^2\, b_{1eq}\,(1-\xi) - \frac{1}{2}\,\gamma\, y_3^2\, b_{3eq} + \frac{1}{2}\,\gamma\, y_3^2\left[b_{3eq} - b_{1eq}(1-\xi)\right] + K_i\,\rho\,(V_2^2 - V_3^2)\,(y_2 + y_3) * (0.5\,\pi\, b_{1eq}\,\xi) - \rho\left(\frac{V_1}{C_*}\right)^2\left[\frac{b_{1eq}\,(1-\xi) + b_{3eq}}{2}\,L_1 + y_1\,L_1\right] - \rho\left(\frac{V_3}{C_*}\right)^2\left[2\,y_3\,(L_2 - L_1) + b_{3eq}(L_2 - L_1)\right] - K_s\,\rho\, V_3^2\, y_3\,(\pi\, b_{3eq}\xi) \quad (3.19)$$

The non-dimensional terms, the discharge ratio $\xi = Q_2/Q_1$, the depth ratio $\eta_2 = y_2/y_1$, $\eta_3 = y_3/y_1$, width ratio $w_2 = b_2/b_{1eq}$, $w_3 = b_{3eq}/b_{1eq}$, and upstream Froude number, $F_1 = Q_1/(g\, b_{1eq}^2\, y_1^3)^{0.5}$ are substituted in Eq. (3-18) and (3-19) leading to

$$\frac{\xi^2}{w_2\eta_2} - \xi = \frac{w_2}{2\,F_1^2}\,(1-\eta_2^2) - K_i\left(\frac{\xi^2}{w_2^2\,\eta_2^2} - \frac{1}{w_3^2\,\eta_3^2} + \frac{2\xi}{w_3^2\,\eta_3^2} - \frac{\xi^2}{w_3^2\,\eta_3^2}\right) * (\eta_2 + \eta_3)\,(0.5\,\pi\,\xi) - \frac{1}{C_*^2}\left[a\,\xi\,\frac{L_1}{b_{1eq}} - a\,w_2\,\xi + \frac{L_1}{b_{1eq}} - w_2\right] - \frac{1}{2C_*^2}\left[\frac{\xi^3\,a}{w_2\eta_2^2}\right] \quad (3.20)$$

and

$$\frac{(1-2\,\xi+\,\xi^2)}{w_3\,\eta_3}-1+\xi=\;\frac{1}{2\,F_1^2}\,[1-\xi-\,\eta_3^2+\,\eta_3^2\,\xi]\;\;+\,K_i\,(\eta_2+\,\eta_3)\,(0.5\,\pi\,\xi)\,*$$
$$\left(\frac{\xi^2}{w_2^2\,\eta_2^2}-\frac{1}{w_3^2\,\eta_3^2}+\frac{2\,\xi}{w_3^2\,\eta_3^2}-\frac{\xi^2}{w_3^2\,\eta_3^2}\right)-\frac{1}{C_*^2}\left[\frac{(1-\,\xi+w_3)}{2}\;a\,\frac{L_1}{b_{1eq}}+\frac{L_1}{b_{1eq}}\right]-$$
$$\frac{1}{C_*^2}\left[\frac{1}{w_3^2\,\eta_3^2}-\frac{2\,\xi}{w_3^2\,\eta_3^2}+\frac{\xi^2}{w_3^2\,\eta_3^2}\right]\left[2\eta_3\left(\frac{L_2}{b_{1eq}}-\frac{L_1}{b_{3eq}}\right)+\,w_3\,\left(\frac{aL_2}{b_{1eq}}-\frac{aL_2}{b_{1eq}}\right)\right]-$$
$$K_s\;\frac{1}{w_3\,\eta_3}\,[\,1-2\,\xi+\,\xi^2]\,(\pi\,\xi) \qquad (3.21)$$

Equations (3.20) and (3.21) are nonlinear equations. The length of CV1 is estimated as twice the breach width for all the experiments, and the length of CV2 is three times the breach width. The values of the non-dimensional ratios for different experiments are reported in Table 3.1. The interfacial shear coefficient, K_i, and separation zone shear coefficient, K_s, are calibrated by using data obtained from measurements.

3.6. Calibration of The Model Coefficients

By substituting the experimental data reported in Table 3-1 into Eq. 3-20 and 3-21, the value of the coefficients K_i and K_s can be estimated for each experiment. The value of K_i decreases when ξ increases as shown in Figure 3.10 indicating that when the breach discharge increases, the interfacial shear coefficient decreases. The opposite happens with K_s, as shown in Figure 3.11. As shown in Figure 3.3, when the downstream water depth increased due to an increase in the weir height, the breach discharge increased and the downstream discharge decreased, leading to an increase in the separation zone length and the stagnation area. Also seen in Figure 3.6 (c) and (d), the streamwise velocity at section Y3 and Y4 decreased when the weir height increased. The interfacial shear coefficient, K_i, and the stagnation shear coefficient, K_s, versus downstream water depth normalized by breach width are plotted in Figure 3.12 and Figure 3.13.

Figure 3.10, Figure 3.11, Figure 3.12, and Figure 3.13 show that the plots of shear coefficients appear in distinct groups according to the breach width. A multi-regression analysis was done to generate the following relations to evaluate K_i, K_s

$$K_i = 0.2 \left(\frac{W_b}{W_c}\right)^{-0.53} (F_1)^{2.31} \quad (3.22)$$

The coefficient of determination (R^2) for this equation is 0.9491. And

$$K_s = 0.72 \left(\frac{W_b}{W_c}\right)^{6.22} (F_1)^{-4.31} \quad (3.23)$$

where $F_1 = V_1/(gD_1)^{0.5}$, and $D_1 = A_1/T_1$ is the hydraulic depth. The coefficient of determination (R^2) for Eq. 3-22 and 3-23, respectively, is 0.95 and 0.89. Equations 3.22 and 3.23 can be used to calculate K_i and K_s. Then, by solving Eq. 3.20 and 3.21 simultaneously, the breach discharge and breach water depth can be estimated.

3.7. Model Validation

To validate this model, eight additional experiments with different and randomly selected discharge were conducted. The experimental condition for these runs is reported in Table 4-2. Discharge and water depth at the breach, water depth upstream and downstream the breach, and downstream discharge were measured from these experiments. Figure 3.14 shows the comparison between the breach discharge calculated by the analytical model and experimental measurement with a coefficient of determination (0.8524). Figure 3.15, shows the comparison between the breach water depth calculated by the analytical model and the measurements with a coefficient of determination (0.8361).

3.8. Summary

Levee breach is one of the most serious problems associated with flooding. Estimation of the breach discharge and the average water depth within the breach area provide the necessary information for flood mitigation and breach closure.

This study has three components: the first one is the experimental measurement of flow velocity and depth, the second component is the development of a 1D analytical model, and the third one is additional experimental work to validate the model. In the first part, twenty-eight experiments were conducted. Four breach widths were tested with seven weir heights at the downstream to control the water depth. It was found from experimental measurements and observation that the breach discharge increased with an increase in the breach width while maintaining a constant downstream water level, and the breach discharge also increased with increasing the downstream water level while maintaining a constant breach width.

In the second part of this study, a one-dimensional analytical model was developed. The momentum principle was applied to two control volumes, developing two equations for two unknowns. This model estimates the breach discharge and average water depth within the breach for known inlet and downstream water depth, and inlet discharge.

Two important coefficients appear in this analysis, the interfacial shear force, K_i, between the control volumes and the separation zone shear coefficient, K_s, that appeared in the main channel downstream of the breach section. These coefficients are calibrated by using the experimental measurements. The variation of these two coefficients depends on the breach and channel width which represents the geometry effect, and Froude number in the upstream channel, which represents the flow effect.

In the third part, eight additional experiments were run to validate the analytical model by considering inlet discharge that higher and lower than the constant discharge in the first set of experiments. in addition, a different breach width of 0.55 m was used. The results show a good agreement between the analytical model results and the measurements.

Table 3.1 Dimensional and non-dimensional experimental data for this study

	b_{1eq}	b_{3eq}	$\xi = Q_2/Q_1$	$\eta_2 = y_2/y_1$	$\eta_3 = y_3/y_1$	$W_2 = b_2/b_{1eq}$	$W_3 = b_{3eq}/b_{1eq}$	$a = b_{1eq}/y_1$	F_{r1}^2
1	0.92	0.945	0.68	0.71	1.19	0.76	1.02	7.56	0.37
2	0.93	0.95	0.74	0.68	1.16	0.75	1.02	7.20	0.31
3	0.935	0.95	0.78	0.68	1.13	0.75	1.01	6.93	0.27
4	0.94	0.96	0.82	0.67	1.11	0.74	1.01	6.67	0.23
5	0.945	0.96	0.86	0.66	1.10	0.74	1.01	6.52	0.21
6	0.95	0.96	0.89	0.65	1.09	0.74	1.01	6.33	0.19
7	0.95	0.97	0.91	0.67	1.10	0.73	1.02	6.26	0.18
8	0.935	0.95	0.68	0.67	1.13	0.64	1.02	6.93	0.26
9	0.94	0.96	0.70	0.67	1.12	0.64	1.02	6.80	0.25
10	0.945	0.96	0.73	0.68	1.11	0.64	1.021	6.55	0.22
11	0.95	0.965	0.76	0.66	1.12	0.63	1.02	6.41	0.20
12	0.95	0.97	0.79	0.66	1.11	0.63	1.02	6.23	0.17
13	0.96	0.975	0.84	0.65	1.09	0.62	1.025	6.00	0.15
14	0.96	0.98	0.87	0.63	1.08	0.62	1.01	5.82	0.13
15	0.94	0.96	0.59	0.71	1.15	0.53	1.02	4.57	0.24
16	0.95	0.97	0.63	0.66	1.12	0.53	1.02	6.33	0.19
17	0.96	0.97	0.69	0.66	1.08	0.52	1.01	6.03	0.15
18	0.96	0.98	0.71	0.65	1.08	0.52	1.01	5.85	0.14
19	0.97	0.98	0.74	0.66	1.06	0.51	1.01	5.71	0.12
20	0.97	0.99	0.78	0.64	1.07	0.51	1.01	5.57	0.11
21	0.98	0.99	0.81	0.63	1.07	0.51	1.01	5.44	0.10
22	0.96	0.97	0.54	0.66	1.10	0.42	1.02	6.09	0.16
23	0.965	0.98	0.57	0.64	1.09	0.41	1.02	5.85	0.14
24	0.97	0.99	0.60	0.67	1.09	0.41	1.02	5.66	0.12
25	0.98	0.99	0.62	0.65	1.08	0.41	1.01	5.49	0.11
26	0.985	1.00	0.66	0.67	1.06	0.40	1.01	5.32	0.09
27	0.99	1.00	0.68	0.65	1.06	0.40	1.01	5.21	0.09
28	1.00	1.01	0.71	0.65	1.04	0.40	1.01	5.04	0.07

Table 3.2 Data for validation experiments

	Breach width (m)	Weir height (m)	Q_1 (m^3/s)	H_1 (m)	Q_2 (m^3/s)	H_2 (m)	Q_3 (m_3/s)	H_3 (m)
1	0.7	0.08	0.083	0.133	0.0568	0.0876	0.026	0.157
2	0.7	0.12	0.0908	0.150	0.0727	0.108	0.18	0.180
3	0.5	0.12	0.0653	0.162	0.0504	0.102	0.148	0.172
4	0.5	0.12	0.0747	0.168	0.0548	0.104	0.198	0.185
5	0.5	0.1	0.0735	0.160	0.0488	0.0985	0.0246	0.175
6	0.5	0.1	0.0577	0.149	0.0414	0.0905	0.0162	0.158
7	0.55	0.1	0.0744	0.167	0.526	0.0905	0.0217	0.168
8	0.55	0.14	0.073	0.19	0.055	0.120	0.0175	0.199

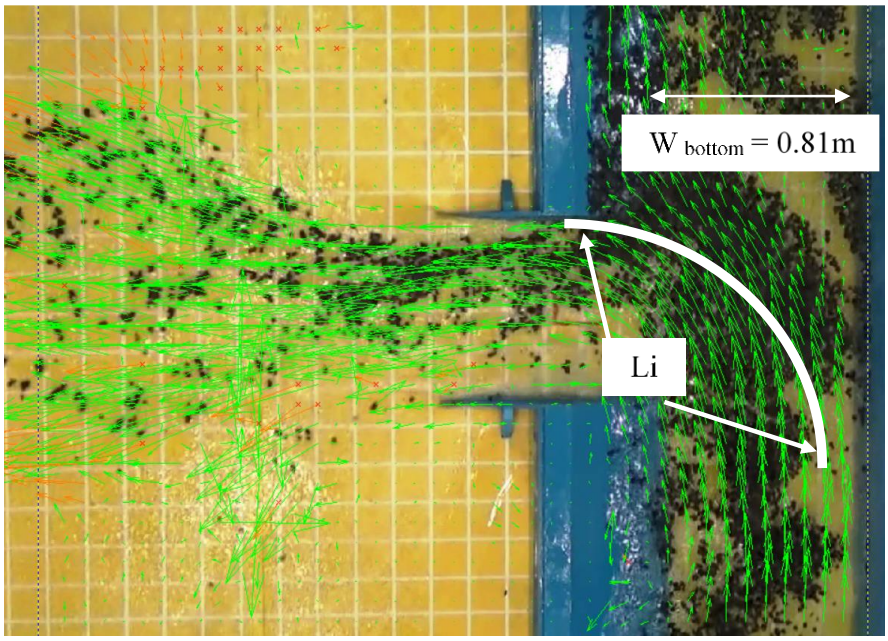

Figure 3.1 The length of the interface, breach = 0.7 m and weir height =0.08 m (image by authors)

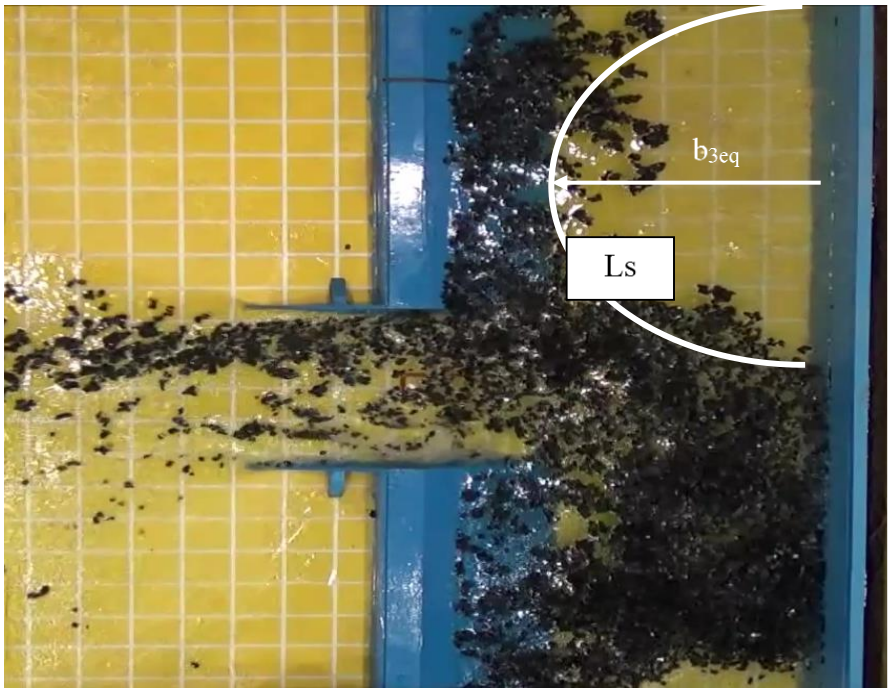

Figure 3.2 The length of the separation zone, breach width = 0.7 m and weir height = 0.12m (image by author)

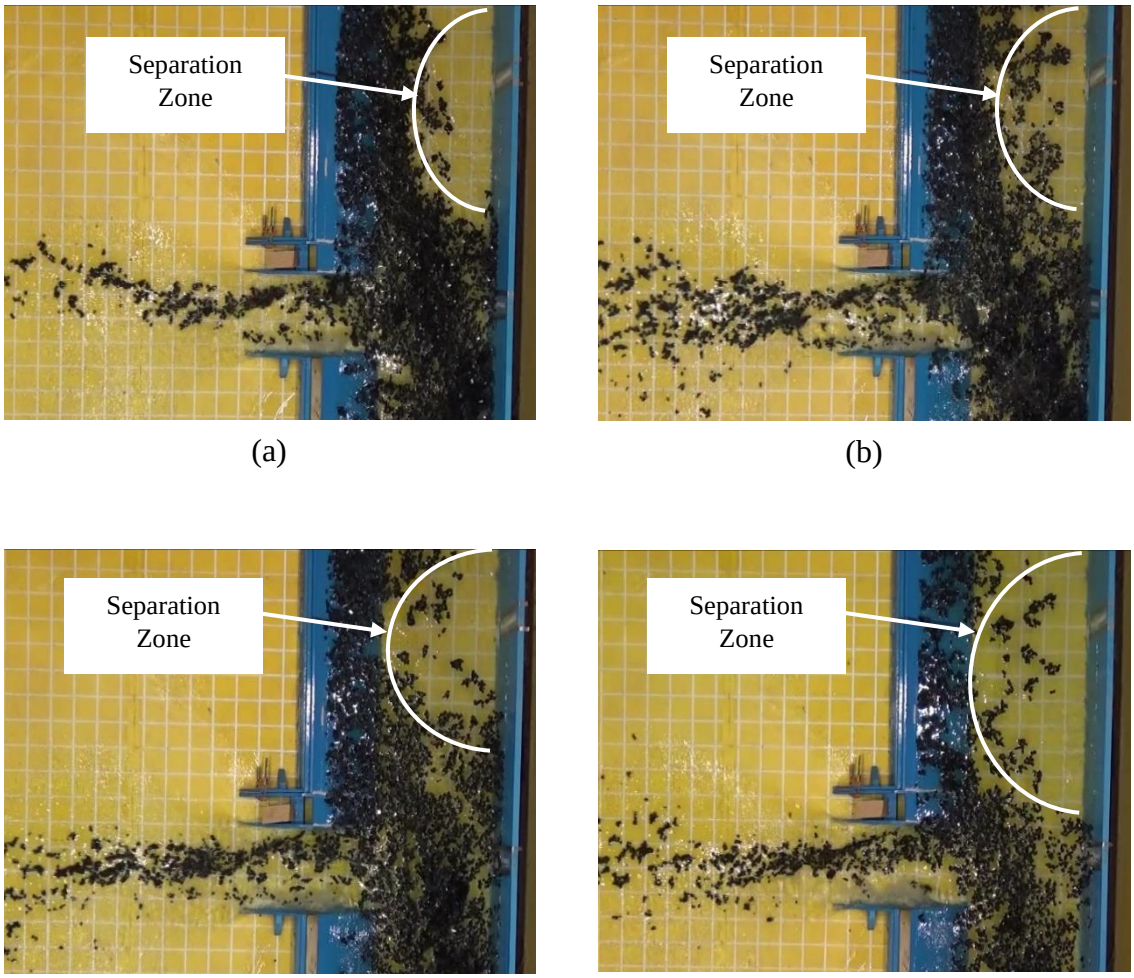

Figure 3.3 Illustration of separation zone for Breach with of 0.5 m; (a) Weir height = 0.08 m; (b) Weir height = 0.1 m; (c) Weir height = 0.12 m; (d) Weir height = 0.14 m. (image by author)

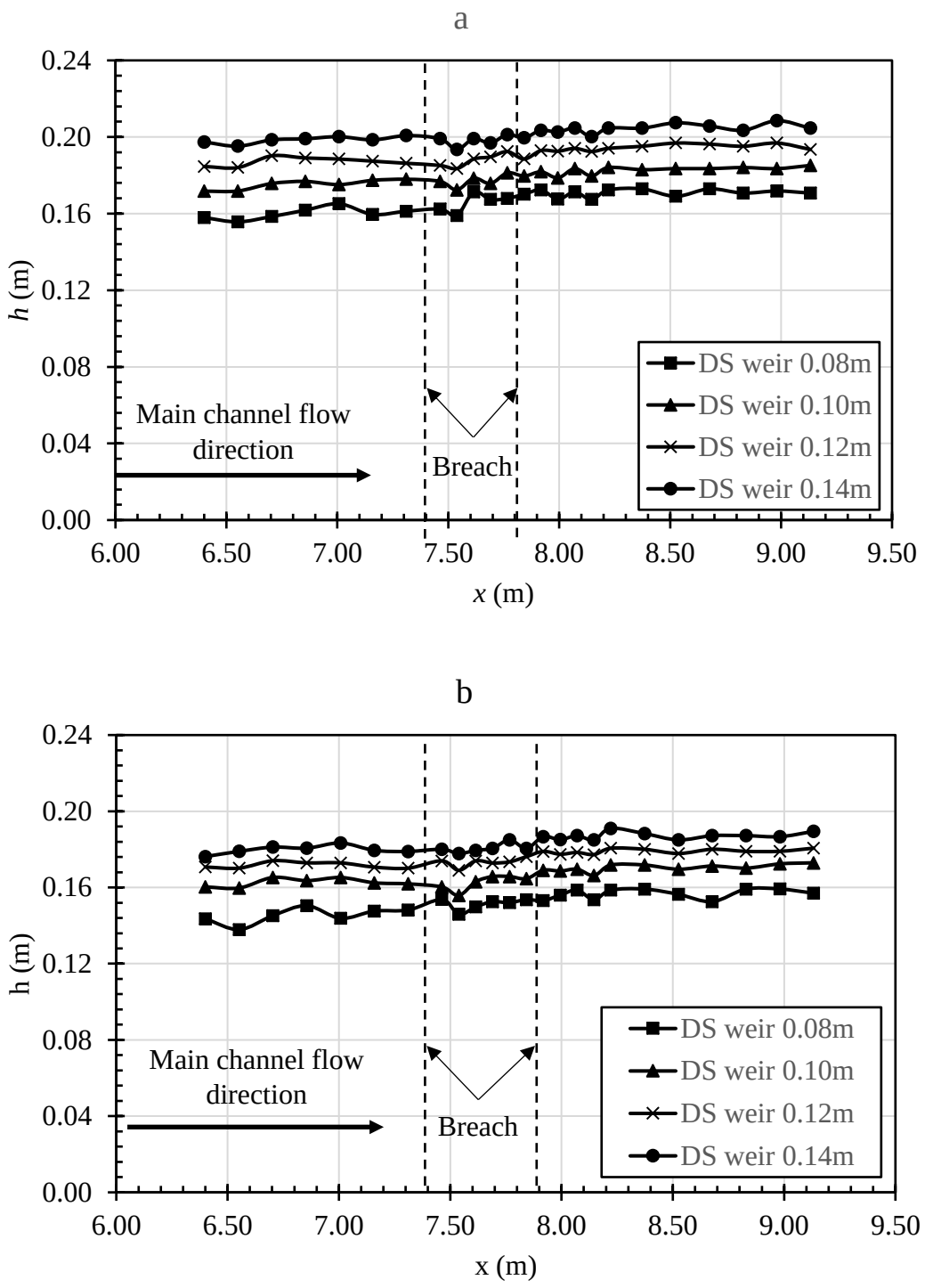

Figure 3.4 Water depth at section Y3: (a) Breach width = 0.4 m; (b) Breach width = 0.5 m; (c) Breach width = 0.6 m; (d) Breach width = 0.7 m

c

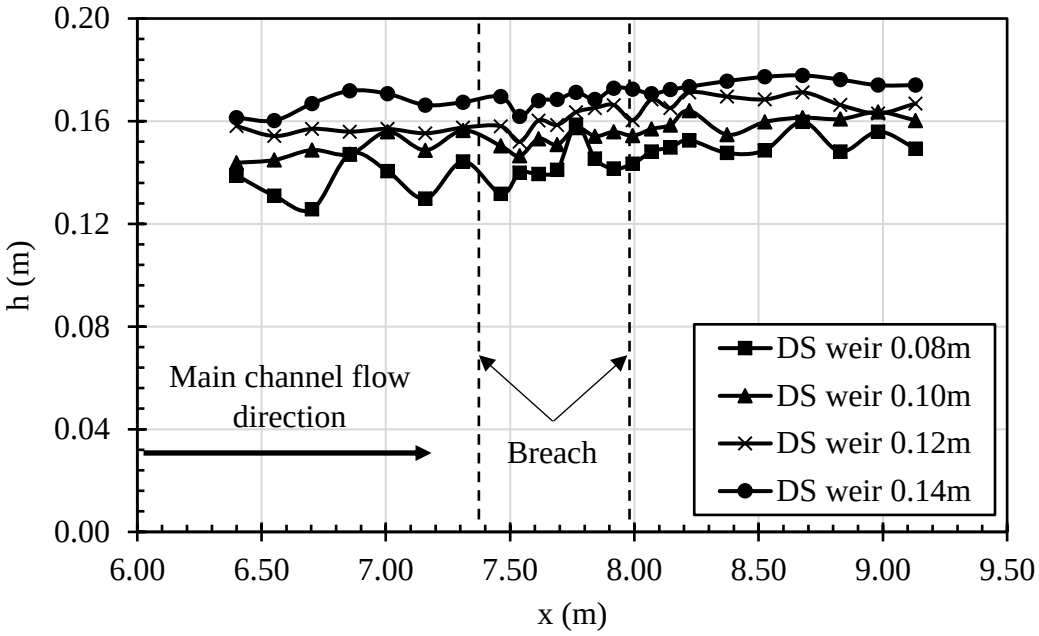

d

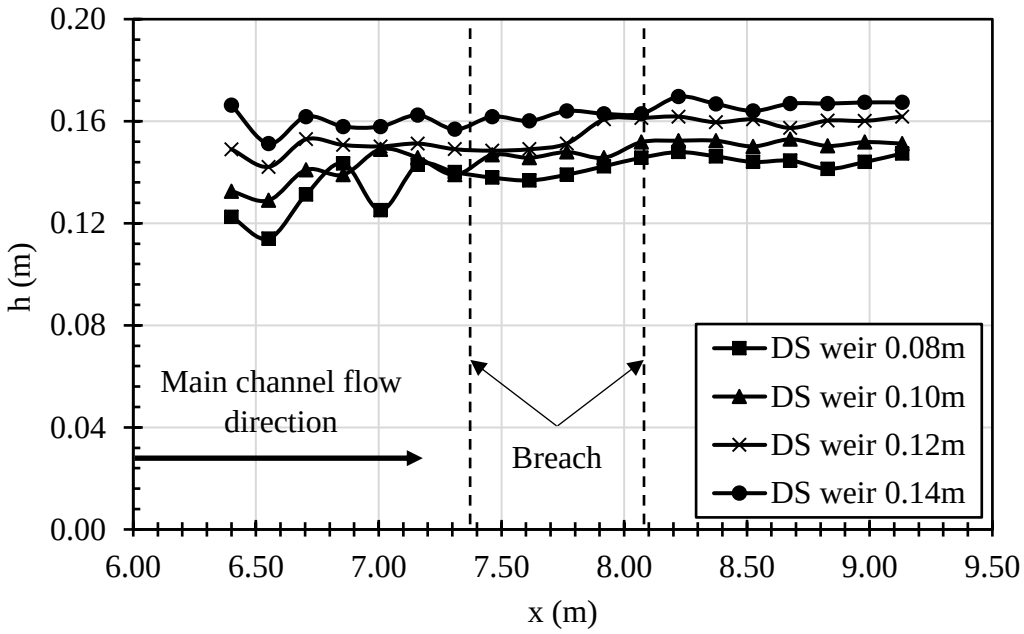

(d)

Figure 3.4 cont'd

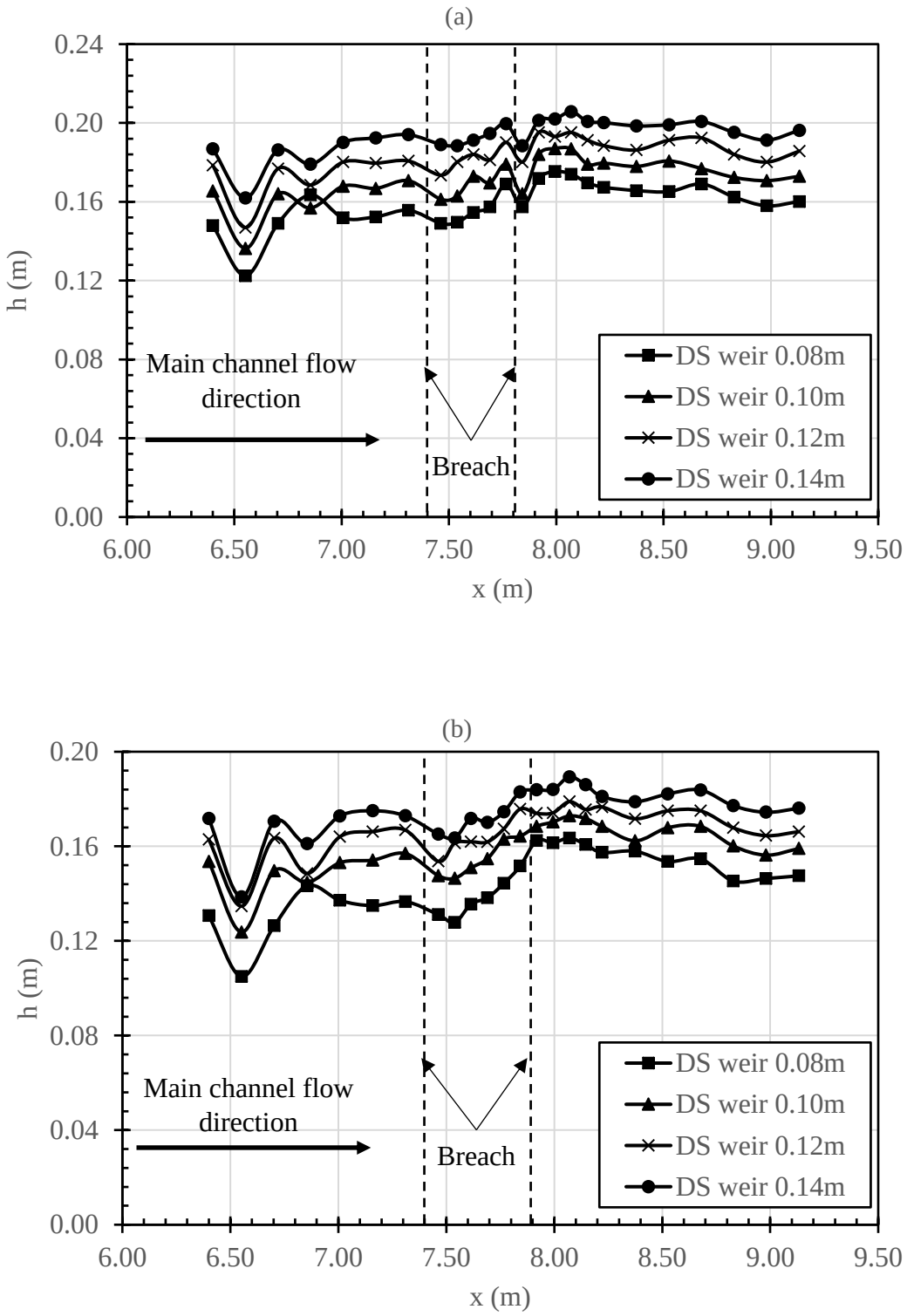

Figure 3.5 Water depth at section Y5: (a) Breach width = 0.4 m; (b) Breach width = 0.5 m; (c) Breach width = 0.6 m; (d) Breach width = 0.7 m

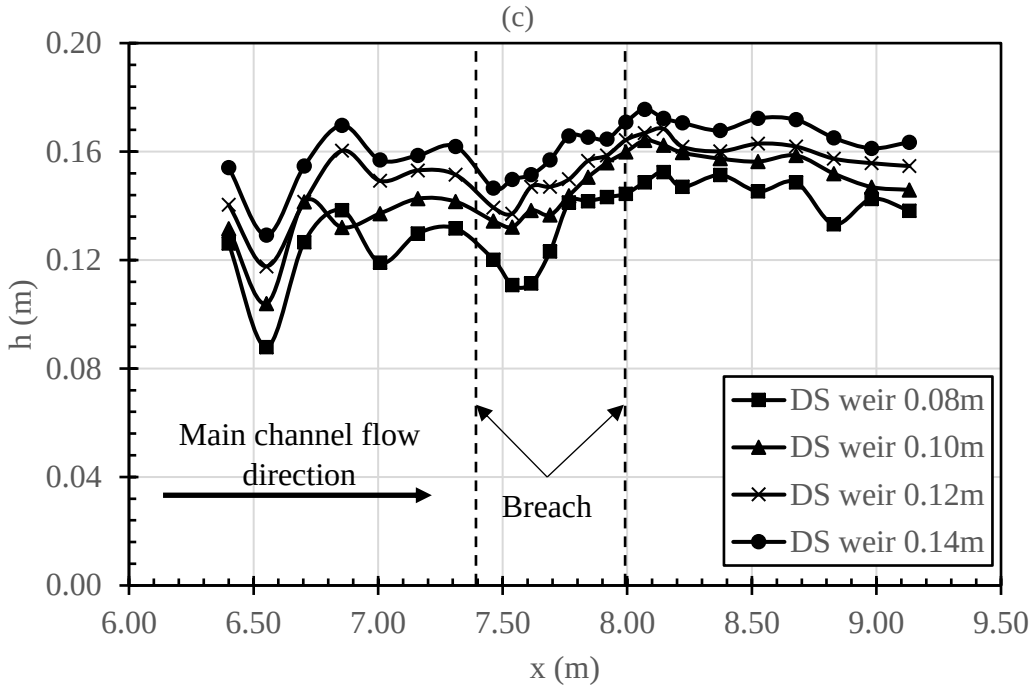

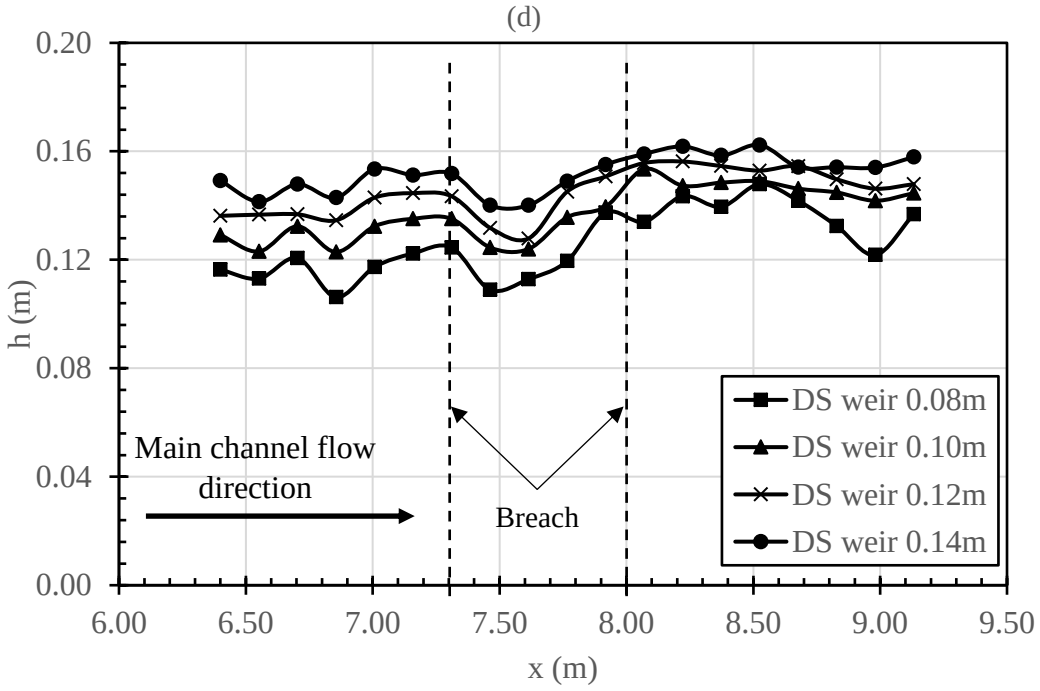

Figure 3.5 cont'd

a

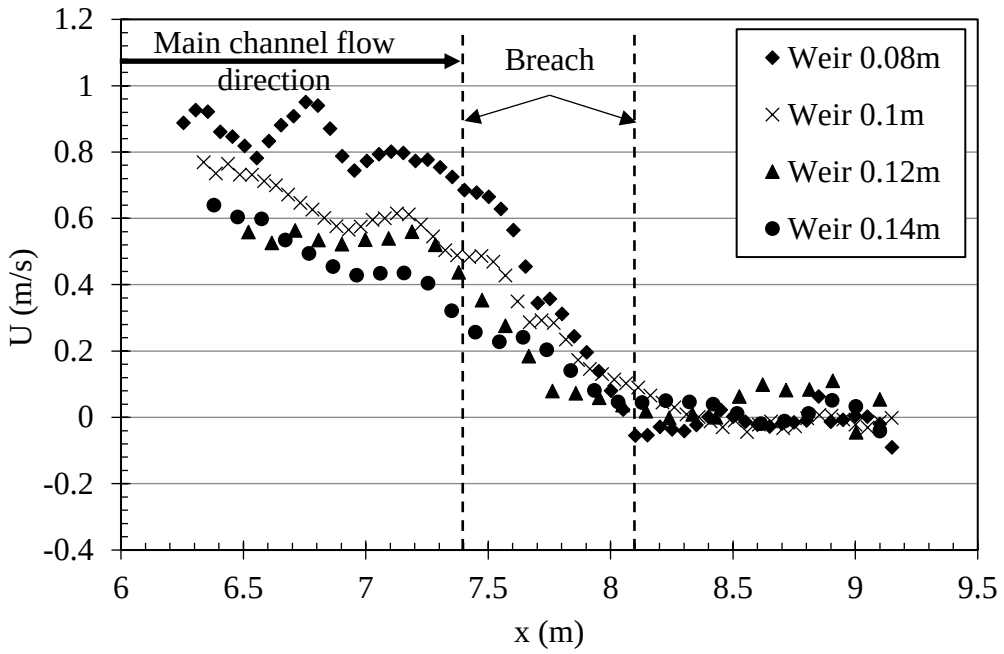

b

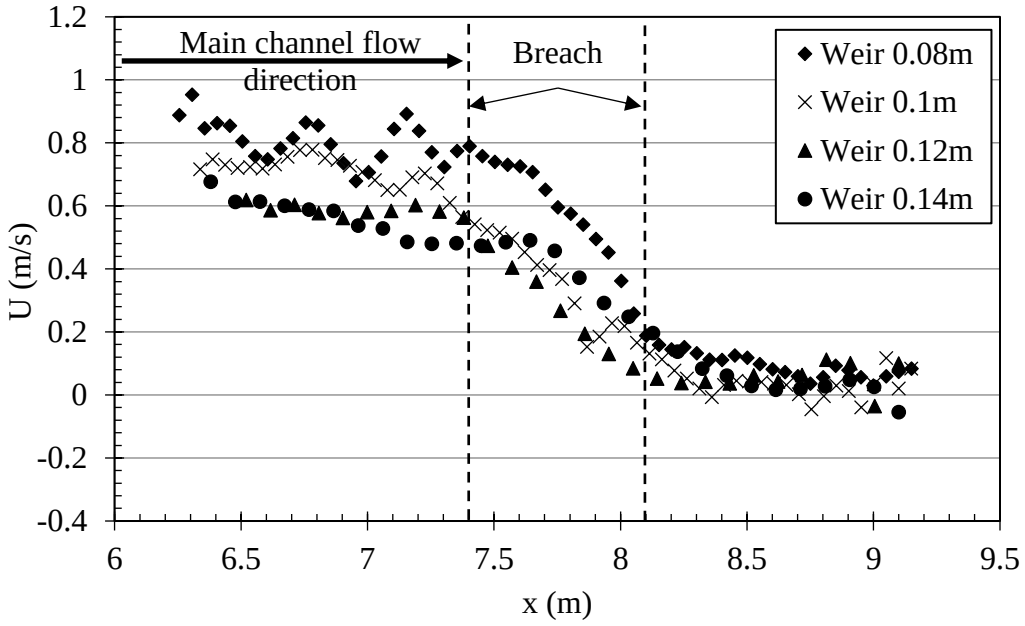

Figure 3.6 Streamwise velocity for breach width 0.7 m for different D.S weir heights at: (a) Y1; (b) Y2; (c) Y3; (d) Y4; (e) Y5; (f) Y6; (g) Y7; (h) Y8; (i) Y9; (j) Y10

(c)

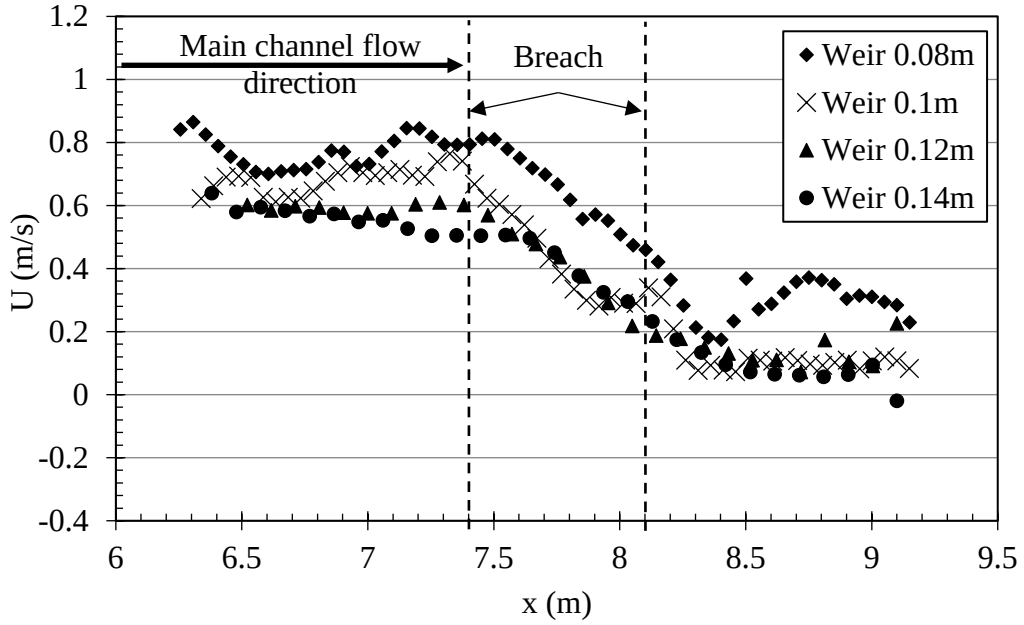

(d)

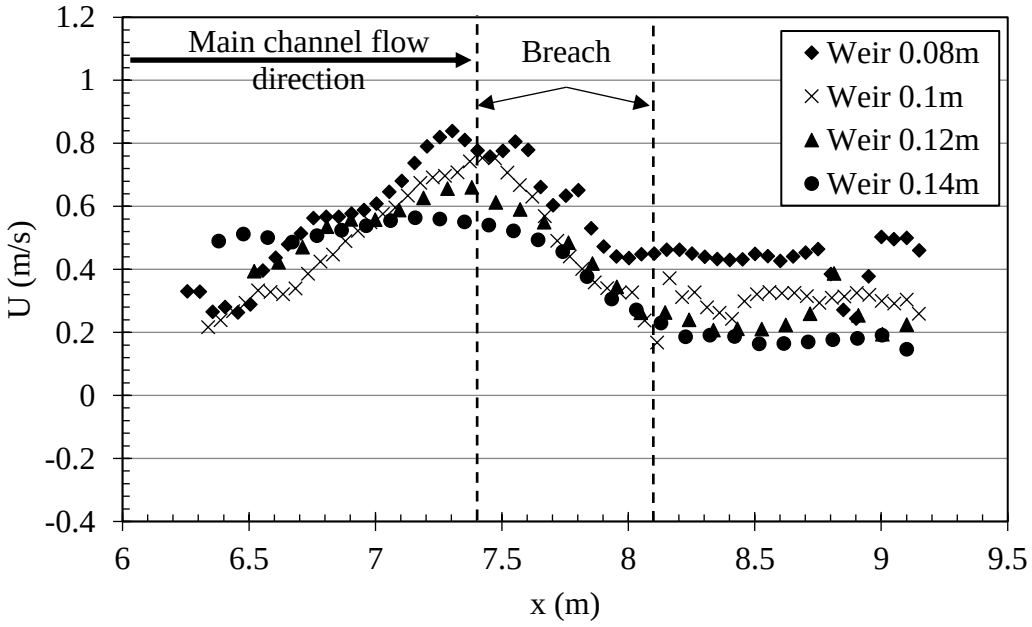

(d)

Figure 3.6 cont'd

(e)

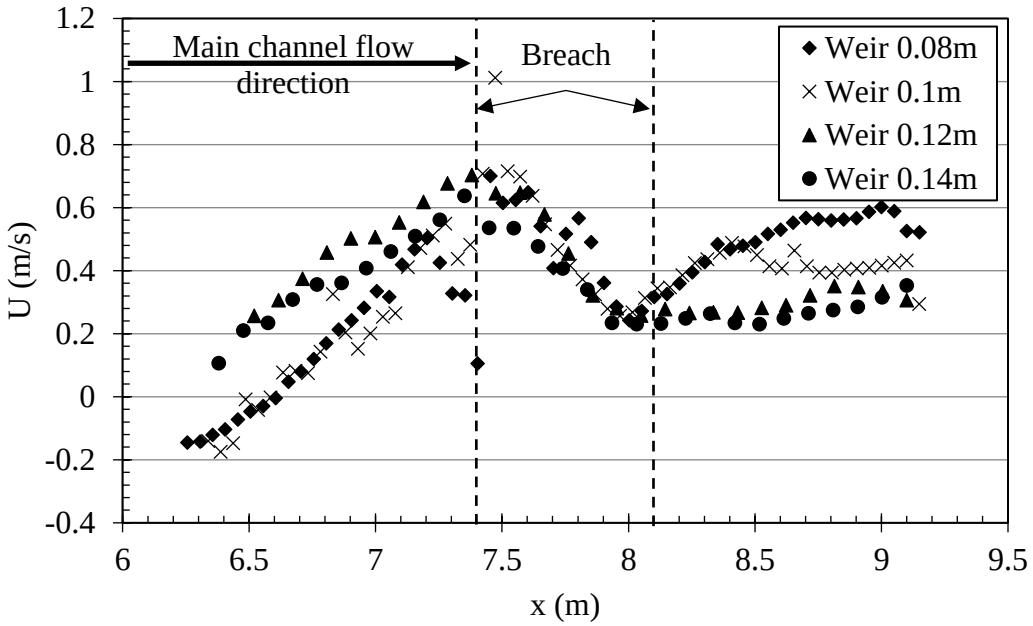

(f)

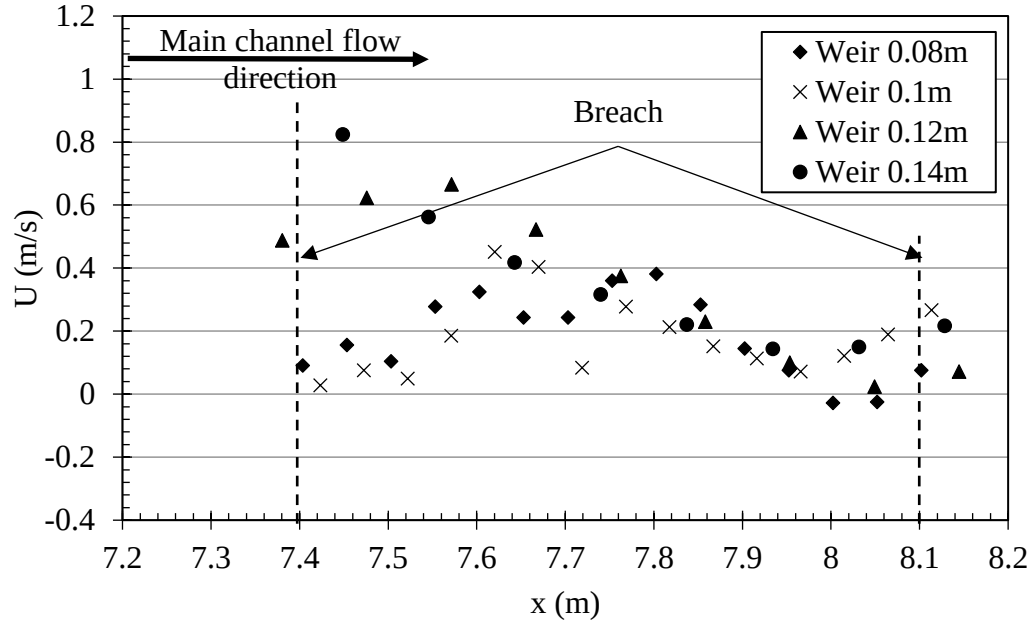

Figure 3.6 cont'd

(g)

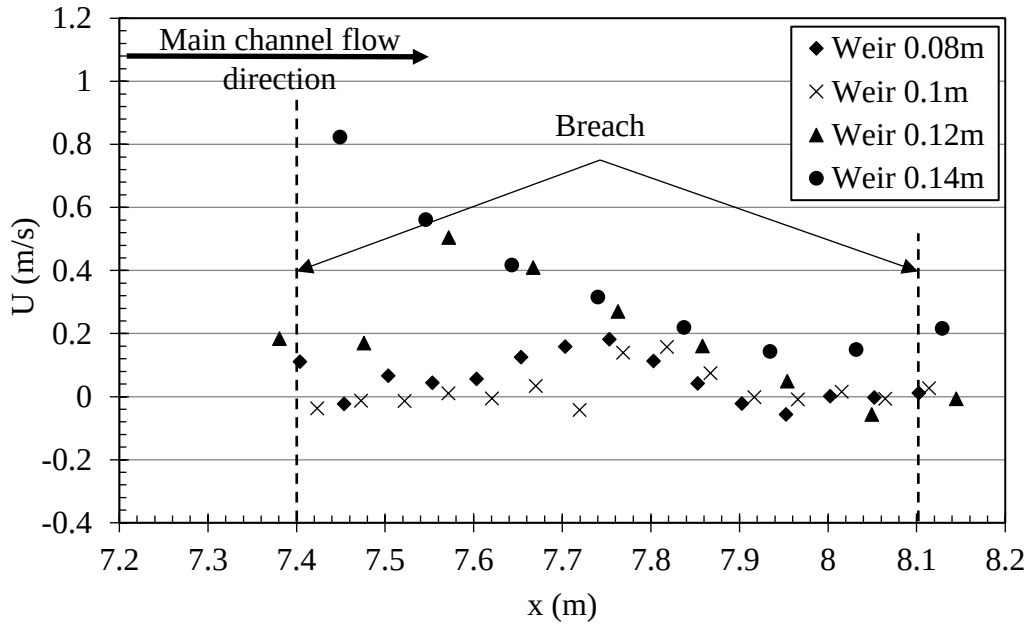

(h)

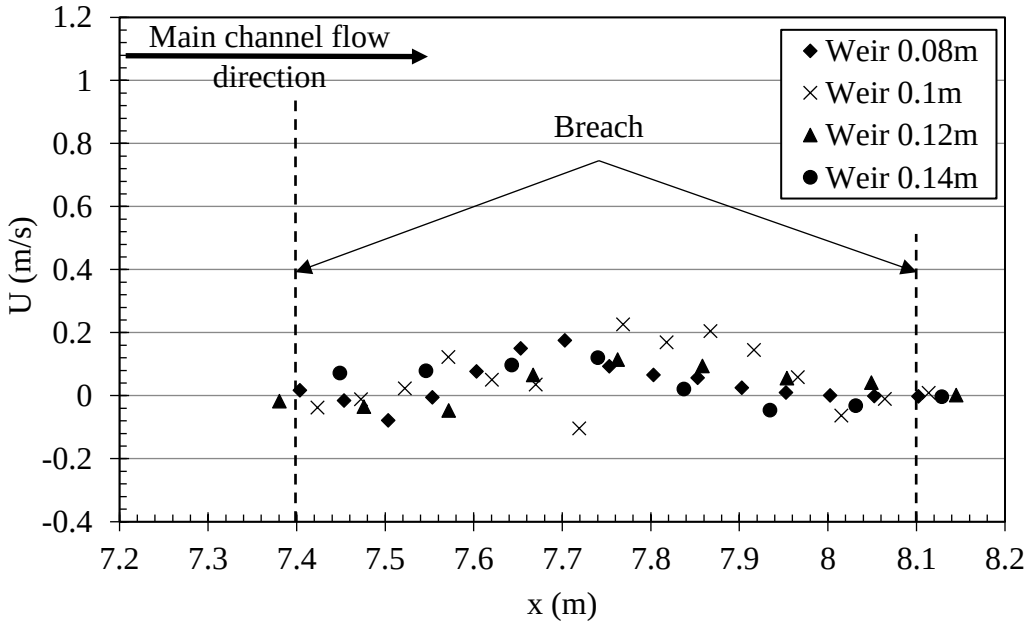

Figure 3.6 cont'd

(i)

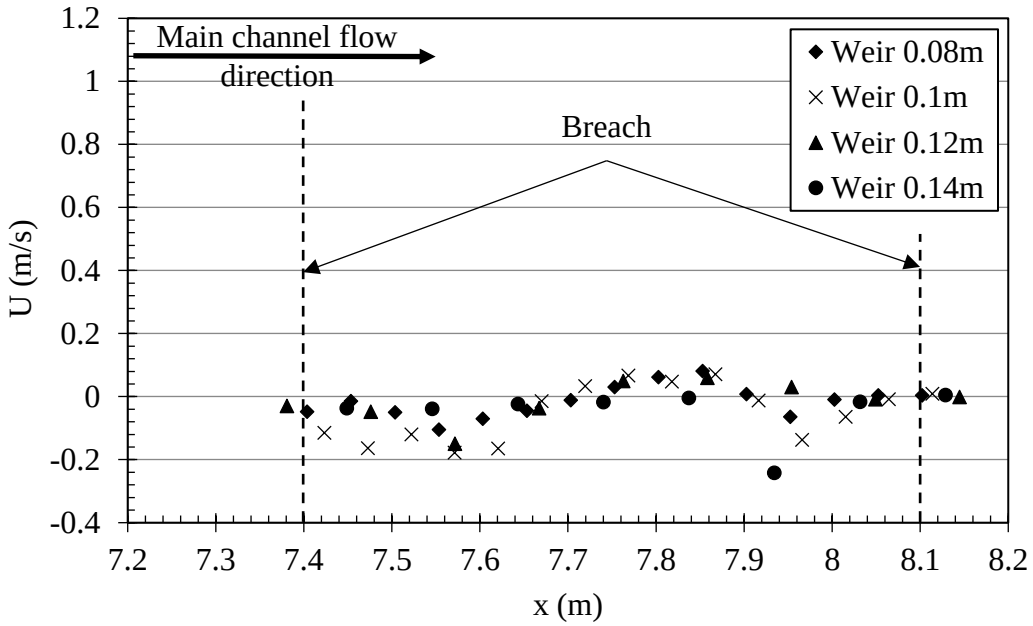

(j)

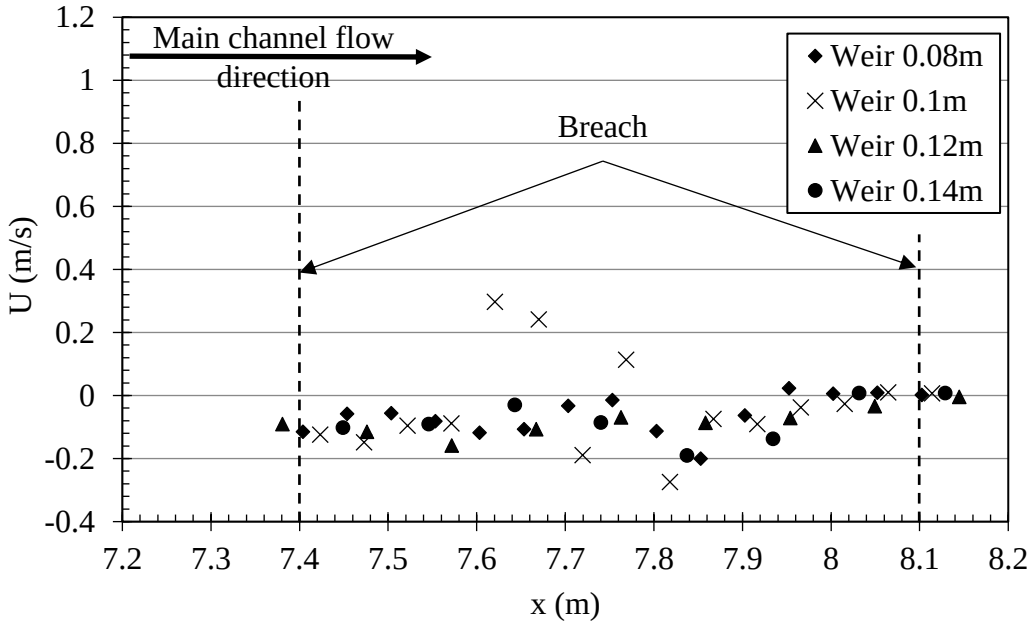

Figure 3.6 cont'd

(a)

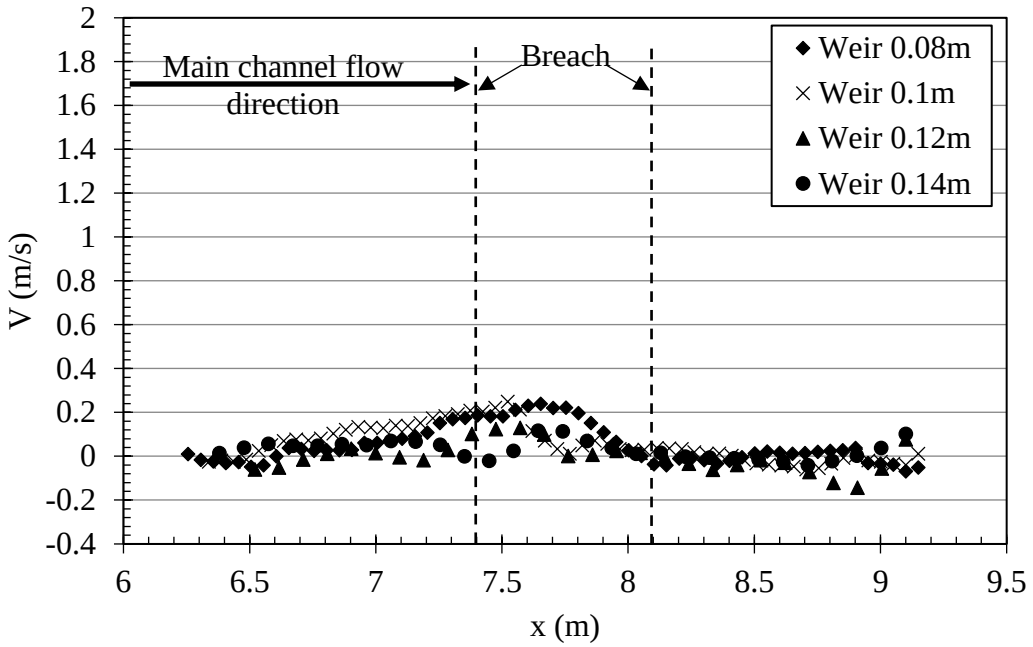

(b)

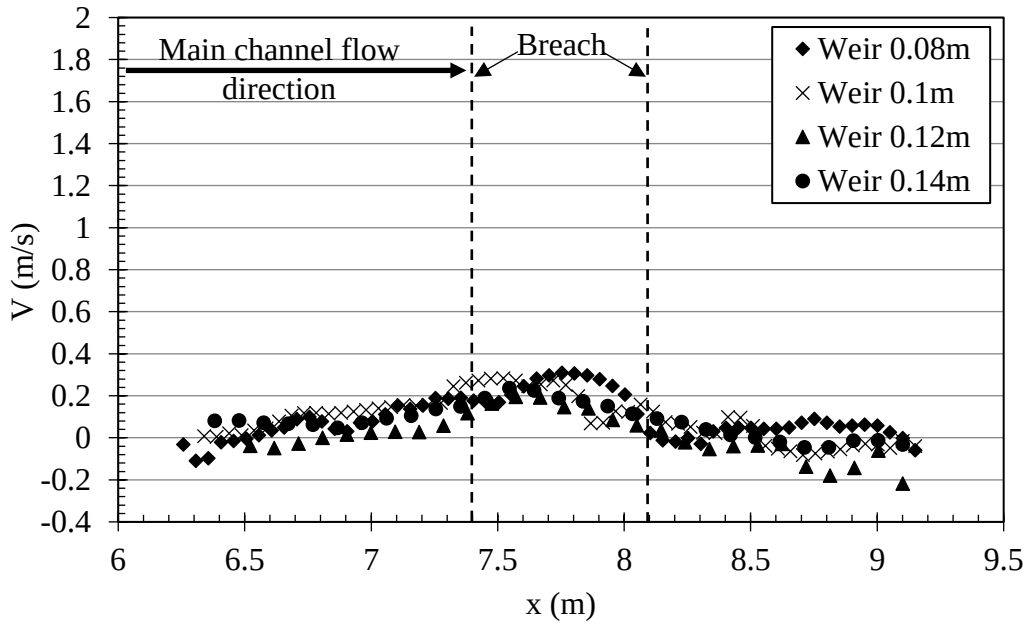

Figure 3.7 Transverse velocity for breach width 0.7 m for different D.S. weir heights at: (a) Y1; (b) Y2; (c) Y3; (d) Y4; (e) Y5; (f) Y6; (g) Y7; (h) Y8; (i) Y9; (j) Y10

(c)

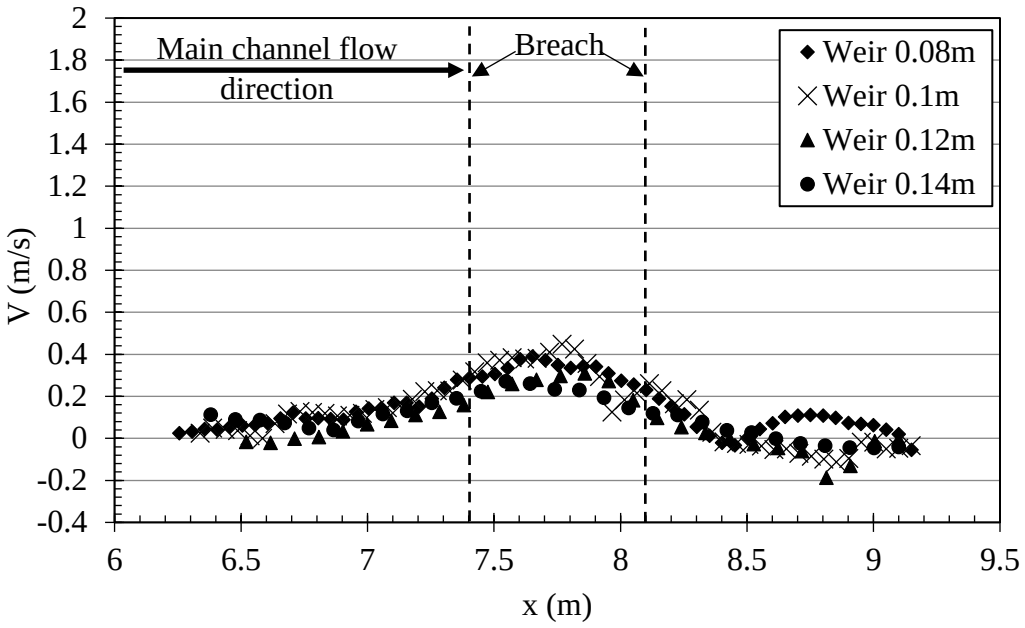

(d)

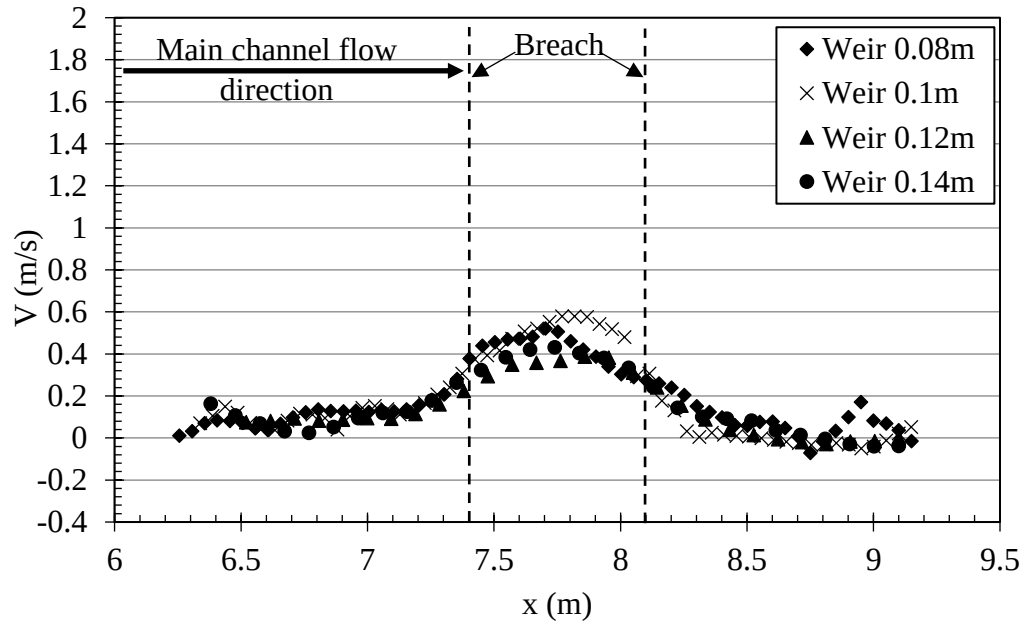

Figure 3.7 cont'd

(e)

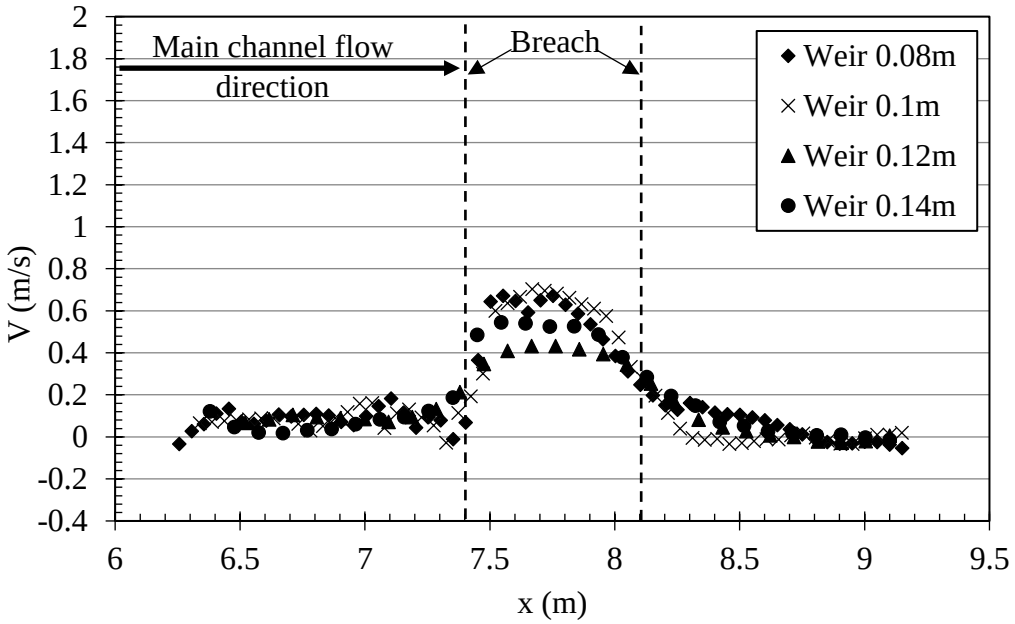

(f)

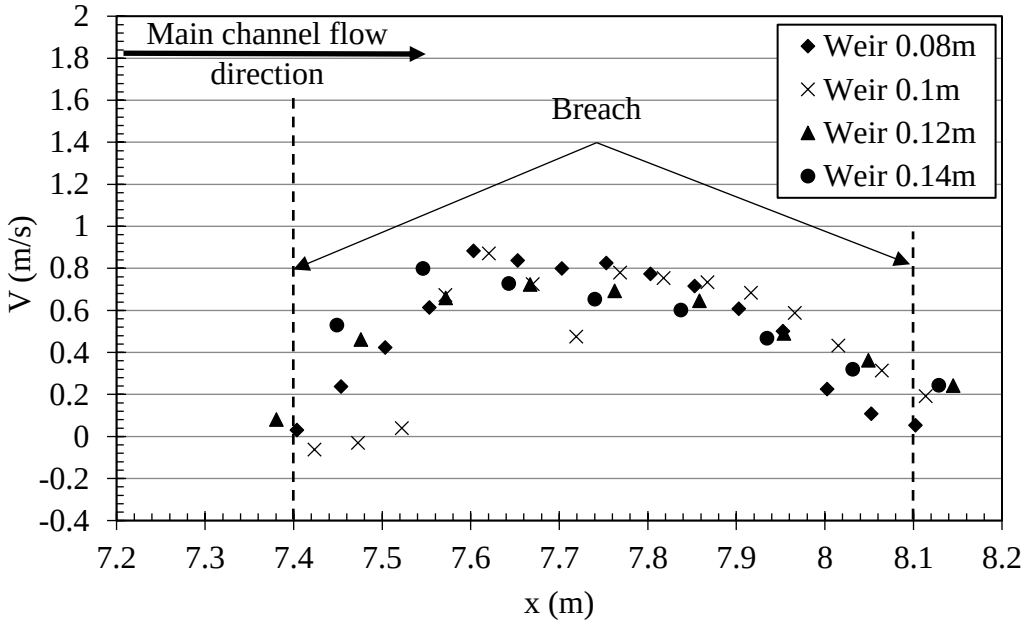

Figure 3.7 cont'd

(g)

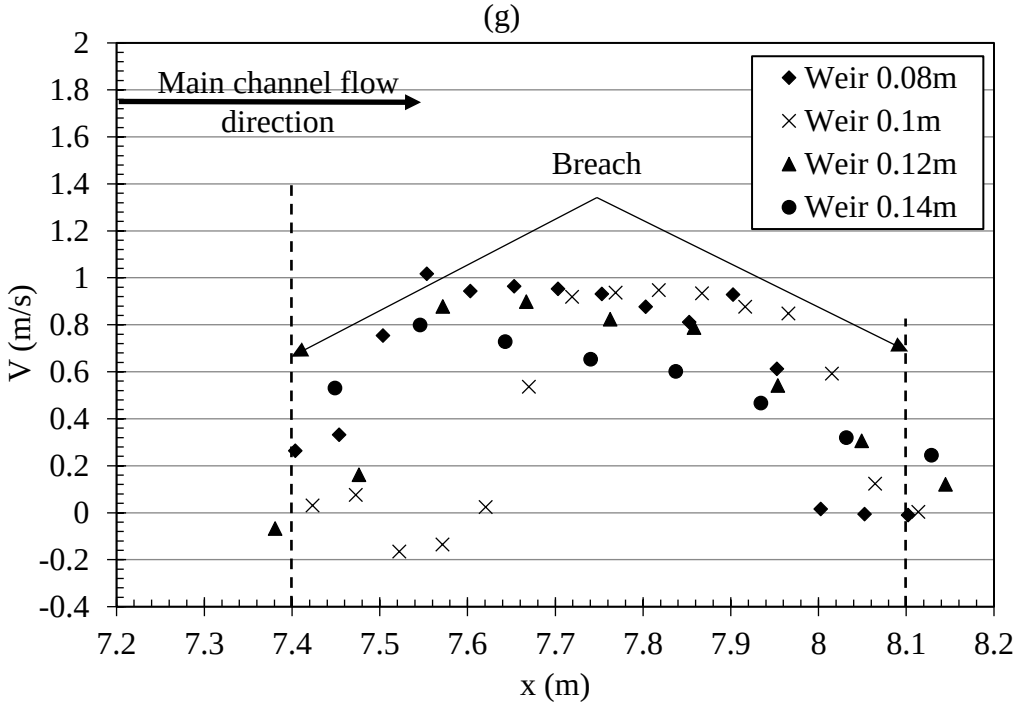

(h)

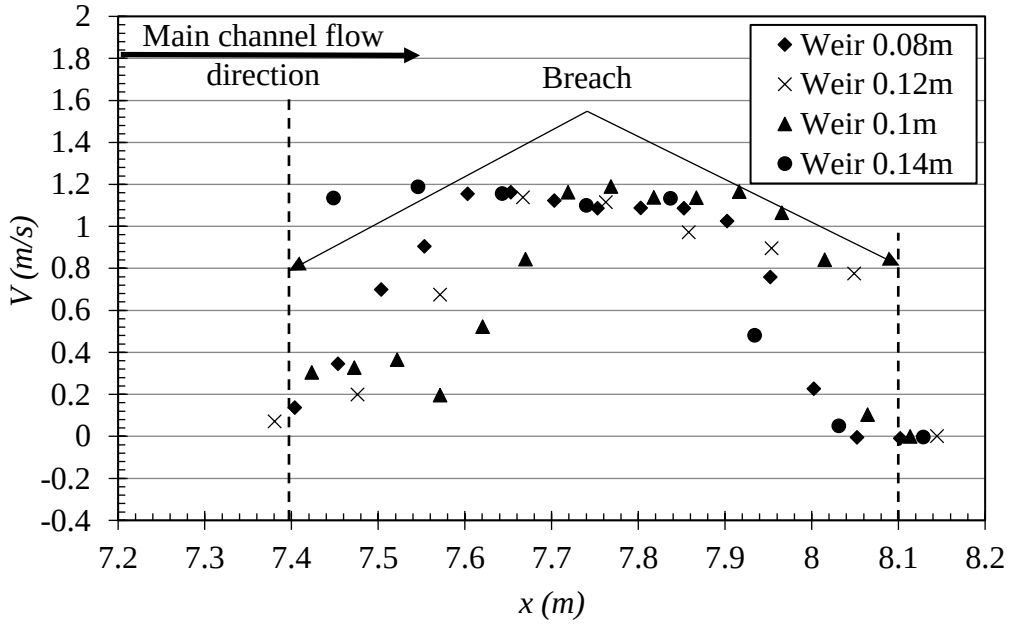

Figure 3.7 cont'd

(i)

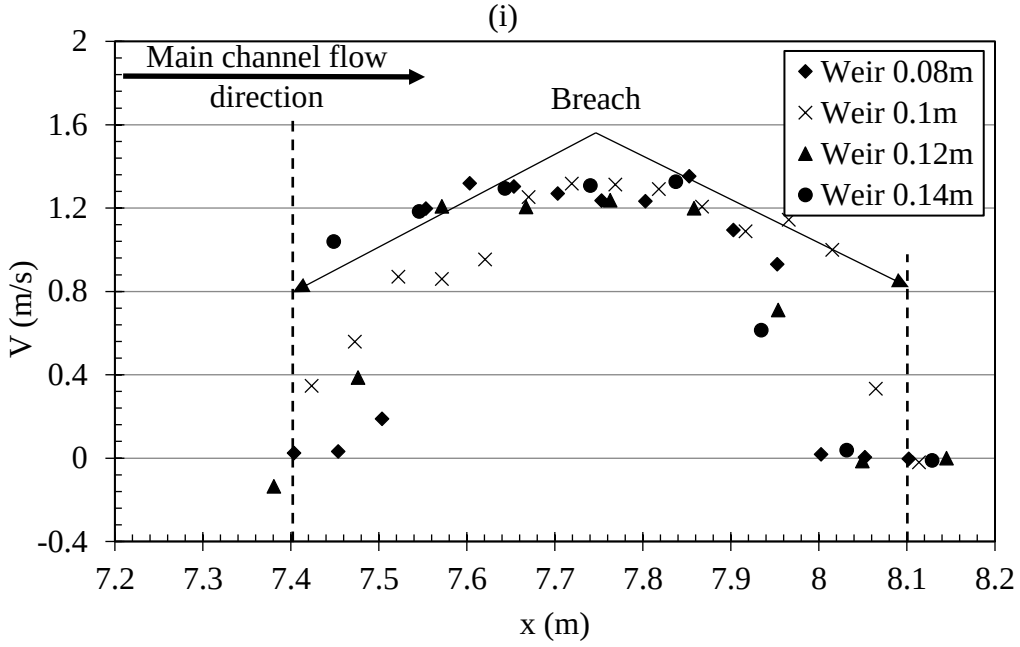

(j)

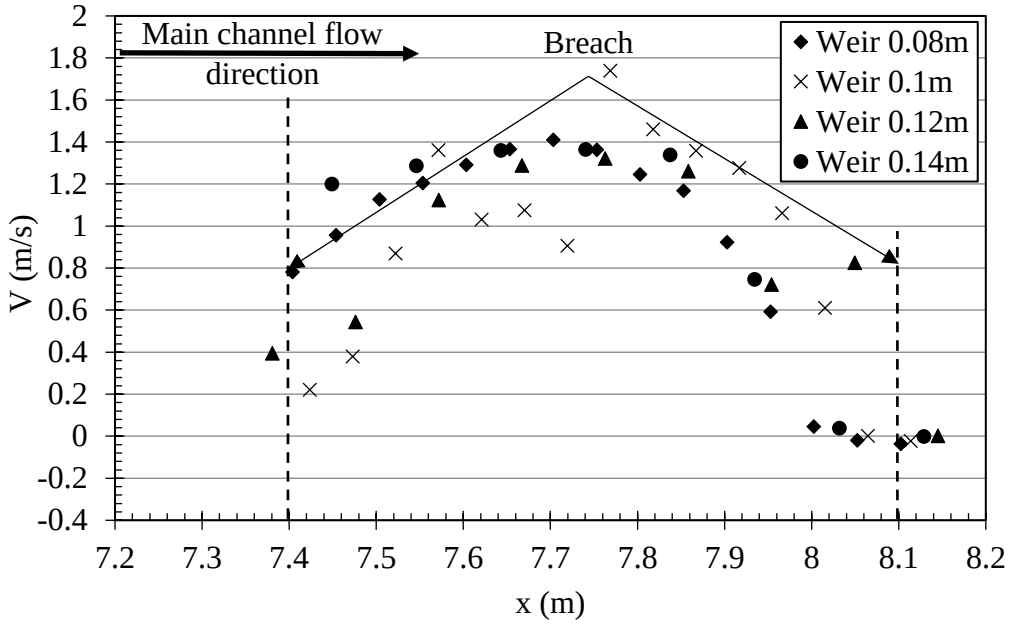

Figure 3.7 cont'd

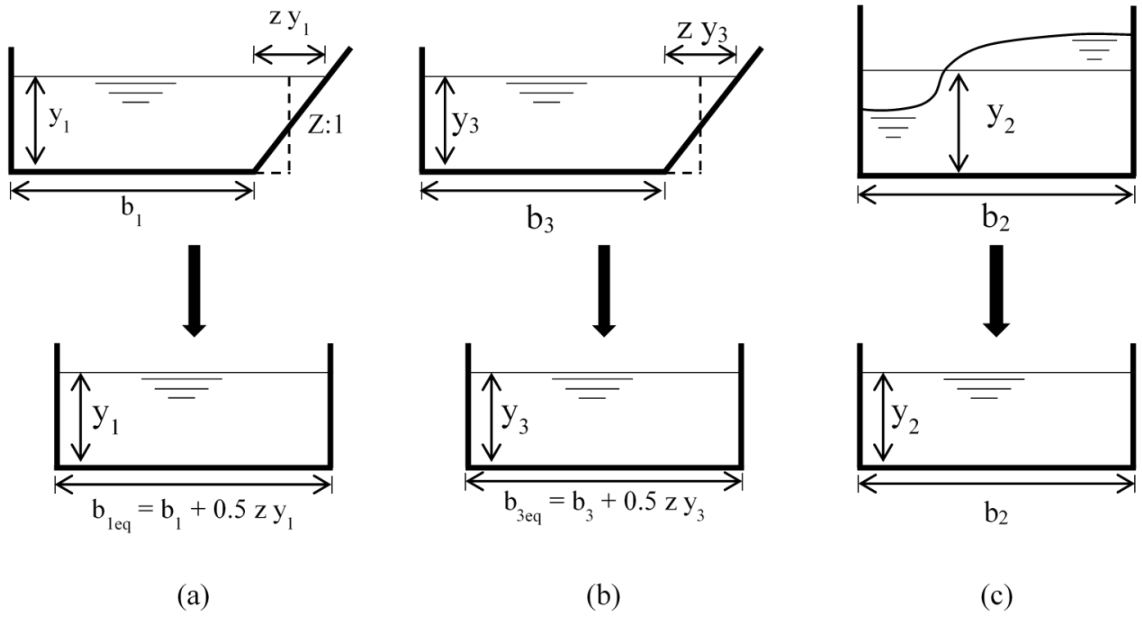

Figure 3.8 Conversion of the cross sectional area for the channel width and water surface profile

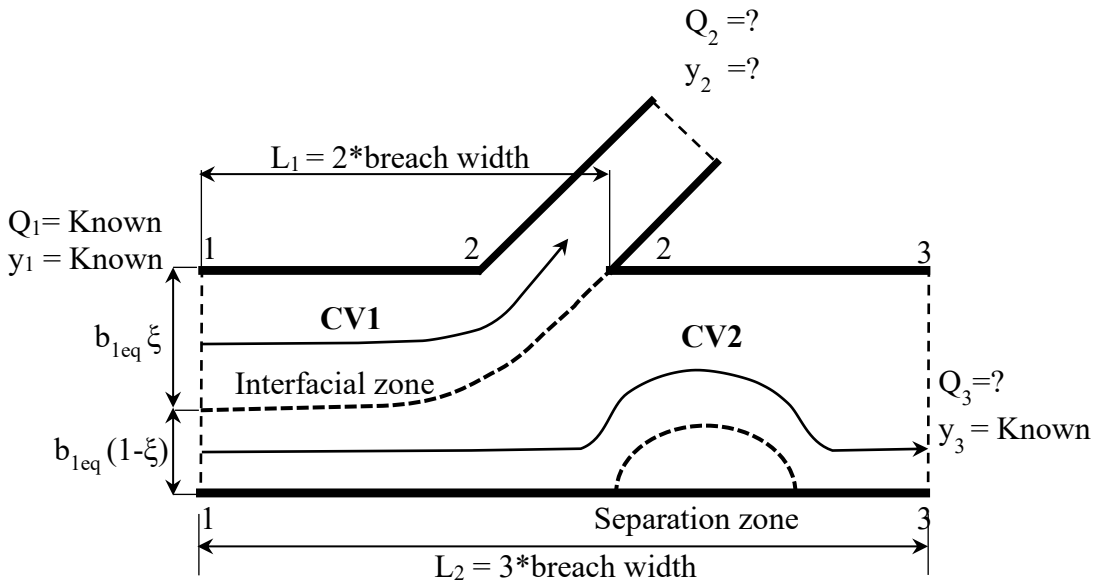

Figure 3.9 Open channel and breach with two control volumes and notation

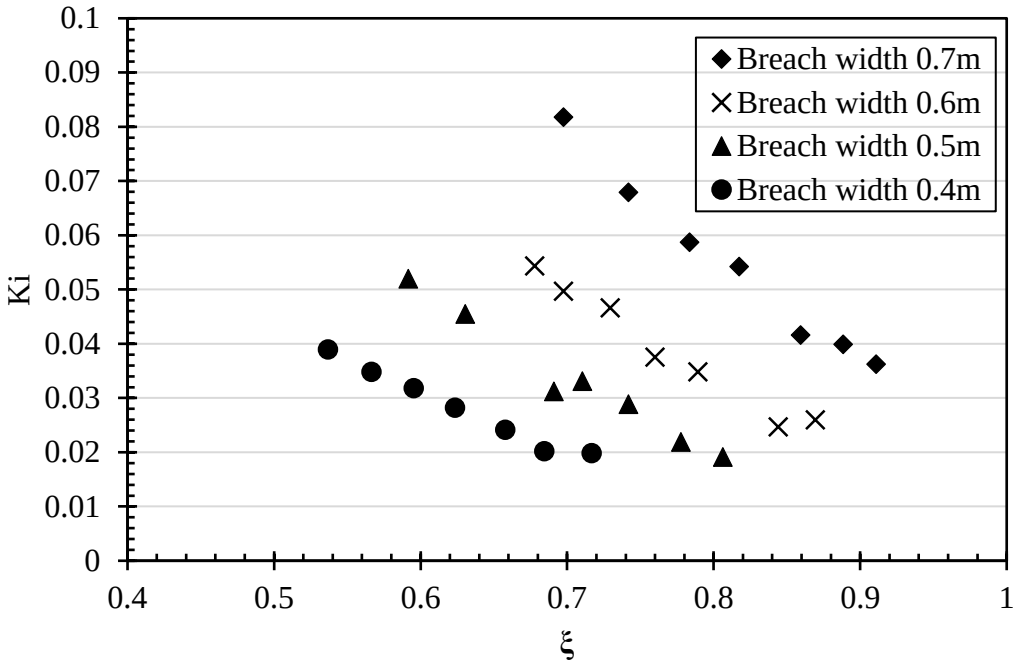

Figure 3.10 the interfacial shear coefficient K_i, versus $\xi=Q_2/Q_1$

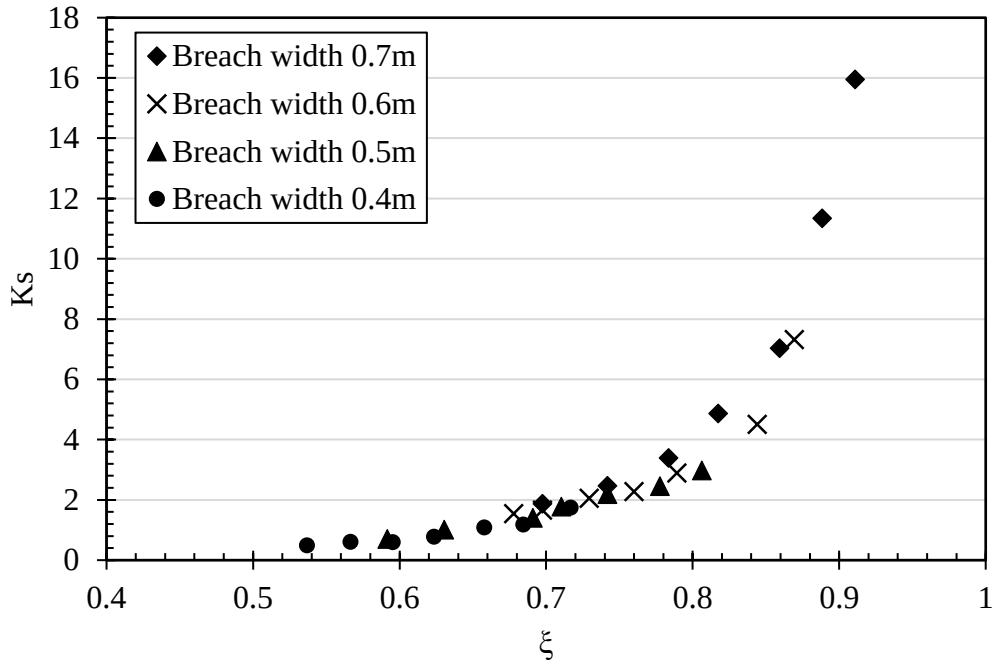

Figure 3.11 the separation zone shear coefficient, K_s, versus $\xi=Q_2/Q_1$

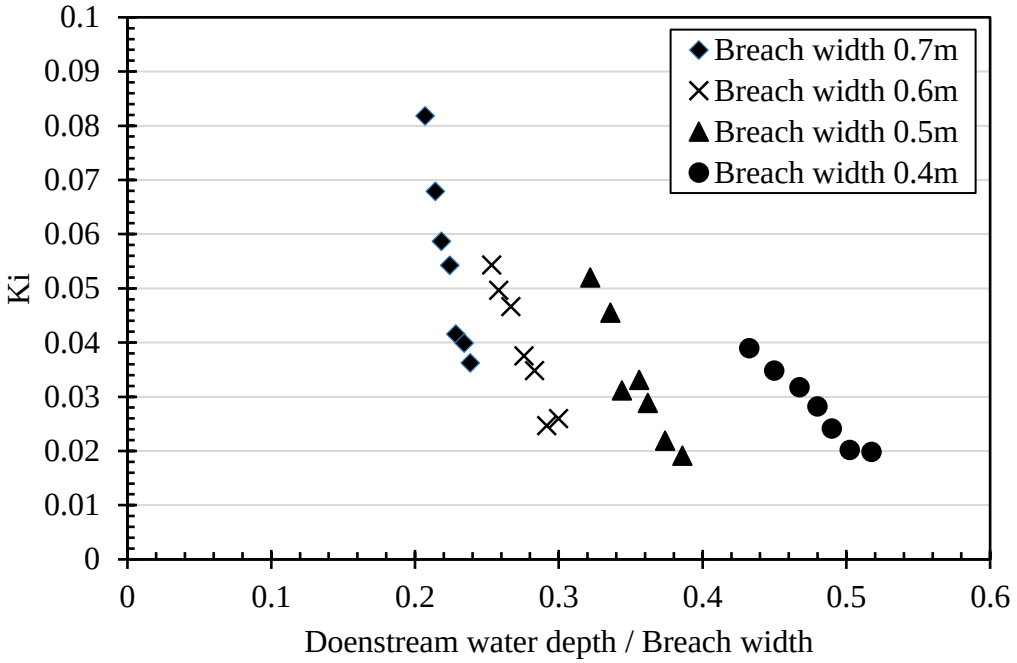

Figure 3.12 K_i versus downstream water depth/Breach Width

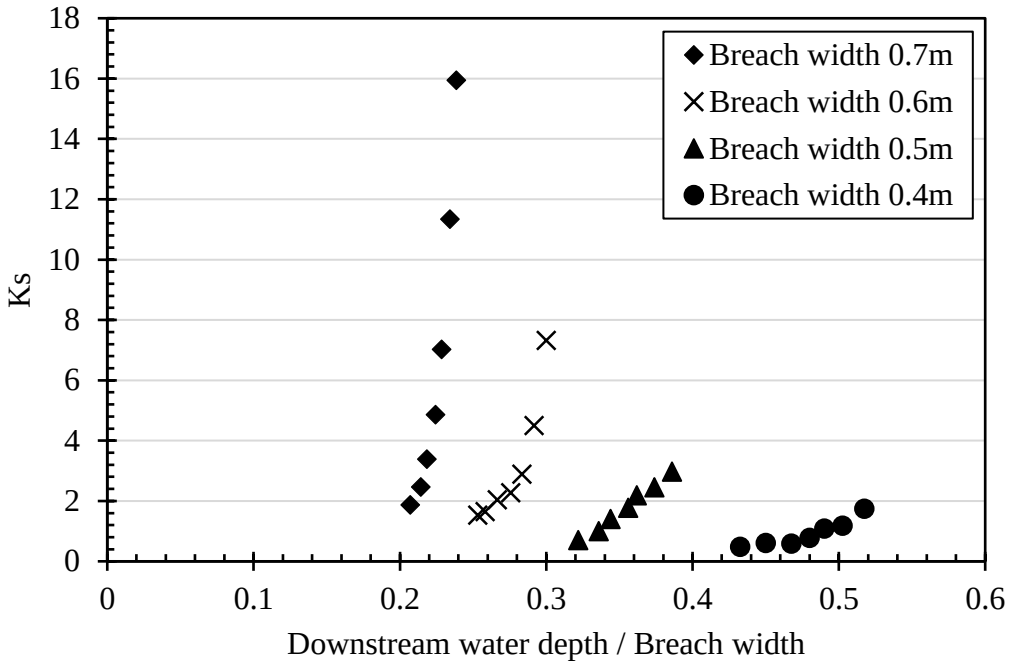

Figure 3.13 K_s versus downstream water depth/Breach Width

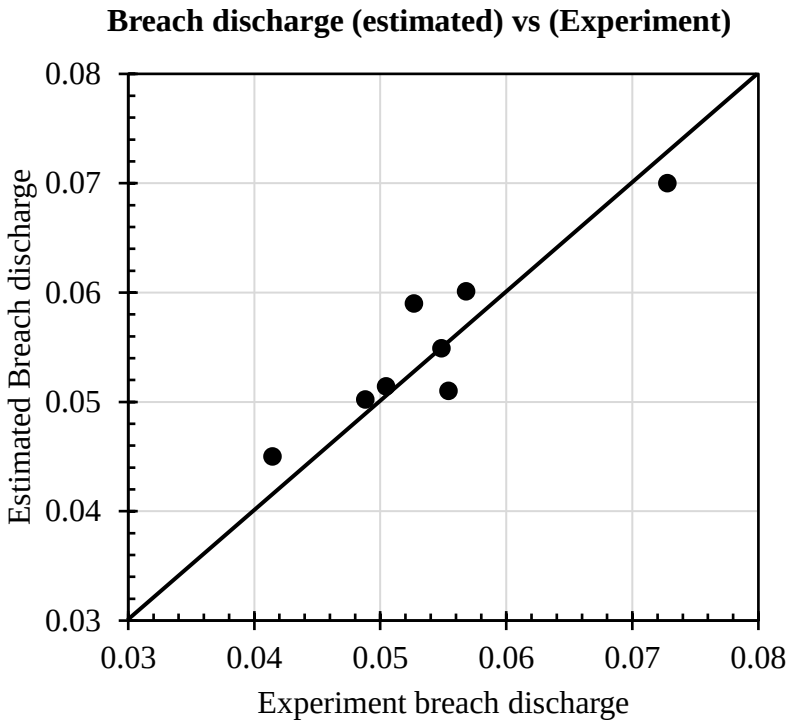

Figure 3.14 Comparison between Predicted and measured breach discharge

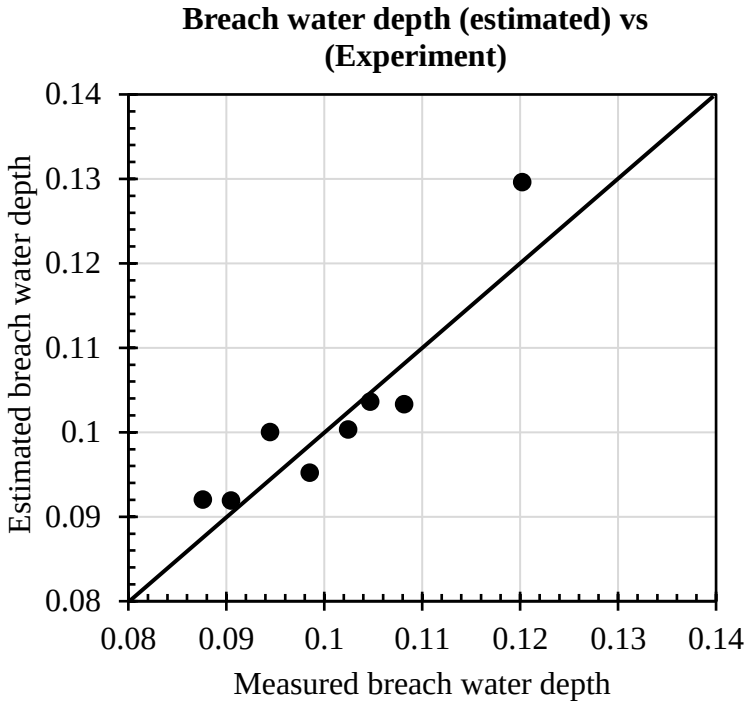

Figure 3.15 Y_2 Comparison between predicted and measured breach water depth

CHAPTER 4
EXPERIMENTAL INVESTIGATION OF FLOOD MANAGEMENT BY AN ENGINEERED LEVEE BREACH

4.1. Overview

Flooding has become more widespread recently around the world as a result of climate change. The increase in flood damage has also grown substantially due to rapid urbanization and floodplain development for commercial and residential purposes. The inland flooding continues to be one of the major natural hazards. Various approaches have been used to manage floods by building dams and reservoirs, constructing levees and floodwalls, and moving small cities away from flood prone areas. Although less common, floodways have been used to divert part of the flow to less populated areas during large floods, thereby alleviating pressure on levees and floodwalls built for protecting populated areas. A similar concept is utilized in the UK by setting aside areas known as washlands where water can move and wash into it during the flood period (Bitesize, n.d.). Floodways may include elaborate hydraulic structures operated year-round such as the Yolo bypass in Sacramento Valley or operated during flood emergencies such as Bonnet Carré Spillway in Louisiana. The Yolo Bypass is used for agricultural purposes most of the year, but during the flood season, it is used for storage and conveyance (CDWR 1984). Engineered breach by detonating a fuse plug at a strategic location along the levee only during extreme floods is another approach of flood management. A well-known example of engineered levee breach along the Mississippi River is the New Madrid Floodway at Birds Point, controlled

by the US Army Corps of Engineers, where a fuse plug design is utilized to detonate a portion of the levee and divert floodwater from the Mississippi River. Fuse plugs are also commonly used to protect dams and other important hydraulic structures. Notwithstanding this, systematic data on flood management by flow diversion to floodways are scarce.

In this study, laboratory experiments were conducted to investigate the effects of an engineered levee breach on the attenuation of the flood stage at upstream and downstream locations of a breach. Two main scenarios were considered during this work. In the first one, the breach was closed completely before the flood wave arrived at the upstream target location and the tailwater depth in the floodplain basin was zero. As the flood wave approached the target location a gate installed on the channel sidewall was lifted instantaneously. This emulated an active flood management strategy. In the second scenario, the breach was kept open and initial tail water depth was present in the floodplain basin, thus emulating a passive flood management strategy. The inflow flood wave was generated by a computer-controlled valve allowing for various peak discharges and flood durations in the channel. Two different sets of hydrographs were used in the experiments. In one, the same volume of water with different duration was released and in the second, different volumes of water with the same duration were released. The tail water effect due to the floodplain storage was assessed by adjusting the basin storage volume and the tailwater depth. The flood stage at target locations was recorded using ultrasonic probes. Comprehensive data were obtained and analysed from the measurement to find the effect of breach width, floodplain area and tailwater depth in the floodplain basin on the reduction of water depth at target locations.

4.2. Results and Discussion

A large amount of data was generated from 80 different experimental runs. The experimental conditions are summarized in Table 4.1. The primary data in these experiments are water level recorded by eight Baumer ultrasonic probes. The primary focus of the analyses is on flow depth at location 3 (upstream of the breach) and location 6 (downstream of the breach).

4.2.1. The response of different inflow hydrographs to an engineered levee breach

The response of flood wave with different duration but same volume to changes in breach width and floodplain storage volume is investigated by comparing results from experimental runs conducted with three breach widths of 0.2 m, 0.4 m, and 0.8 m, three different storage areas 6 m^2, 9 m^2, and the open area.

Figure 4.1 shows the water depth at target locations 3 and 6 for the case of active management i.e. without tail water in the flood basin for a breach width of 0.2 m and storage area of 9 m^2 from the release of hydrographs 1-3 (Run 6, 8 and 10). Figure 4.2 shows the corresponding cases of passive flood management with initial tail water depth in the floodplain (Run 7, 9, and 11).

Comparison of Figure 2.11 and Figure 4.1 shows a reduction of flood stage at both upstream and downstream of the breach, with greater reduction occurring at the upstream location. The upstream location also shows the appearance of secondary wave peaks. Comparison of Figure 4.1 and Figure 4.2 shows that the flood stage reduction is less at both upstream and downstream locations in the case of the passive management i.e. a priori

connection between the channel and the flood basin. The secondary waves are less prominent at the downstream location for both cases.

Figure 4.3 and Figure 4.4 respectively shows the combined effects of floodplain area and breach width on the reduction of peak water depth at target location 3 and 6 for the active management scenario, i.e., no a priori connection between the channel and the floodplain. Figure 4.5 and Figure 4.6 show the same relationship for the passive management scenario, i.e., initial water depth in the floodplain. These figures show a) a power law relation between water depth and breach width, b) The effect of increasing breach width on peak flood stage diminishes as breach width increases, c) active flood management is more effective in reducing peak flood stage.

The percent decrease of water depth at target locations are computed for input hydrographs 1-3 for the cases presented in Figure 4.3 to Figure 4.6. Figure 4.7 and Figure 4.8 show the percent water depth reduction for the active management cases and Figure 4.9 and Figure 4.10 show the same results for the passive management case. For the active flood management scenario when the flood basin was small (6 m^2), a systematic increase in peak depth attenuation at the upstream target location occurred with a decrease of flood duration (Figure 4.7 (a)). As the flood basin area increased to 9 m^2, the stage reduction for input hydrograph 1 and 2 were similar, and the same was less for hydrograph 3 (Figure 4.7 (b)). An open flood basin was similarly effective in flood stage reduction at the upstream target location for all three input hydrographs as shown in Figure 4.7 (c). Figure 4.8 shows the percentage of nondimensional water depth reduction at the downstream target location for the active flood management scenario. A flood basin area of 6 and 9 m^2 is similarly effective for hydrograph 1 and 2, but less effective for hydrograph 3. An open flood basin

was more effective for the peak stage reduction in the case of the long duration flood as seen in Figure 4.8 (c).

In the passive flood management scenario, the percent flood stage reduction at the upstream target location is more for a shorter duration flood in both cases of 6 m^2 and 9 m^2 basin area as seen in Figure 4.9. However, at the downstream target location flood reduction is similar for input hydrographs 1 and 2, and less for hydrograph 3 as seen in Figure 4.10.

4.2.2. The effect of breach width

The effect of breach width on flood stage reduction for a given input hydrograph is analysed by comparing the stage hydrograph at location 3 and 6 for the cases with the same floodplain area, but different breach width. Figure 4.11 shows a comparison of water depth at location 3 for the active flood management scenario considered with a breach width of 0, 0.2, 0.4, and 0.4 m (Test 1, 6, 31, 56) run with input hydrograph 1 and floodplain area of 9 m^2. The stage hydrographs show significant depth reduction at the upstream target location. The percent reduction ranged between 8.7% and 50%. The increase of breach width from 0.4 m or channel width to 0.8 m or twice the channel width had no significant effect. In all the runs, multiple secondary peaks appeared on the reduced flood stage hydrograph. The water depth was not significantly reduced at the downstream target location, and the water depth hydrographs for different breach width are quite similar in terms of duration and magnitude. Figure 4.12 shows the upstream and downstream stage hydrograph for the corresponding cases under the passive flood management scenario in which the flood basin had an initial water depth the same as the channel depth. The flood

depth reduction in this scenario is less - between 2.6% and 28%. Changes in breach width had minimal effect in flood reduction at both upstream and downstream locations.

4.2.3. The effect of the floodplain area

The effect of the floodplain basin area on water depth at upstream and downstream target locations is analysed by comparing stage hydrographs at these locations from four tests with the same inflow condition (hydrograph 1), same breach width of 0.4 m and four different floodplain areas (Test run 1, 31, 41, 51). Figure 4.13 shows a significant reduction of water depth at target location 3 and modest reduction at location 6. In the case of the open flood plain storage basin with an infinite area, the main channel water level dropped below the original steady state water level during the receding stage of the flood. The flood wave was significantly modified in shape upstream of the breach. Figure 4.14 and Figure 4.15 show the combined effect of storage area and breach width on the average flood stage at target locations 3 and 6 respectively.

4.2.4. The volume of flood water at floodplain basin

The floodwater discharge can be obtained from the manometer reading and the outflow discharge at the downstream of the channel can be obtained from the nearby Baumer reading (location 4). The flow volume can be obtained by integrating the area under these hydrographs, and the flow diverted to the flood basin would be the balance of the two. An analysis of volume removed from the channel using the levee breach is done for three runs involving Hydrographs 1 to 3. These runs involve active flood management with an open floodplain i.e. infinite storage volume. Table 4.5 summarizes the result. The percent removal of floodwater varies between 38% and 78%. The smallest value is for Run

26 with hydrograph 1 and a breach width of 0.2. The largest value is for Run 78 with hydrograph 3 and a breach width of 0.8 m. Figure 4.16, Figure 4.17, and Figure 4.18 show the inflow and outflow hydrographs for these runs grouped according to the inflow hydrograph. Figure 4.19 and Figure 4.20 respectively show the volume of water at the downstream end of the channel and the percentage volume into the flood basin. The figures show that a flood basin with a wider breach most effectively removes floodwater from a long duration low peak flooding event.

4.3. Dimensional Analysis

The water depth at a target point located upstream and downstream of the breach, Y_t, is considered to be a function of the flood hydrograph, breach width, floodplain basin size, and flow characteristics. The Buckingham Pi-theorem can be used to propose a non-dimensional relationship between the water depth at the target point and the independent variables in this study. The functional relationship between the dependent and the independent variables can be expressed as:

$$Y_t = f\ (Q_p, T_p, T_b, A_b\ , W_b, W_c, \rho, g\ , X_t) \tag{4.2}$$

where, Y_t= Water depth at target point, dependent variable (L), A_b= Area of the basin (L^2), W_b= Width of the breach (L), W_c = Width of the channel (L), ρ = Density of water (M L^{-3}), T_b = Base time (total time of flood) (T), T_p =Time to peak (T), g = Gravity (L T^{-2}), X_t = Distance to target location (L), Q_p = Peak discharge (L^3T^{-1}). The non-dimensional form of the above equation is:

$$\frac{Y_t}{W_b} = f\left(\frac{W_c}{W_b}, \frac{X_t}{W_b}, \frac{t_p\, Q_p}{W_b^3}, \frac{t_b\, Q_p}{W_b^3}, \frac{A}{W_b^2}, \frac{Q_p^2}{W_b^5\, \mathrm{g}}\right) \tag{4.3}$$

Three target points are considered to develop a generalized non-dimensional relation. These are at Baumer locations 3, 6 and 5. Table 4.2, shows the average flood depth at three target locations (L3, L6, and L5) along with the peak water depth at the same locations. The reduction in flood stage, ΔY_t, is obtained by subtracting the average flood depth from the reference depth at the relevant target location. The reference depth is measured at the same locations by running experiments with hydrograph 1, 2, 3, 4, and 5 in the channel without a breach. Since ΔY_t and Y_t have the same dimension, equation (4.3) can be recast as:

$$\frac{\Delta Y_t}{W_b} = f\left(\frac{W_c}{W_b}, \frac{X_t}{W_b}, \frac{A}{W_b^2}, \frac{t_p\, Q_p}{W_b^3}, \frac{t_b\, Q_p}{W_b^3}, \frac{Q_p^2}{W_b^5\, \mathrm{g}}\right) \tag{4.4}$$

The experimental data are divided into two sets. The first set involves experiments in which the breach was closed at the beginning of the experiment and it was opened as soon as the flood wave approached location 3. In this case, the floodplain was initially completely empty and there was no initial tail water depth. This set of data represents an active flood management approach. The data, in this case, are analysed as three different groups. The first group, G I, consists of all the data of the active flood management tests. However, the nondimensional area is excluded from the equation since some of the tests involved an infinite floodplain storage area represented by an open floodplain. The second group, GII includes data from experiments with a flood basin area of 6 m^2 and 9 m^2. The

third group, G III includes data from experiments that had an open flood basin i.e. infinite storage area. The second set of data corresponds to tests conducted to emulate a passive flood management approach. The floodplain was connected to the channel during the initial steady state condition and had the same water depth of 0.13 m as in the main channel. Experiments were run with a flood basin storage area of 6 and 9 m^2. The flood basin walls were closed. This data set constitutes the fourth Group, G IV. Multi-variate analysis is done separately for the four groups of data and regression equations are developed in the following section.

4.4. Multivariate Regression Analysis

4.4.1. Active flood management with initially empty flood basin

The data pertaining to experimental runs with the initially closed breach are used in multiple regression analysis for developing a relationship between the nondimensional variables in Equation (4.4). The analysis is done by organizing the data into three groups as follows.

1- G I. Data from all the experiments in which the breach was initiated as the flood wave approached target location 3 are used for the regression analysis. A relationship between the dependent variable ($\Delta Y_t/W_b$), and the independent variables (W_c/W_b, X_t/W_b, T_pQ_p/W_b^3, T_bQ_p/W_b^3, *and* Q_p^2/gW_b^5), is obtained. The analysis gives R^2 of 0.68. In this case, 68.1% of the variation in the independent variable is explained by dependent variables and 31.9% is unexplained. The standard error is 0.0483, which is a measure of how far the actual points are from the regression line. From Anova analysis, the sum of squared regression (SSR) is

found to be 0.78. The Residual of error, SSE is 0.364 which is the measure of unexplained variation. The significant F is 4.92E-37 which is less than 0.05. Therefore, the overall regression model is significant. Column two of Table 4.3 shows the significance of each independent variable. Comparing with the value of alpha, 0.05, all the independent variables are accepted as a significant predictor of the dependent variables ($\Delta Y_t/W_b$) except for (T_bQ_p/W_b^3).

The proposed predictive relation after dropping the insignificant term is:

$$\frac{\Delta Yt}{W_b} = 0.0334 + 0.157\ \frac{W_c}{W_b} - 0.005\ \frac{X_t}{Wb} - 0.00175\ \frac{T_p\ Q_p}{W_b^3} + 0.082\ \frac{Q_p^2}{g\ W_b^5} \qquad (4.5)$$

A comparison between prediction made by Eq. (4.5) and the measurement is shown in Figure 4.21 along with the line of perfect agreement and 25% bounds.

2- G II. Multivariate regression analysis is performed using a subgroup of the data set G-I in which the floodplain area was finite (9, 6) m^2. In this analysis, the dependent variable ($\Delta Y_t/W_b$) is considered to be a function of the independent variables (A/W_b^2, W_c/W_b, X_t/W_b, T_pQ_p/W_b^3, T_bQ_p/W_b^3, and Q_p^2/gW_b^5). Note the inclusion of the variable A/W_b^2. The predictive relation obtained from this analysis has an R^2 equal to 0.76 which is higher than the value when all the data were used in the previous step. The standard error, in this case, is 0.0401. Moreover, Anova analysis gives SSR, Sum of squared regression equal to 0.516 and SSE, the Residual of error equal to 0.162. The significant F is 3.551E-29 which is far less than 0.05. Therefore, the overall regression model is significant. Table 4.3, column four shows the significance of each variable individually. Comparing with the value

of alpha, 0.05, all the independent variables are considered as a significant predictor of the dependent variables ($\Delta Y_t/W_b$) except (T_bQ_p/W_b^3).

The regression equation after dropping the insignificant term is:

$$\frac{\Delta Yt}{W_b} = 0.0378 + 0.00066246\ \frac{A}{W_b^2} + \ 0.1165\ \frac{W_c}{W_b} - 0.0045\ \frac{X_{tc}}{Wb} - 0.001936\ \frac{T_p\ Q_p}{W_b^3} + 0.1\ \frac{Q_p^2}{g\ W_b^5} \tag{4.6}$$

A comparison between data and prediction along with the line of perfect agreement and the 25% bound is shown in Figure 4.22.

3- G III. Mutivariate analysis is done using a second subgroup of the data considered in G I. These experiments pertain to the condition in which the flood basin had an opening allowing for the floodwater to freely leave the basin, thus creating the condition of an infinite basin area. The dependent and independent variables are the same as those considered in G I analysis. The analysis gives a predictive relation with an R^2 value of 0.763 and a standard error of 0.0446. From Anova analysis the SSR, Sum of squared regression is, 0.307, and the Residual of error, SSE is 0.0955 the amount of unexplained variation. The significant F, in this case, is 6.343E-14 which gives an indication that the overall regression model is significant. Table 4.3, column six, shows the significance of each independent variable individually. Comparing with the value of alpha, 0.05, all the independent variables are considered as a significant predictor of the dependent variables ($\Delta Y_t/W_b$) except (T_bQ_p/W_b^3). After dropping the insignificant variable, the predictive relation assumes the following form:

$$\frac{\Delta Yt}{W_b} = 0.05695 + 0.1567\ \frac{W_c}{W_b} - 0.0059\ \frac{X_{tc}}{Wb} - 0.00309\ \frac{T_p\ Q_p}{W_b^3} - 0.000305\ \frac{T_b\ Q_p}{W_b^3} + 0.065\ \frac{Q_p^2}{g\ W_b^5} \quad (4.7)$$

Figure 4.23 shows a comparison between measurements and prediction along with the line of agreement and lines of 25% bound.

4.4.2. Passive flood management with initial tailwater depth in the flood basin.

1- G IV. Data in this group pertain to experiments with an open breach and the flood basin having an initial tailwater depth of 0.13 m. The storage basin area in these experiments was either 6 or 9 m^2. In conducting the multivariate analysis, the nondimensional variable ($\Delta Y_t/W_b$) is considered to be a function of dependent variables (A/W_b^2, W_c/W_b, X_t/W_b, T_pQ_p/W_b^3, T_bQ_p/W_b^3, and Q_p^2/gW_b^5). The resulting equation has an R^2 value equal to 0.7726, and standard error equal to 0.0288. From Anova analysis, the SSR Sum of squared regression is 0.285, which represents the amount of variation explained by the regression of independent variables on $\Delta Y_t/W_b$. The Residual of error, SSE is 0.084 and the significant F is 2.66E-30 which is less than 0.05. Therefore, the overall regression model is significant. The P-values for the independent variables are shown in Table 4.4. The results show that all the independent variables are significant with values less than alpha, 0.05.

The resulting regression equation is:

$$\frac{\Delta Yt}{W_b} = 0.02448 + 0.0003644\ \frac{A}{W_b^2} + \ 0.084\ \frac{W_c}{W_b} - 0.00295\ \frac{X_{tc}}{Wb} - 0.0014$$
$$\frac{T_p\ Q_p}{W_b^3} - 0.000194\ \frac{T_b\ Q_p}{W_b^3} + 0.097\ \frac{Q_p^2}{g\ W_b^5} \quad (4.8)$$

Figure 4.24 shows the predicted nondimensional dependent variables $\frac{\Delta Yt}{W_b}$ versus the measurement with lines of perfect agreement and 25% bound.

4.5. Summary

Engineered levee breach and flood diversion by side weir are commonly used to control and mitigate floods in rivers and channels. However, systematic studies of the effectiveness of these approaches are rare. The present study provides a laboratory study on in-channel flood stage reduction by an engineered levee breach. The study has led to the generation of an important data set that can be utilized for future model validation. Predictive relations for flood stage reduction as a function of flood hydrograph characteristics, breach width, flood storage areas, and tailwater depth have been developed.

This study has three main components: (1) measurements and analysis of water depth at several locations upstream and downstream of the breach, (2) dimensional analysis by using Buckingham PI-theorem to obtain a nondimensional group of dependent and independent variables, (3) a multiple regression analysis of the nondimensional variables to find predictive relationships for practical application.

In the first part, eighty unique experiments were conducted. Three different breach widths, three floodplain basin areas, and five different hydrographs were tested. A sharp

crested weir was installed at the downstream end of the channel to control the water depth in the channel. The experiments were divided into two main groups. At first, the breach was closed at the beginning of the experiment and the floodplain basin was dry. The breach was opened instantaneously as soon as the flood wave arrived at a specific location upstream of the breach. The experiments were repeated by keeping the breach open completely with the floodplain basin having an initial tail water depth equal to the initial water depth in the main channel, 0.13 m.

The results show that the water depth at two target locations was higher when the duration of the flood wave for the same volume of water was shorter. However, flood waves having shorter duration experienced a higher percentage of depth reduction. It has been also found that an increase in the breach width leads to a decrease in the water level in the main channel. The decrease was between 8.7-50 % in case of an active flood management scenario with zero tailwater depth in the flood basin and 2.6-28 % in case of a passive flood management scenario with the presence of tailwater in the basin. Furthermore, the floodplain area had a strong effect on water depth reduction at target locations. However, when the breach size was small, and the flood duration was short the flood basin area had a diminished effect. Another important observation was that flood reduction was higher at upstream target locations than at downstream target locations.

The volume of water that passed through the breach to the flood basin was calculated. The percentage volume of flood water that passes to the floodplain increased with an increase in the breach width. The volume of water passed to the floodplain basin also

dependent on the flood duration. More floodwater entered the basin for hydrographs with a longer duration.

In the second component the Buckingham Pi-theorem was used to obtain a non-dimensional relationship between the dependent variable; i.e., the decrease in water depth at target locations (ΔY_t) and the independent variables, i.e. (Q_p, T_p, T_b, A_b, W_b, W_c, ρ, g, X_t), peak discharge, time to peak, base time, floodplain basin area, width of the breach, width of the channel, water density, gravitational acceleration, and target location, respectively. The resulting non-dimensional variables are, dependent variable ($\Delta Y_t/W_b$) and independent variables (A/W_b^2, W_c/W_b, X_t/W_b, T_pQ_p/W_b^3, T_bQ_p/W_b^3, and Q_p^2/gW_b^5).

The third component involved multi-regression analysis to obtain mathematical equations relating to the dependent and independent nondimensional groups. In this analysis, the data was divided in to two main parts according to initial tailwater depth in the floodplain basin. The data were divided into four groups based on experimental conditions. For each group, a satisfactory agreement was found between measurements and prediction. It was shown from the analysis that all the independent variables are significant except ($T_b\ Q_p/W_b^3$).

Table 4.1 The plan of experiments

No. of Experiment	Breach width (m)	Floodplain Area (m^2)	Hydrograph No.	Breach Case
1	Closed	Zero	1	Close
2			2	Close
3			3	Close
4			4	Close
5			5	Close
6	0.2	9	1	Active flood management
7				Passive flood management
8			2	Active flood management
9				Passive flood management
10			3	Active flood management
11				Passive flood management
12			4	Active flood management
13				Passive flood management
14			5	Active flood management
15				Passive flood management
16		6	1	Active flood management
17				Passive flood management
18			2	Active flood management
19				Passive flood management
20			3	Active flood management
21				Passive flood management
22			4	Active flood management
23				Passive flood management
24			5	Active flood management
25				Passive flood management
26		Open Area	1	Active flood management
27			2	Active flood management
28			3	Active flood management
29			4	Active flood management
30			5	Active flood management
31	0.4	9	1	Active flood management
32				Passive flood management

33			2	Active flood management
34				Passive flood management
35			3	Active flood management
36				Passive flood management
37			4	Active flood management
38				Passive flood management
39			5	Active flood management
40				Passive flood management
41		6	1	Active flood management
42				Passive flood management
43			2	Active flood management
44				Passive flood management
45			3	Active flood management
46				Passive flood management
47			4	Active flood management
48				Passive flood management
49			5	Active flood management
50				Passive flood management
51		Open Area	1	Active flood management
52			2	Active flood management
53			3	Active flood management
54			4	Active flood management
55			5	Active flood management
56	0.8	9	1	Active flood management
57				Passive flood management
58			2	Active flood management
59				Passive flood management
60			3	Active flood management
61				Passive flood management
62			4	Active flood management
63				Passive flood management
64			5	Active flood management
65				Passive flood management
66		6	1	Active flood management
67				Passive flood management

68			2	Active flood management
69				Passive flood management
70			3	Active flood management
71				Passive flood management
72			4	Active flood management
73				Passive flood management
74			5	Active flood management
75				Passive flood management
76		Open area	1	Active flood management
77			2	Active flood management
78			3	Active flood management
79			4	Active flood management
80			5	Active flood management

Table 4.2 Data of experiments

Breach Width (m)	Constant	Area (m^2)	No. of experiments	Average water depth (*Yt*) (m)			Peak Water Depth		
0.2	Volume of water		1	0.298			0.302		
			2	0.278			0.282		
			3	0.23			0.234		
		9		L3	L6	L5	L3	L6	L5
			6	0.2245	0.242	0.249	0.249	0.258	0.264
			7	0.245	0.255	0.264	0.255	0.272	0.272
			8	0.210	0.225	0.23	0.221	0.234	0.235
			9	0.230	0.24	0.245	0.239	0.248	0.25
			10	0.188	0.201	0.203	0.21	0.21	0.22
			11	0.212	0.214	0.215	0.23	0.221	0.224
		6		L3	L6	L5	L3	L6	L5
			16	0.228	0.26	0.259	0.261	0.265	0.27
			17	0.250	0.263	0.27	0.27	0.275	0.274
			18	0.228	0.241	0.24	0.225	0.245	0.242
			19	0.231	0.245	0.251	0.254	0.26	0.26
			20	0.202	0.210	0.212	0.215	0.22	0.23
			21	0.220	0.224	0.224	0.235	0.23	0.24
	Time		1	0.298			0.302		
			4	0.271			0.274		
			5	0.23			0.232		
				L3	L6	L5	L3	L6	L5
		9	6	0.2245	0.249	0.253	0.249	0.258	0.264
			7	0.245	0.26	0.264	0.255	0.272	0.272
			12	0.205	0.223	0.23	0.2207	0.23	0.234
			13	0.225	0.238	0.242	0.2307	0.25	0.246
			14	0.174	0.183	0.19	0.1807	0.189	0.187
			15	0.1915	0.202	0.204	0.20	0.208	0.21

				L3	L6	L5	L3	L6	L5
		6	16	0.228	0.263	0.257	0.261	0.265	0.27
			17	0.25	0.267	0.27	0.27	0.275	0.274
			22	0.209	0.236	0.236	0.225	0.24	0.24
			23	0.23	0.241	0.246	0.238	0.252	0.25
			24	0.176	0.196	0.197	0.19	0.199	0.188
			25	0.2	0.203	0.21	0.21	0.212	0.215
	Volume of Water	Open Area		L3	L6	L5	L3	L6	L5
			26	0.218	0.236	0.246	0.235	0.256	0.266
			27	0.20	0.22	0.228	0.203	0.229	0.23
			28	0.167	0.183	0.184	0.182	0.194	0.193
	Time		26	0.22	0.248	0.25	0.235	0.254	0.269
			29	0.20	0.225	0.23	0.215	0.235	0.236
			30	0.17	0.19	0.19	0.18	0.192	0.19
0.4	Volume of Water	9		L3	L6	L5	L3	L6	L5
			31	0.198	0.23	0.24	0.222	0.252	0.26
			32	0.228	0.244	0.25	0.248	0.261	0.266
			33	0.187	0.213	0.221	0.21	0.225	0.226
			34	0.222	0.229	0.234	0.233	0.242	0.244
			35	0.172	0.19	0.192	0.206	0.206	0.211
			36	0.201	0.21	0.215	0.227	0.219	0.23
		6		L3	L6	L5	L3	L6	L5
			41	0.208	0.249	0.25	0.251	0.256	0.258
			42	0.24	0.257	0.262	0.264	0.27	0.28
			43	0.219	0.23	0.232	0.223	0.24	0.24
			44	0.243	0.244	0.246	0.25	0.256	0.255
			45	0.195	0.205	0.206	0.20	0.213	0.225
			46	0.212	0.22	0.219	0.23	0.234	0.236
	Time	9		L3	L6	L5	L3	L6	L5
			31	0.19	0.24	0.246	0.222	0.252	0.26
			32	0.228	0.25	0.256	0.248	0.261	0.266
			37	0.164	0.218	0.22	0.186	0.223	0.225
			38	0.215	0.228	0.233	0.225	0.242	0.24
			39	0.146	0.18	0.18	0.143	0.163	0.168
			40	0.183	0.192	0.195	0.193	0.197	0.198

		6		L3	L6	L5	L3	L6	L5
			41	0.208	0.245	0.25	0.251	0.255	0.265
			42	0.24	0.257	0.262	0.264	0.27	0.28
			47	0.193	0.22	0.23	0.21	0.235	0.227
			48	0.224	0.233	0.239	0.237	0.249	0.245
			49	0.168	0.18	0.19	0.176	0.185	0.173
			50	0.194	0.2	0.206	0.197	0.207	0.208
	Volume of Water			L3	L6	L5	L3	L6	L5
			51	0.17	0.237	0.239	0.196	0.248	0.25
			52	0.152	0.22	0.22	0.179	0.22	0.222
			53	0.132	0.17	0.173	0.148	0.167	0.173
	Time		51	0.177	0.237	0.24	0.201	0.248	0.250
			54	0.174	0.216	0.22	0.186	0.234	0.227
			55	0.15	0.185	0.18	0.145	0.168	0.172
0.8	Volume of Water	9		L3	L6	L5	L3	L6	L5
			56	0.177	0.22	0.228	0.208	0.245	0.245
			57	0.218	0.24	0.245	0.246	0.258	0.265
			58	0.171	0.201	0.211	0.231	0.222	0.215
			59	0.2	0.222	0.229	0.23	0.24	0.245
			60	0.16	0.182	0.186	0.197	0.201	0.215
			61	0.19	0.201	0.201	0.224	0.211	0.226
		6		L3	L6	L5	L3	L6	L5
			66	0.195	0.234	0.238	0.24	0.25	0.256
			67	0.228	0.252	0.254	0.257	0.265	0.268
			68	0.208	0.218	0.22	0.226	0.235	0.229
			69	0.236	0.238	0.24	0.246	0.253	0.25
			70	0.182	0.196	0.195	0.19	0.21	0.22
			71	0.203	0.212	0.208	0.227	0.227	0.226
	Time	9		L3	L6	L5	L3	L6	L5
			56	0.177	0.222	0.233	0.208	0.245	0.245
			57	0.211	0.24	0.245	0.246	0.258	0.265
			62	0.152	0.196	0.208	0.165	0.206	0.217
			63	0.206	0.22	0.227	0.216	0.236	0.234
			64	0.133	0.16	0.17	0.14	0.161	0.17
			65	0.18	0.186	0.191	0.188	0.191	0.187

		6		L3	L6	L5	L3	L6	L5
			66	0.195	0.234	0.244	0.24	0.25	0.256
			67	0.228	0.252	0.254	0.257	0.265	0.268
			72	0.188	0.219	0.223	0.19	0.221	0.220
			73	0.210	0.229	0.23	0.23	0.245	0.240
			74	0.157	0.175	0.185	0.158	0.170	0.189
			75	0.185	0.195	0.198	0.191	0.205	0.206
	Volume of Water			L3	L6	L5	L3	L6	L5
			76	0.160	0.209	0.21	0.194	0.227	0.234
			77	0.149	0.19	0.197	0.169	0.200	0.208
			78	0.115	0.141	0.152	0.130	0.148	0.160
	Time		76	0.164	0.209	0.220	0.194	0.227	0.234
			79	0.160	0.184	0.200	0.165	0.193	0.205
			80	0.130	0.150	0.160	0.123	0.145	0.164

Table 4.3 P-value for the independent variables in first part of regression analysis

	G I		G II		G III	
Independent variables	P-value		P-value		P-value	
A/W_b^2	-----		0.000282	Significant	-----	
W_c/W_b	2.456E-09	Significant	5.073E-05	Significant	0.000260	Significant
X_t/W_b	7.078E-12	Significant	1.873E-09	Significant	1.39E-06	Significant
T_pQ_p/W_b^3	0.059513	Significant	0.047844	Significant	0.041662	Significant
T_bQ_p/W_b^3	0.648620	Not Significant	0.083935	Not Significant	0.095059	Not Significant
Q_p^2/gW_b^5	4.113E-06	Significant	1.358E-07	Significant	0.021706	Significant

Table 4.4 P-value for the independent variables in the second part of regression analysis

G IV		
Independent variables	P-value	
A/W_{b2}	0.002969308	Significant
Wc/W_b	4.90506E-05	Significant
X_t/W_b	2.68929E-08	Significant
T_pQ_p/W_{b3}	0.045475857	Significant
T_bQ_p/W_{b3}	0.019849155	Significant
Q_{p2}/gW_{b5}	1.0049E-11	Significant

Table 4.5 Percentage volume of water pass to the floodplain basin

	Breach Width (m)	The volume of water at downstream (m^3)	% Volume of water that released to floodplain basin
Hydrograph 1	0	3.788	
Run 26	0.2	2.42	36.1
Run 51	0.4	2.06	45.6
Run 76	0.8	1.63	57.1
Hydrograph 2	0	3.81	
Run 27	0.2	2.32	39.1
Run 52	0.4	1.80	52.7
Run 77	0.8	1.33	65.0
Hydrograph 3	0	4.13	
Run 28	0.2	2.13	48.3
Run 53	0.4	1.35	67.3
Run 78	0.8	0.90	78.1

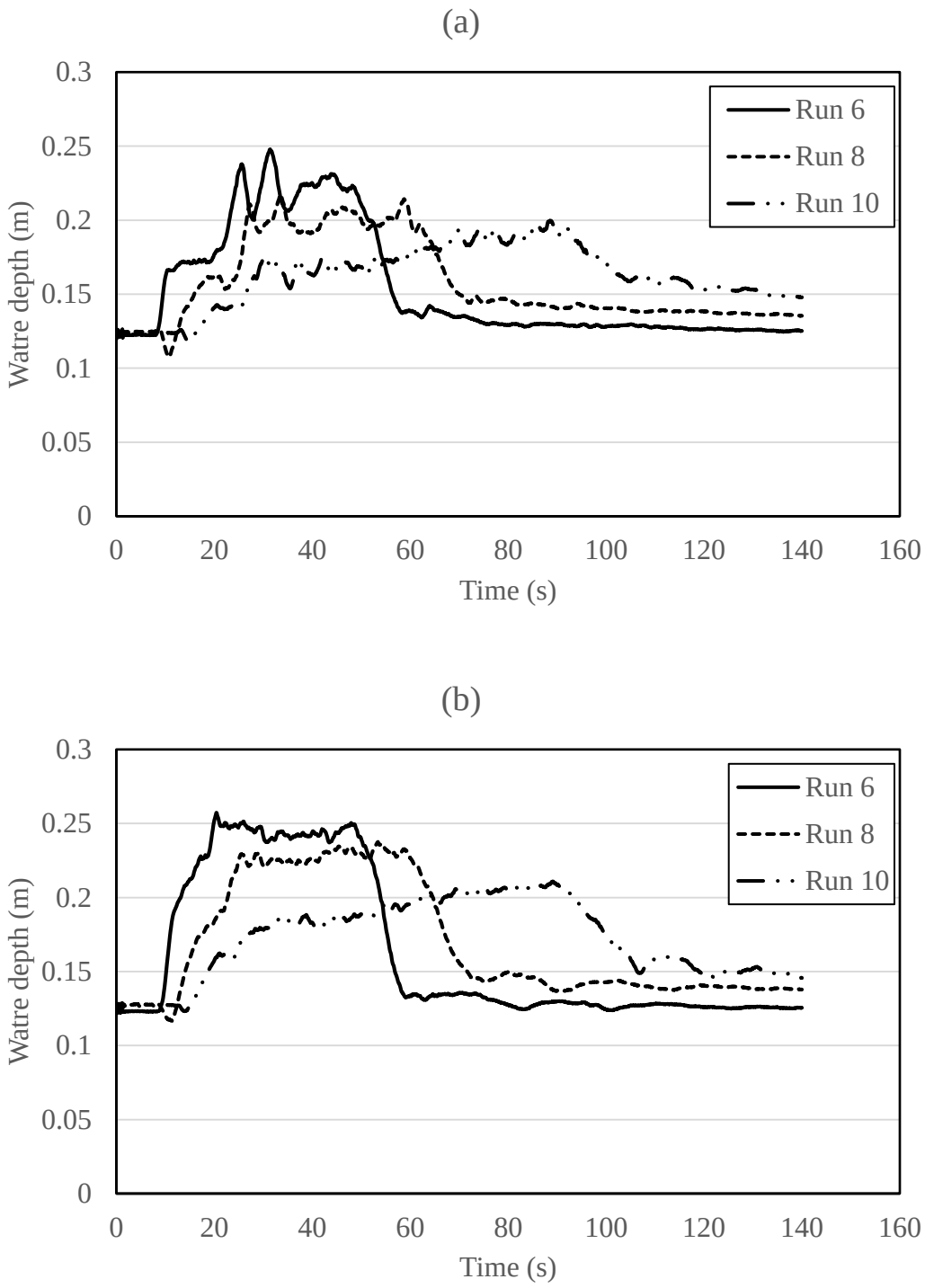

Figure 4.1 Flood stage due to inflow hydrograph (1,2,3) at the target location (a) upstream of the beach (b) downstream of the breach, in case of the empty flood basin

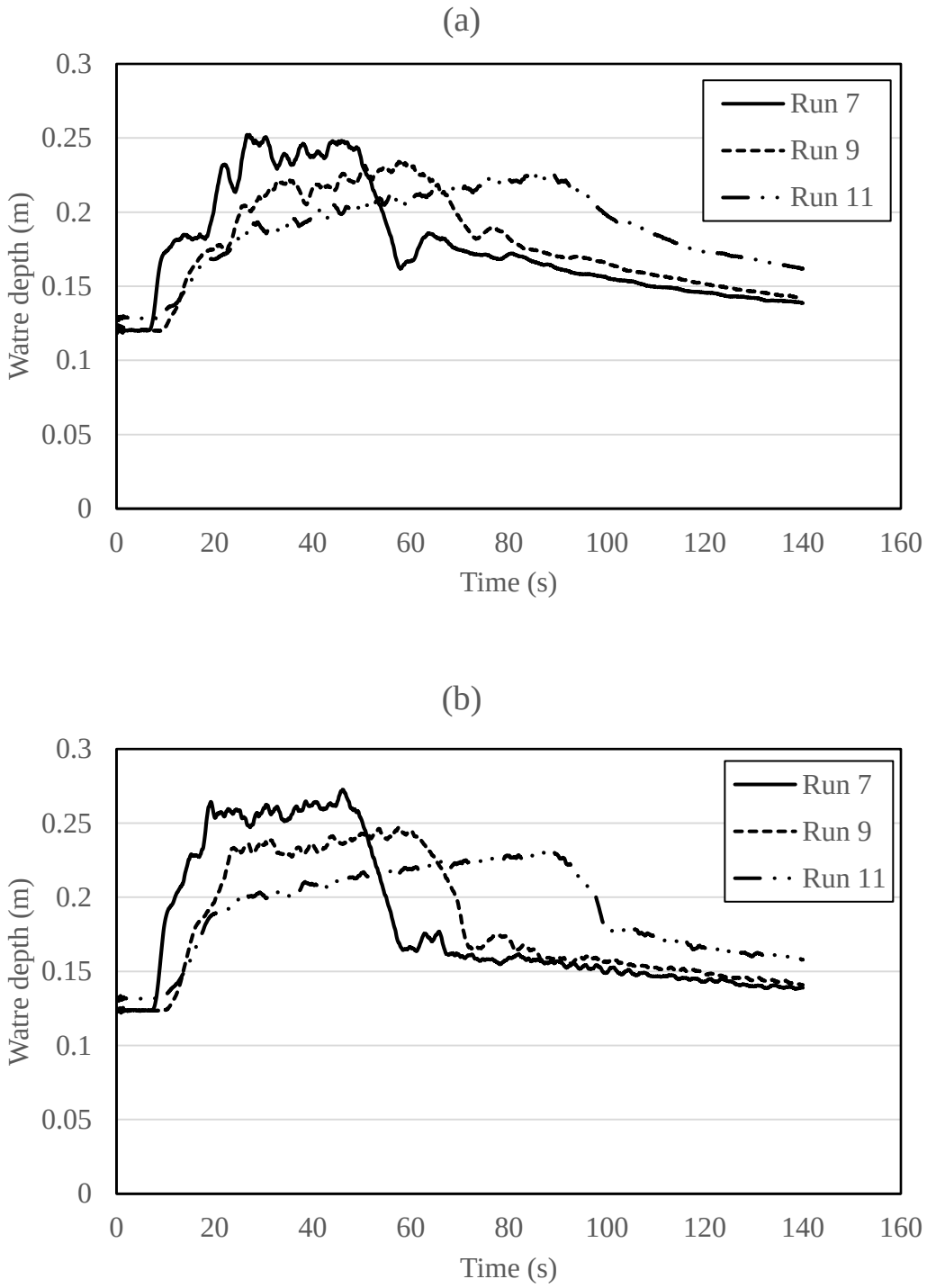

Figure 4.2 Flood stage due to inflow hydrographs (1,2,3) in case of initial tailwater depth in the floodplain basin at the target location (a) upstream of the beach (b) downstream of the breach

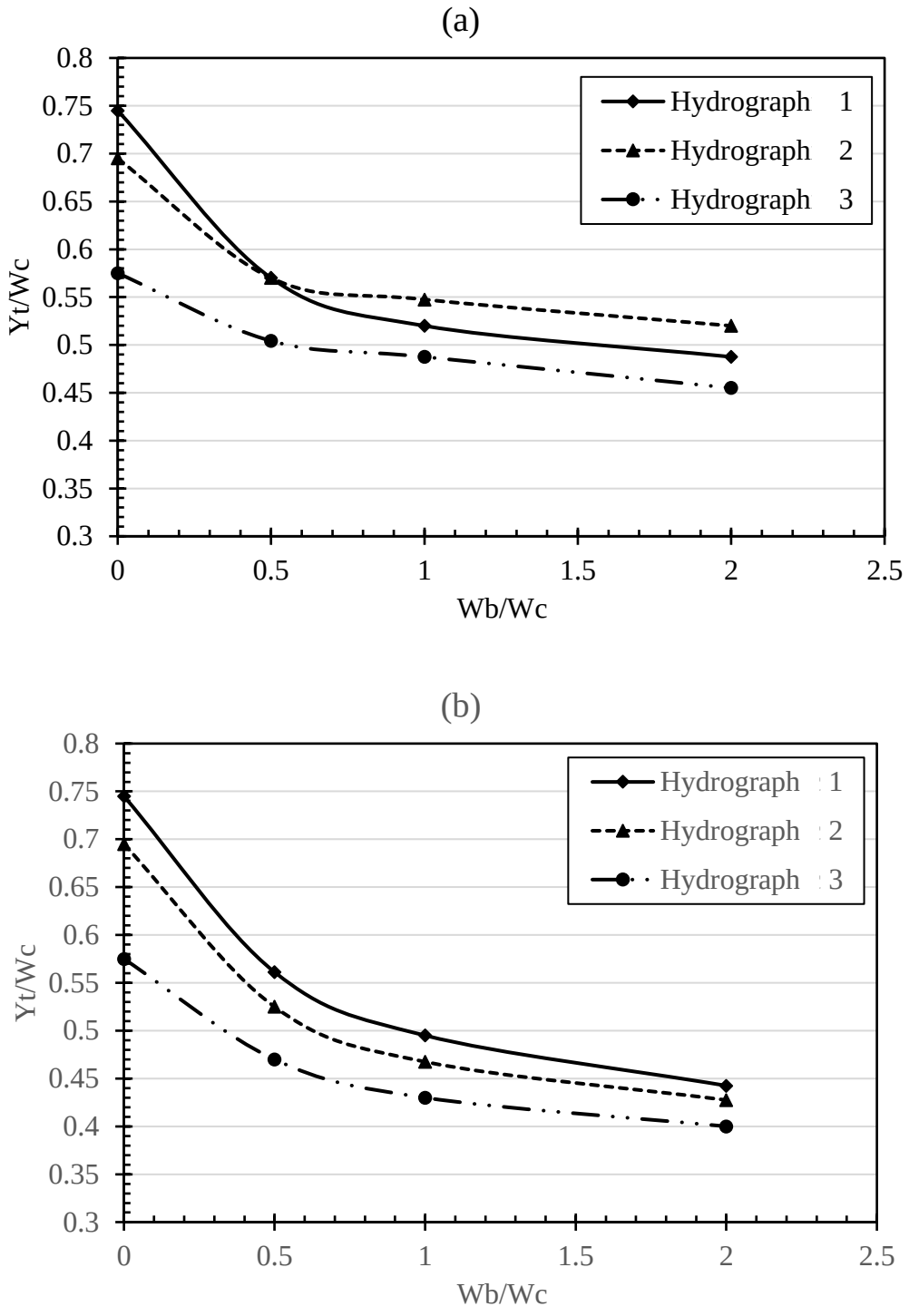

Figure 4.3 Nondimensional water depth upstream of the breach target location when there is no tailwater depth in the floodplain (a) Area 6 m^2, (b) Area 9 m^2, (c) Open Area

(c)

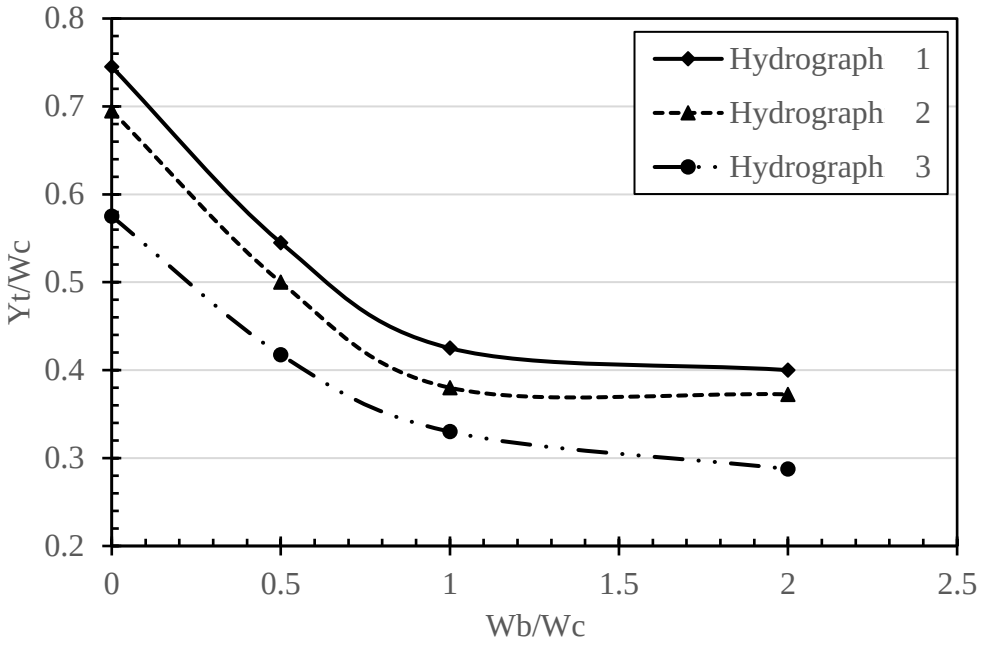

Figure 4.3 cont'd

(a)

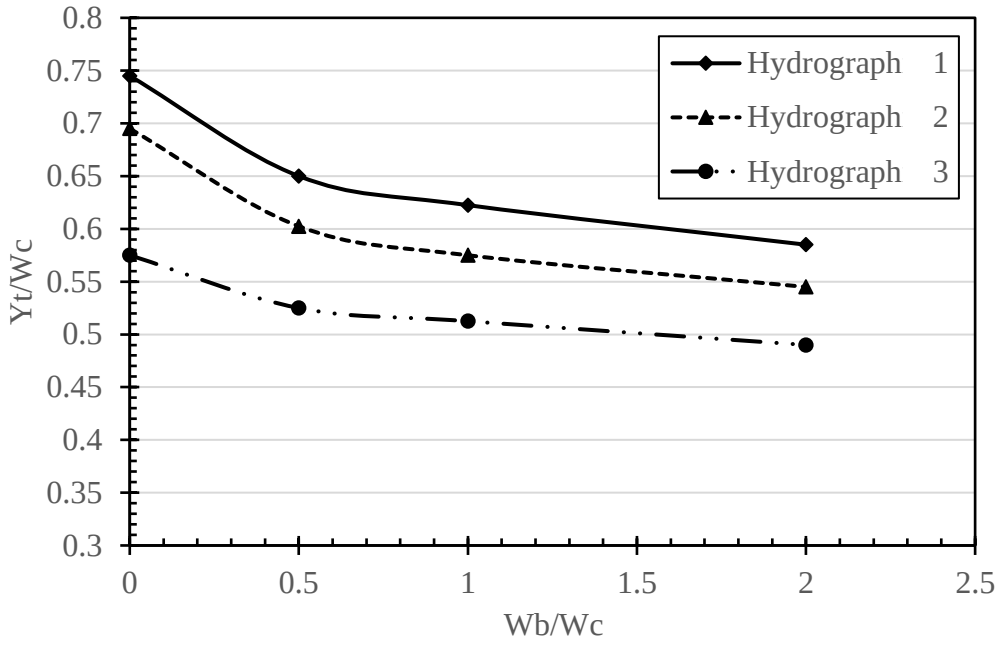

Figure 4.4 Nondimensional water depth at the downstream target location when there is no tailwater depth in floodplain basin (a) Area 6 m^2, (b) Area 9 m^2, (c) Open Area

(b)

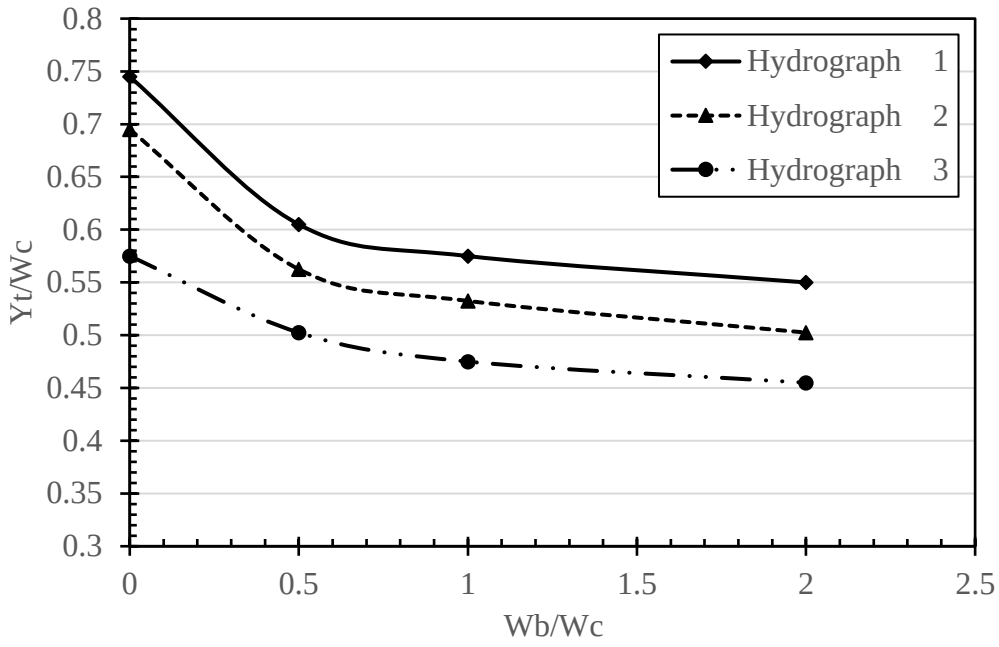

(c)

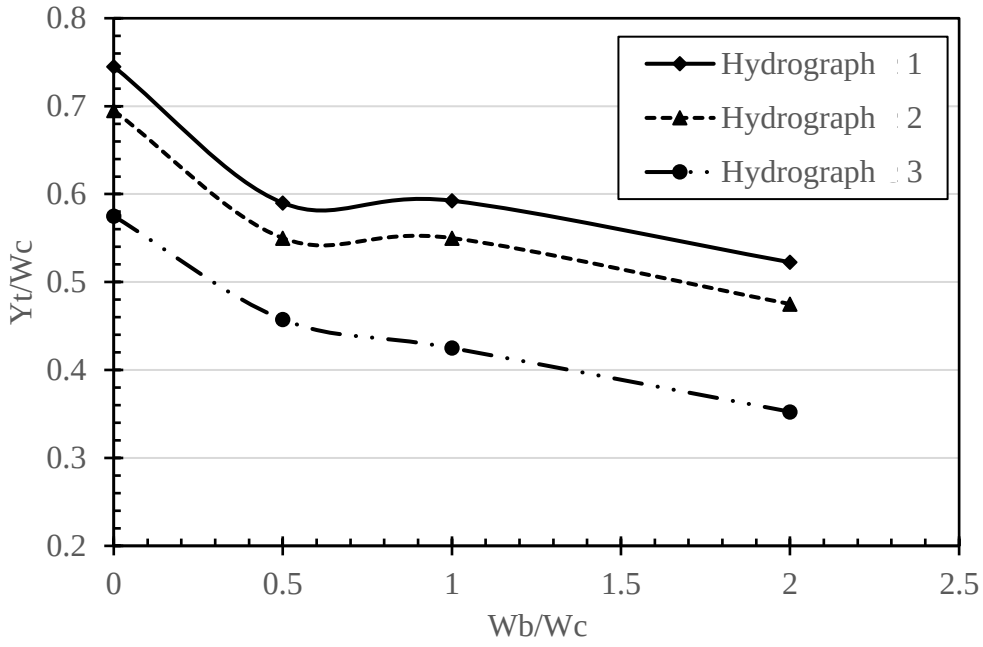

Figure 4.4 cont'd

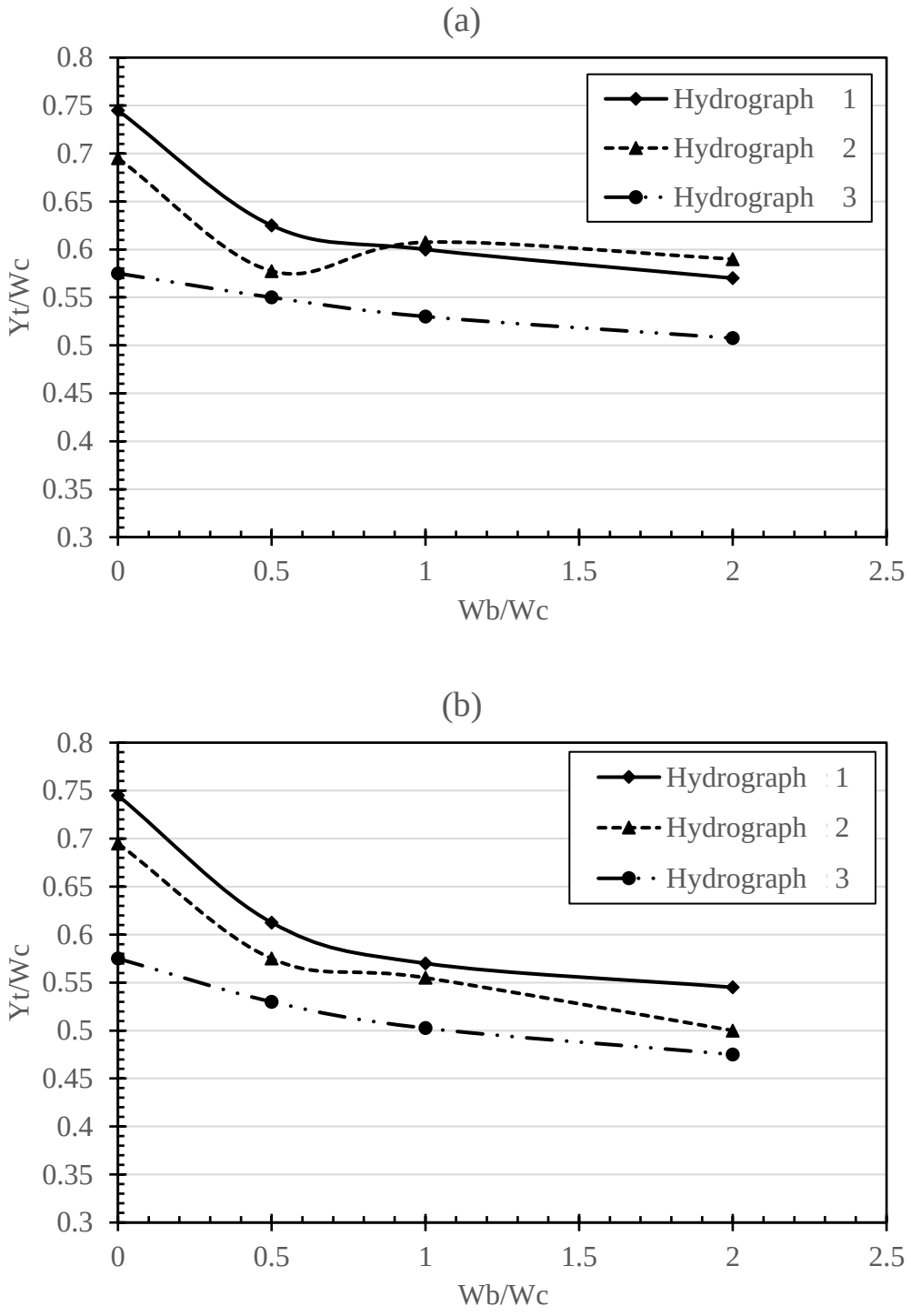

Figure 4.5 Nondimensional water depth at the upstream target location when there is initial tailwater depth in floodplain basin (a) Area 6 m^2, (b) Area 9 m^2

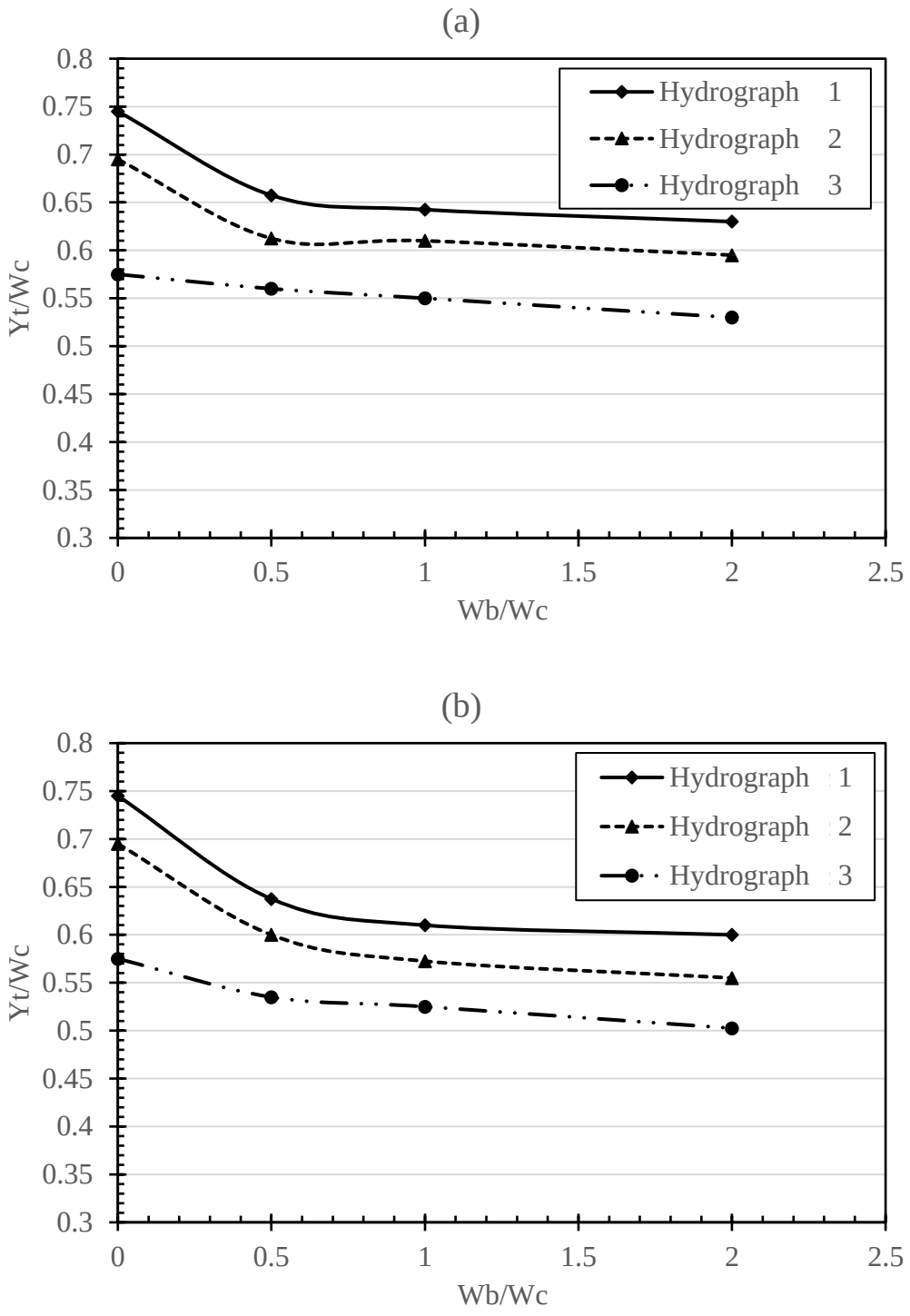

Figure 4.6 Nondimensional water depth at the downstream target location when there is initial tailwater depth in floodplain basin (a)Area 6 m^2, (b) Area 9 m^2

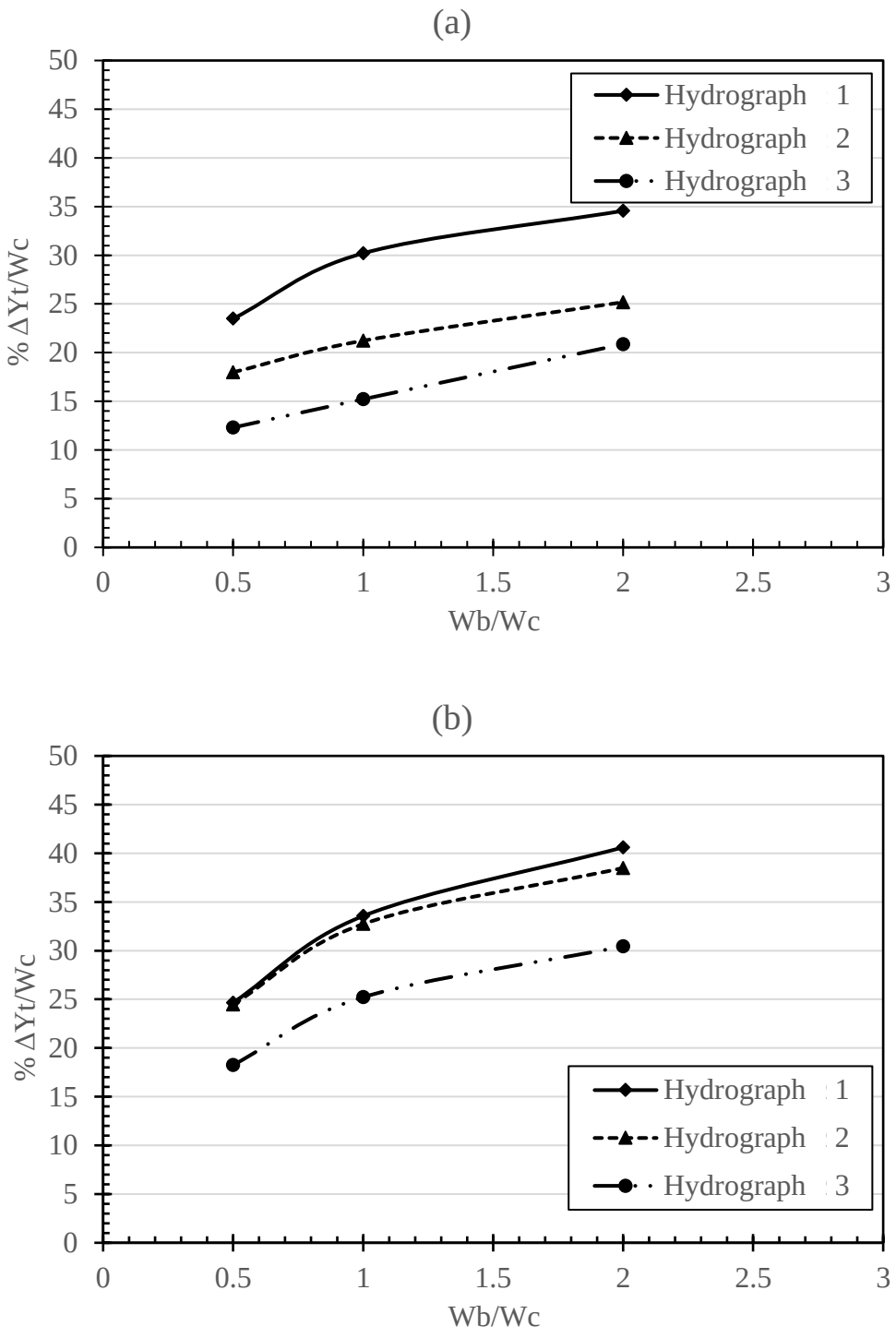

Figure 4.7 The percent of water depth reduction at the upstream target location when there is no tailwater depth in the floodplain (a) Area 6 m^2, (b) Area 9 m^2, (c) Open Area

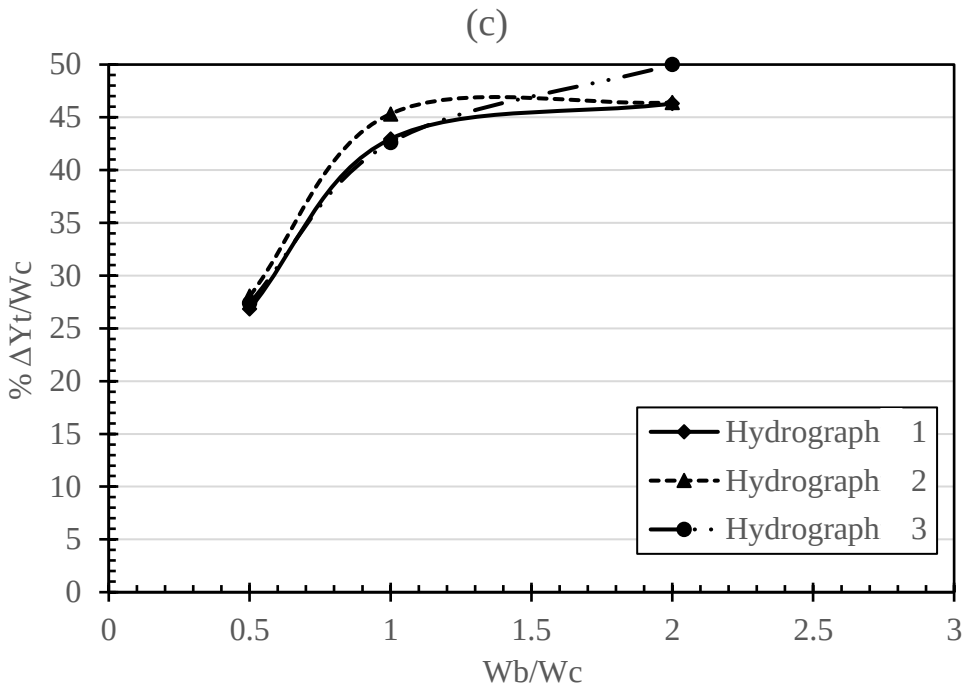

Figure 4.7 cont'd

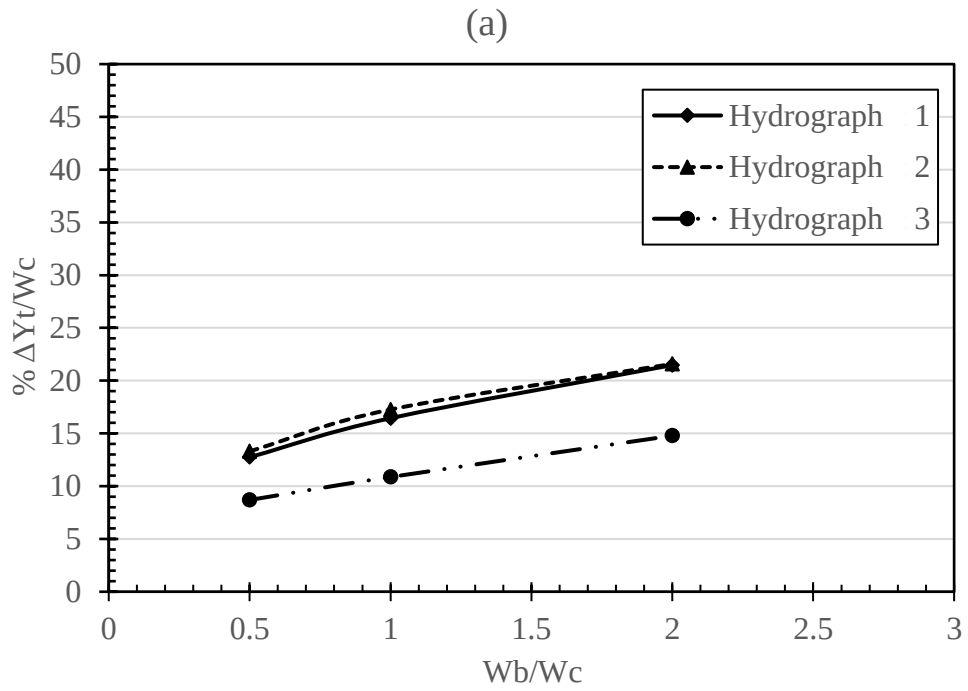

Figure 4.8 The percent water depth reduction at the downstream target location when there is no tailwater depth in the floodplain (a) Area 6 m^2, (b) Area 9 m^2, (c) Open Area

(b)

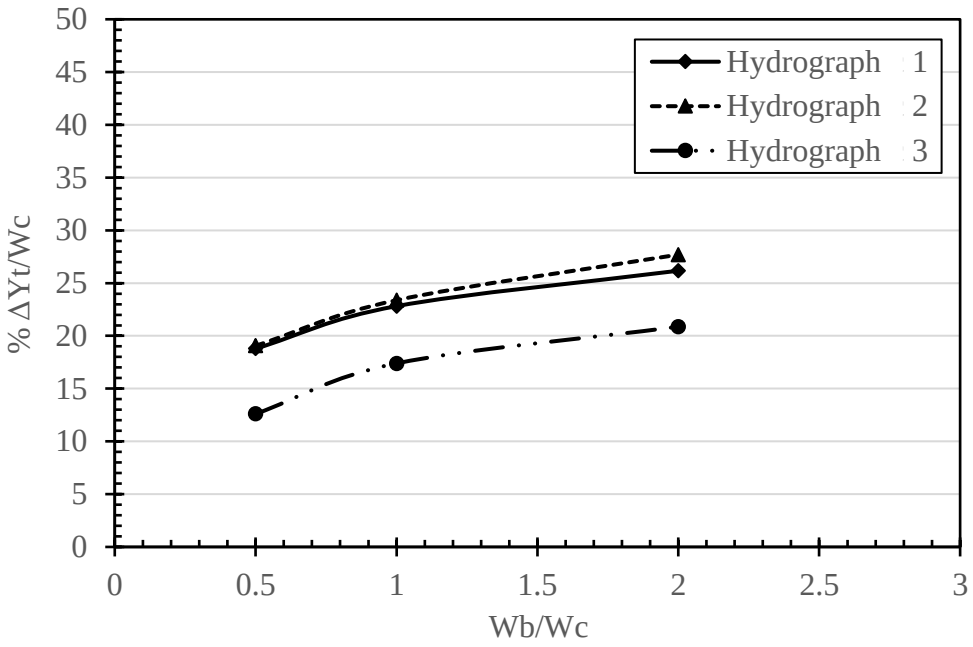

(c)

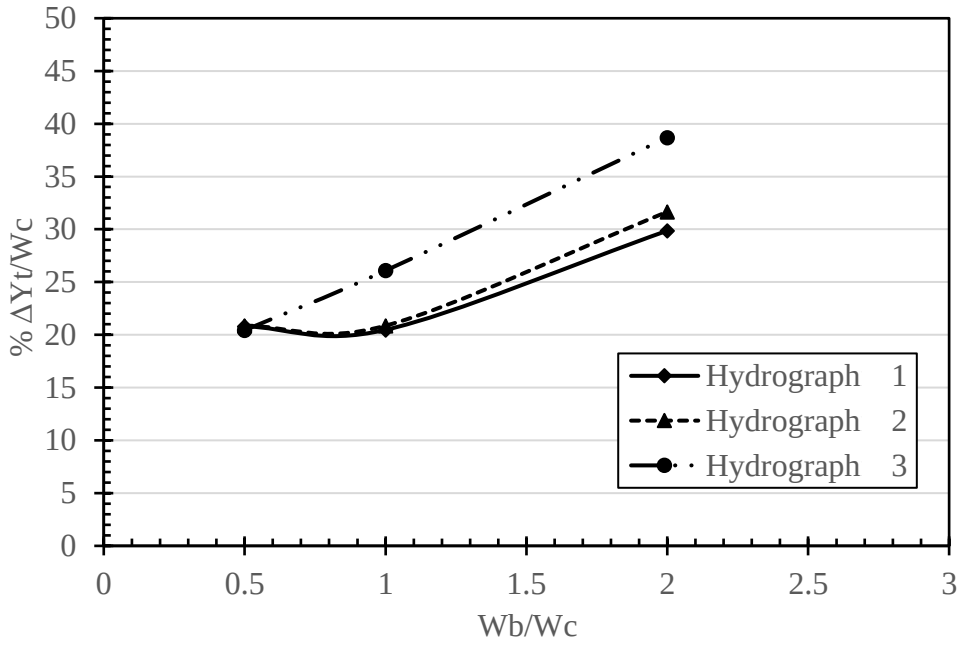

Figure 4.8 cont'd

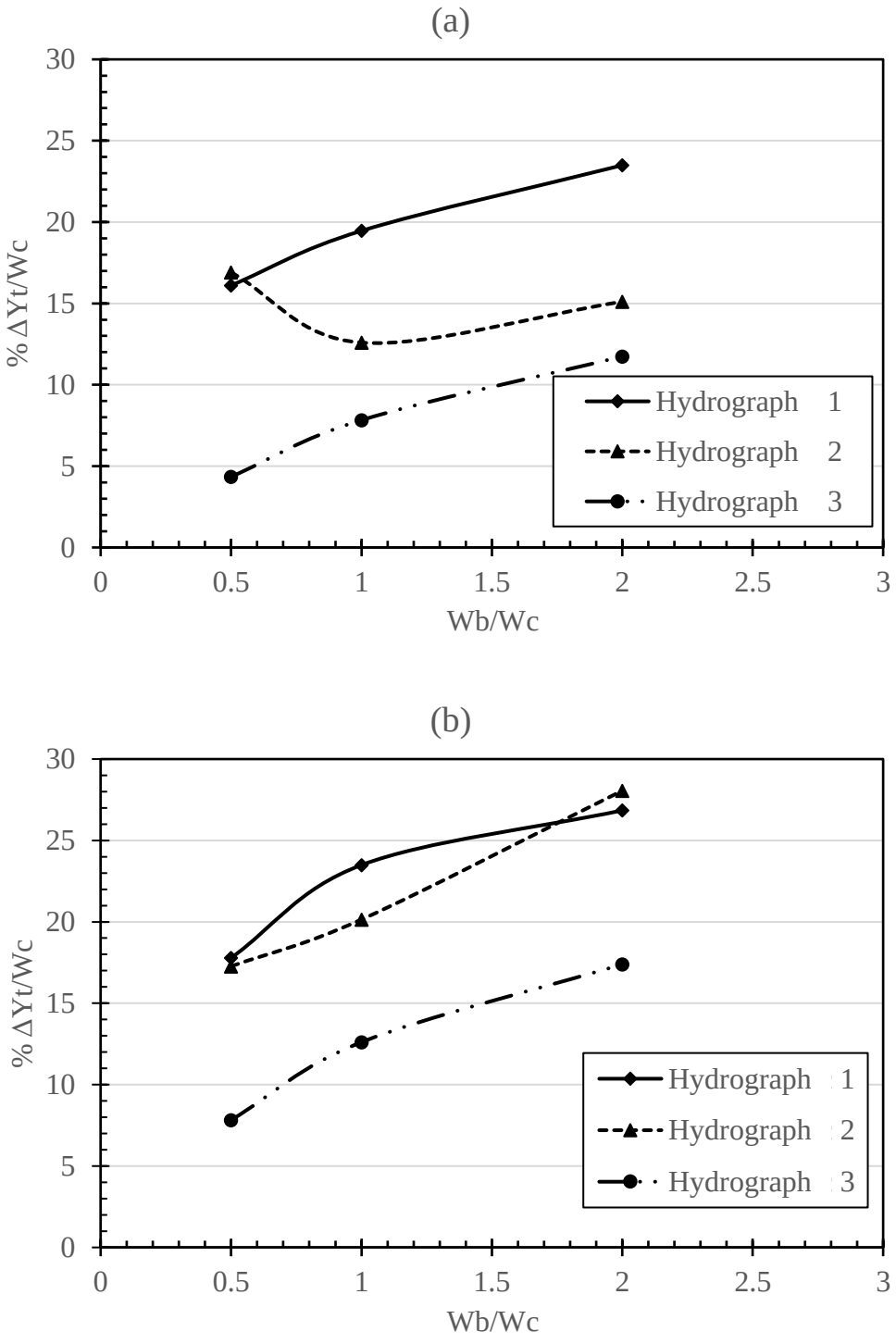

Figure 4.9 The percent water depth reduction at the upstream target location when there is initial tailwater depth in the floodplain (a) Area 6 m^2, (b) Area 9 m^2

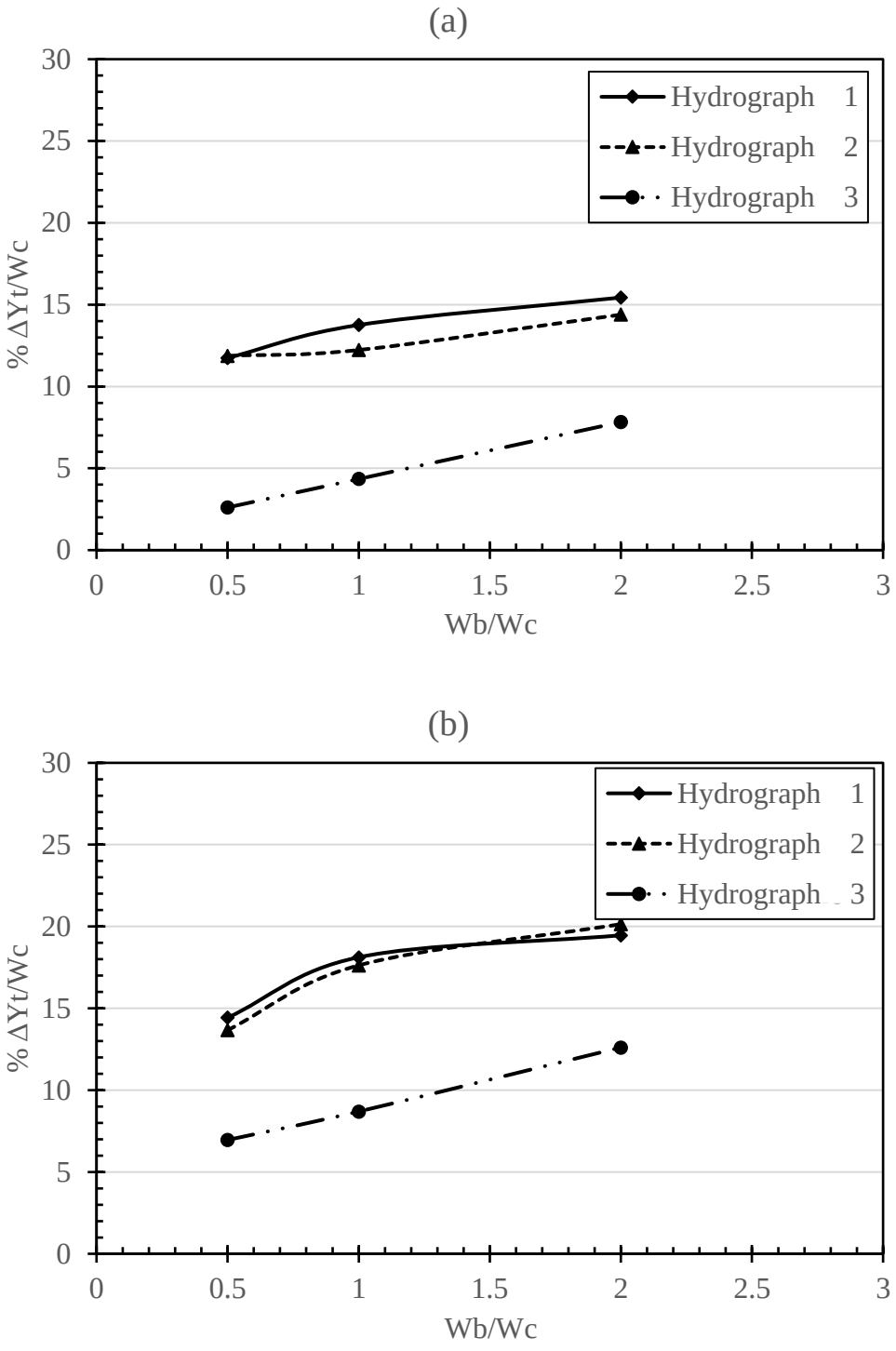

Figure 4.10 The percent water depth reduction at the downstream target location when there is initial tailwater depth in the floodplain (a) Area 6 m^2, (b) Area 9 m^2

(a)

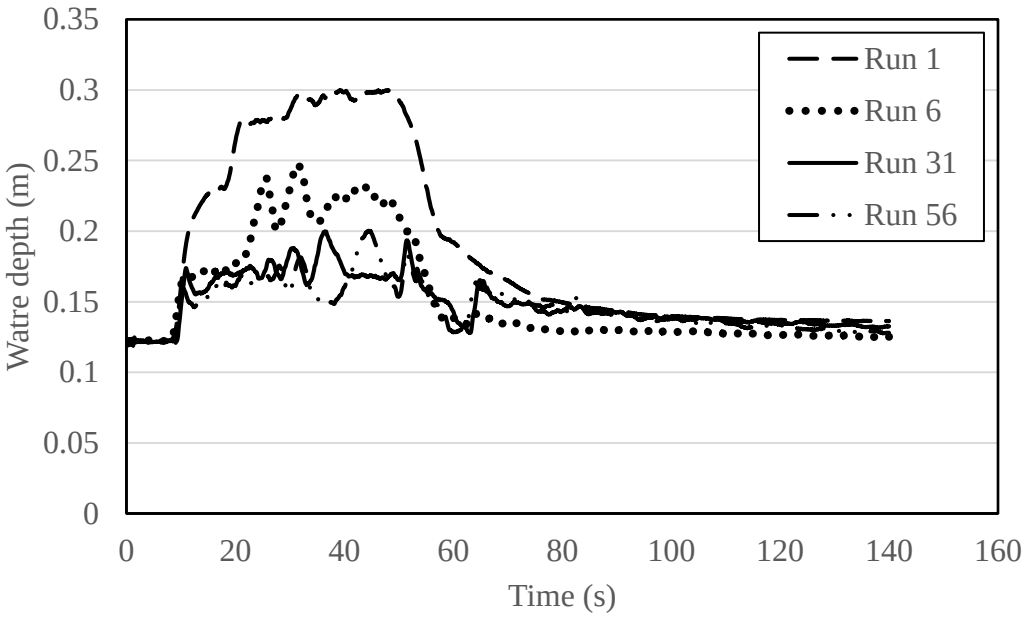

(b)

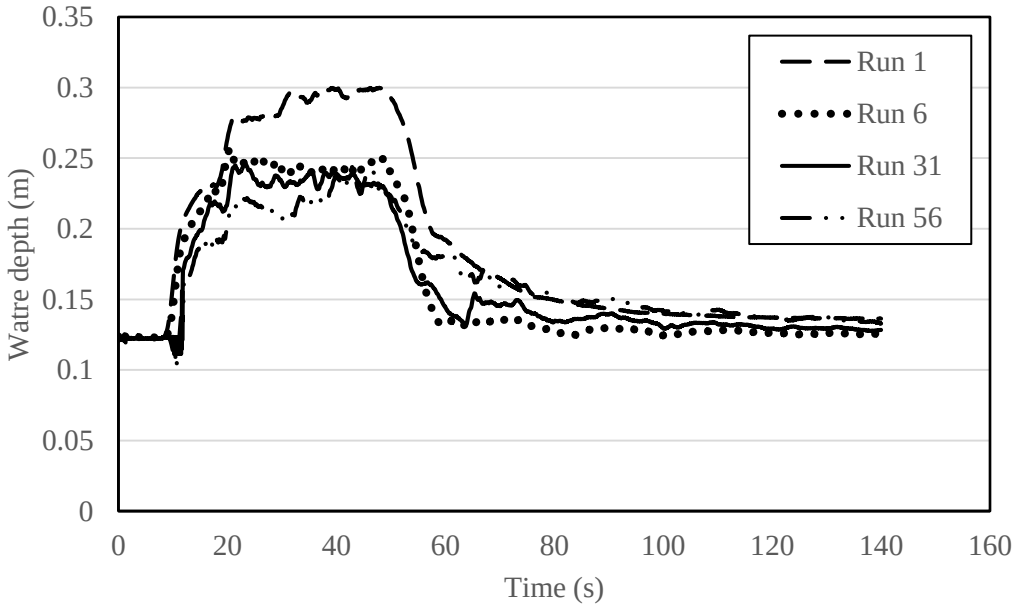

Figure 4.11 Depth due to the release of Hydrograph 1 in case of empty floodplain basin at the target location (a) upstream of the beach (b) downstream of the breach

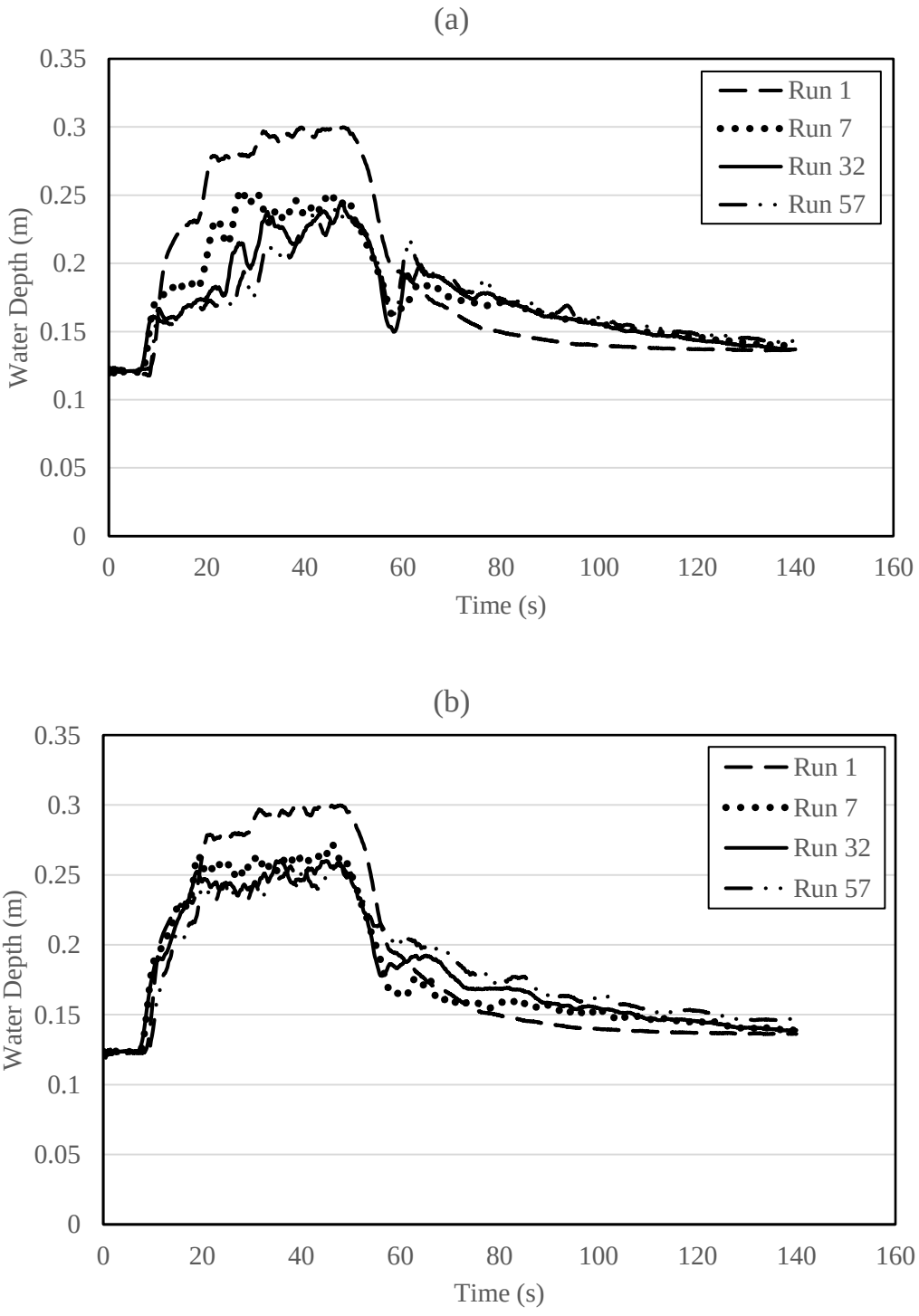

Figure 4.12 Depth due to the releases of Hydrograph 1 in case of initial tailwater depth floodplain basin at the target location (a) upstream of the beach (b) downstream of the breach

(a)

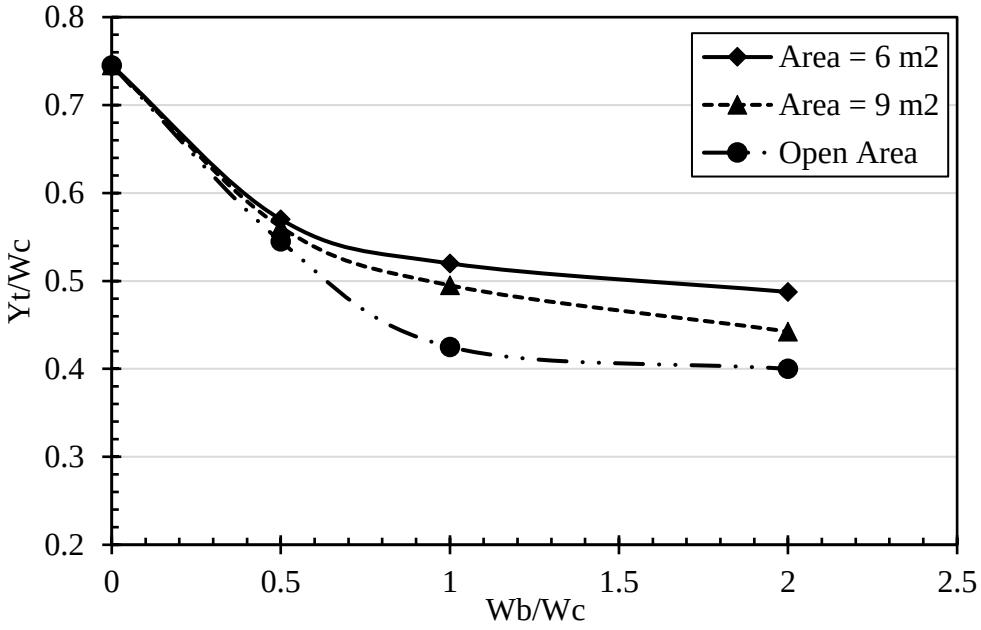

(b)

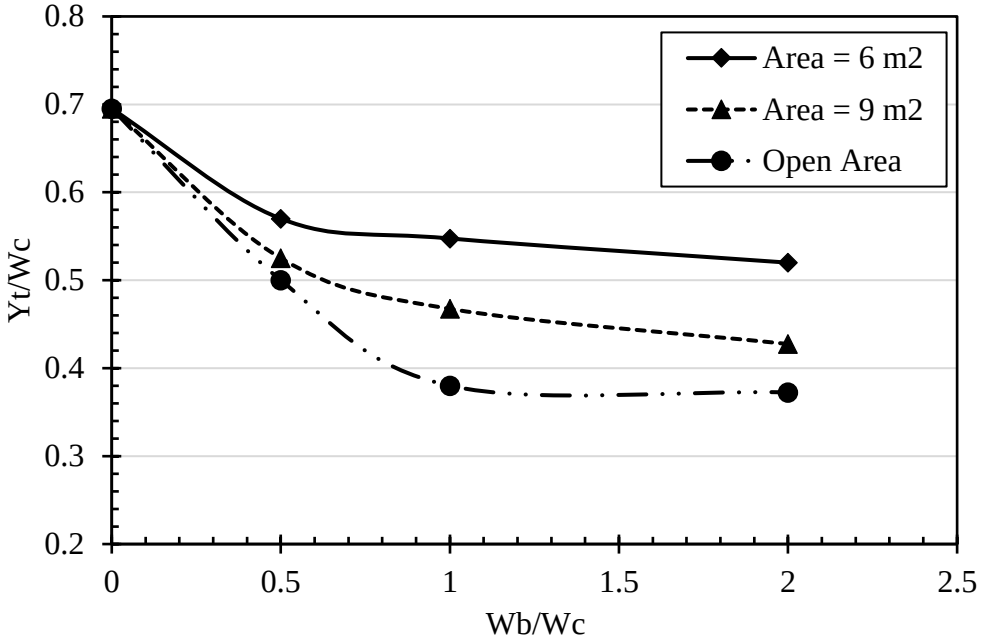

Figure 4.13 Non-dimensional water depth due to Hydrograph 1 at target location (a) upstream breach (b) downstream breach, in case of empty floodplain basin

(a)

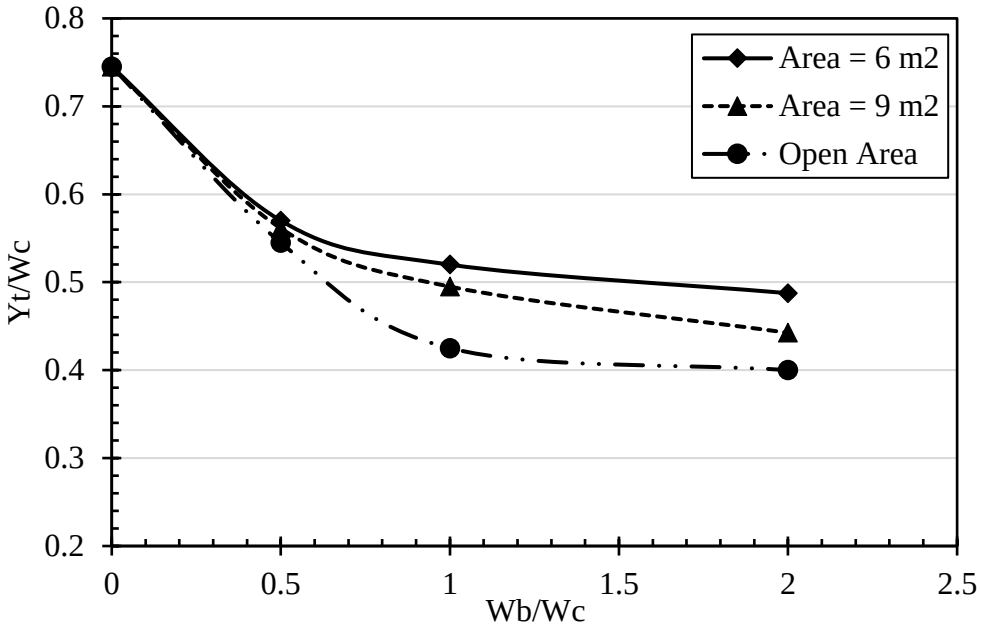

(b)

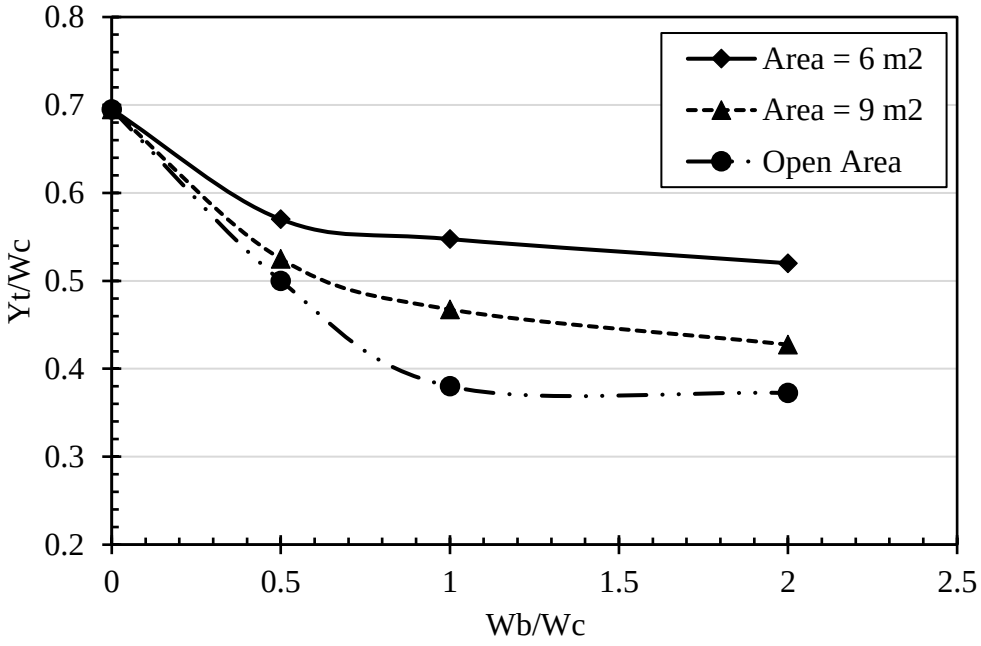

Figure 4.14 The effect of floodplain area on the water depth at the upstream target location when there is no tailwater depth in the floodplain (a) Hydrograph 1, (b) Hydrograph 2, (c) Hydrograph 3

(c)

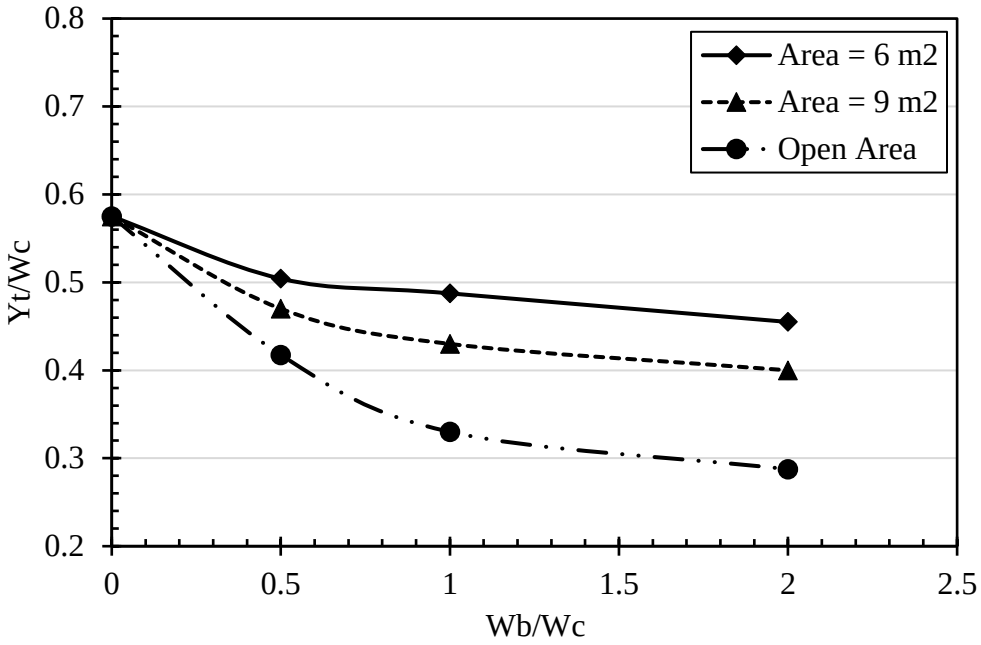

Figure 4.14 cont'd

(a)

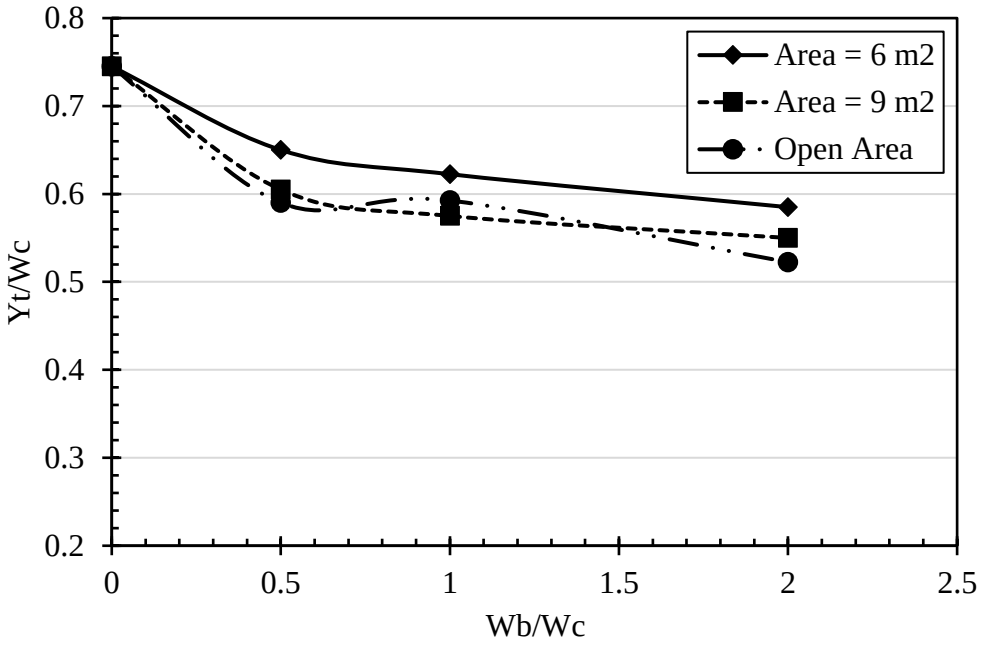

Figure 4.15 The effect of floodplain area on the water depth at the downstream target location when there is no tailwater depth in the floodplain (a) Hydrograph 1, (b) Hydrograph 2, (c) Hydrograph 3

(b)

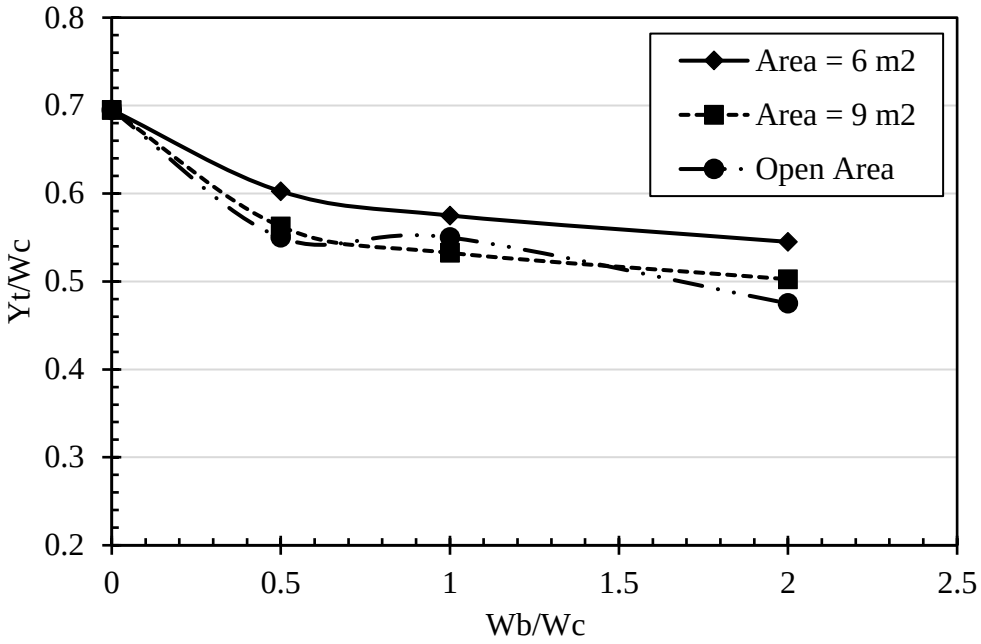

(c)

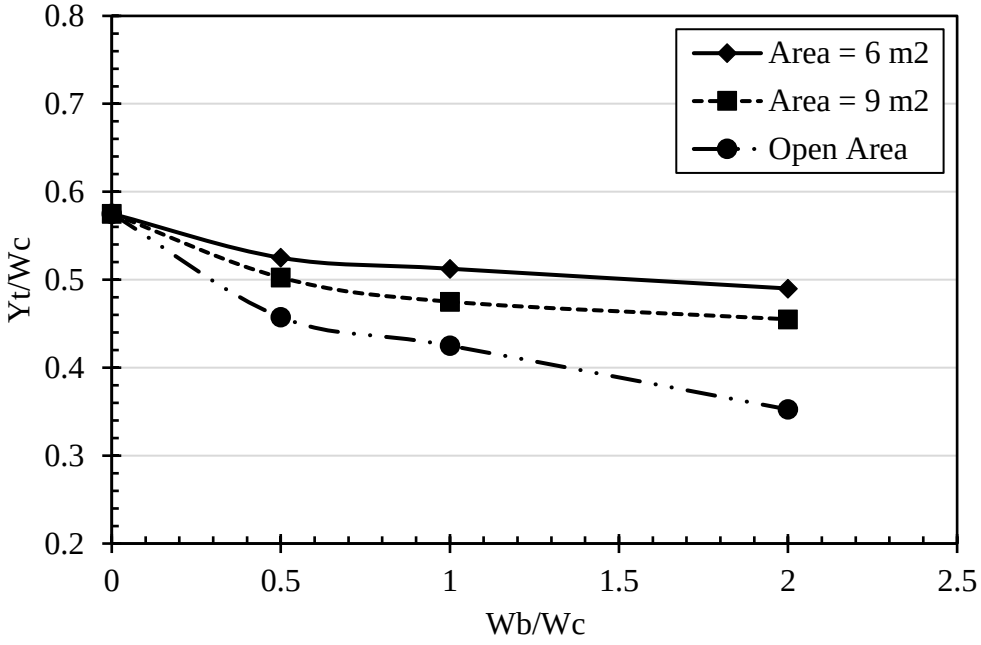

Figure 4.15 cont'd

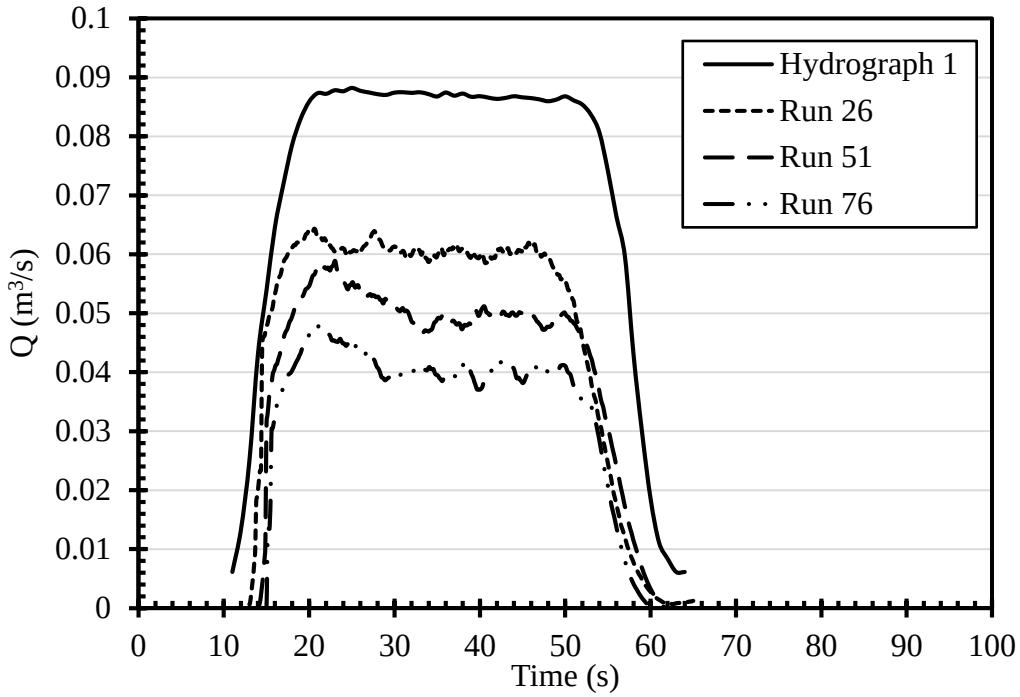

Figure 4.16 Inflow Hydrograph 1 and outflow hydrographs

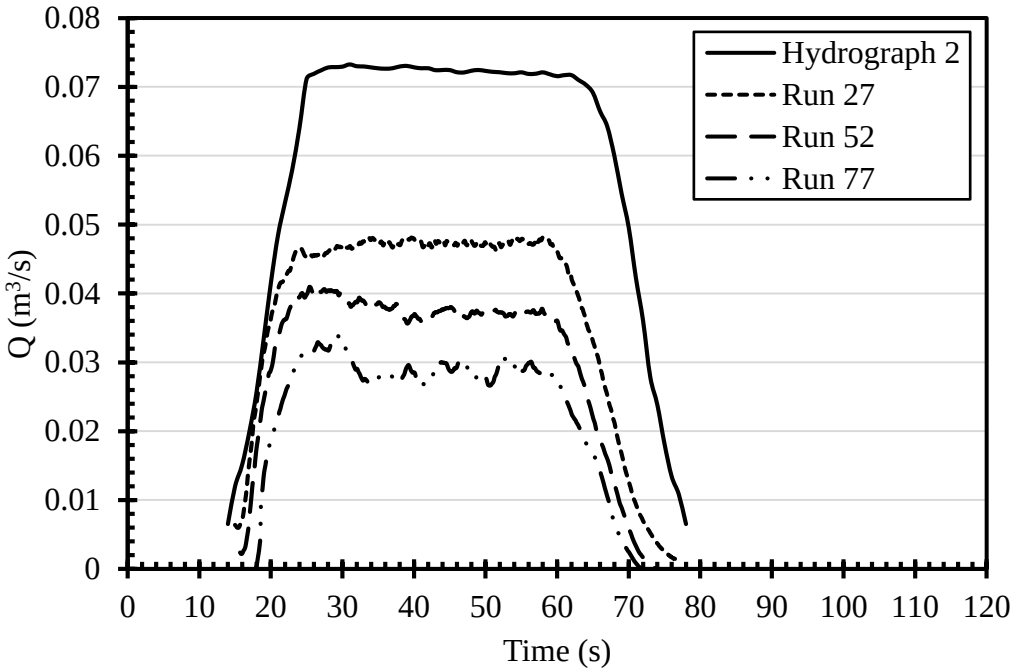

Figure 4.17 Inflow Hydrograph 2 and outflow hydrographs

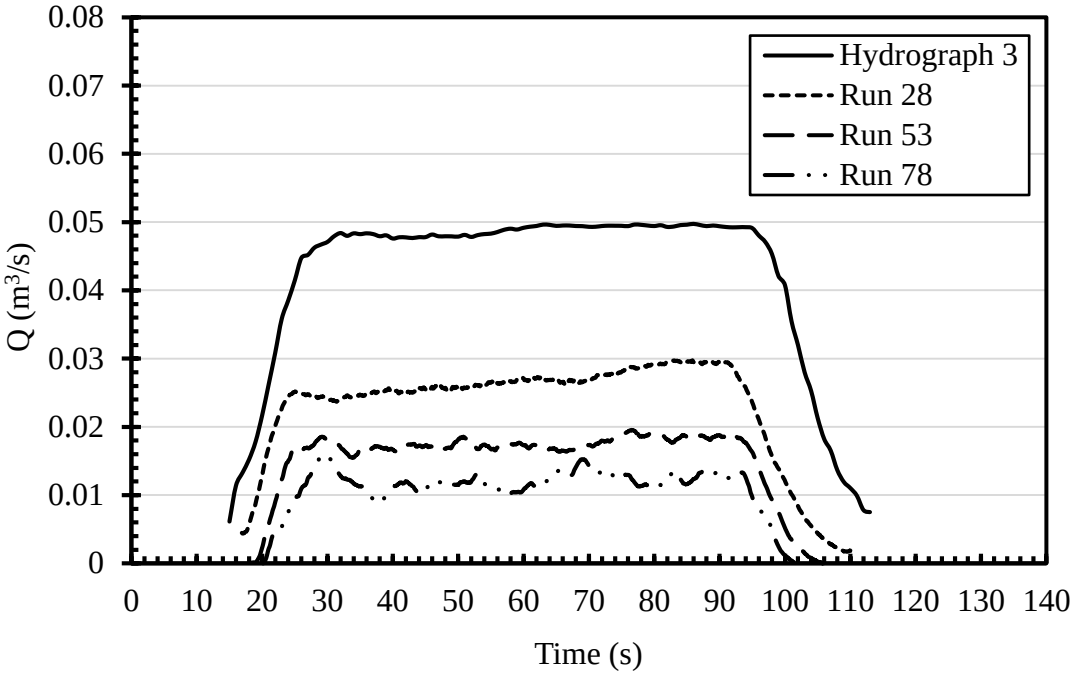

Figure 4.18 Inflow Hydrograph 3 and outflow hydrographs

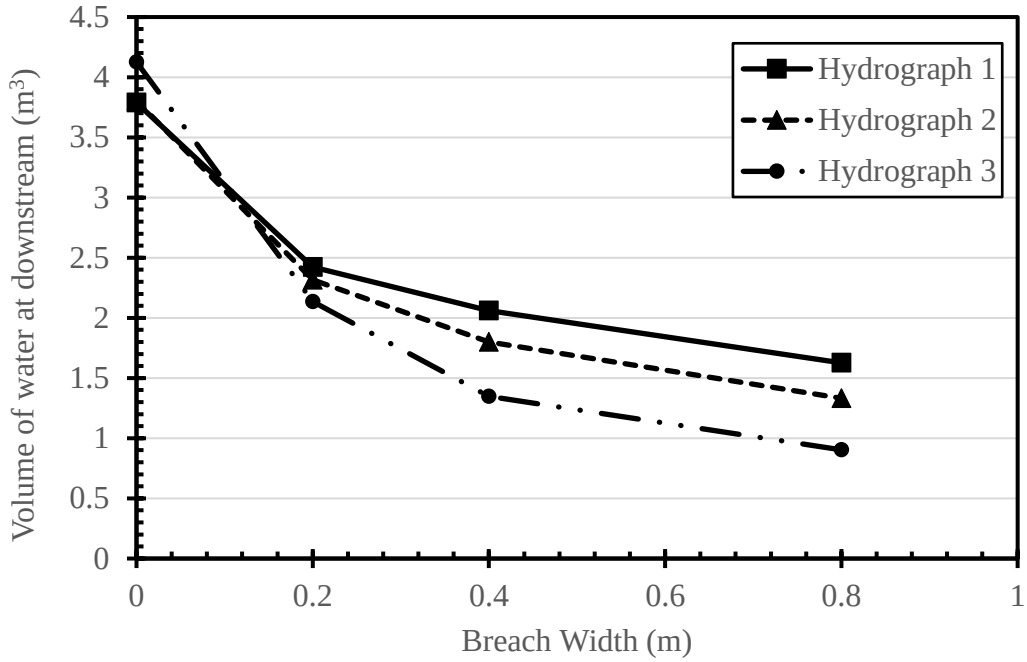

Figure 4.19 Reduction in volume of flood water at channel downstream for different inflow hydrographs

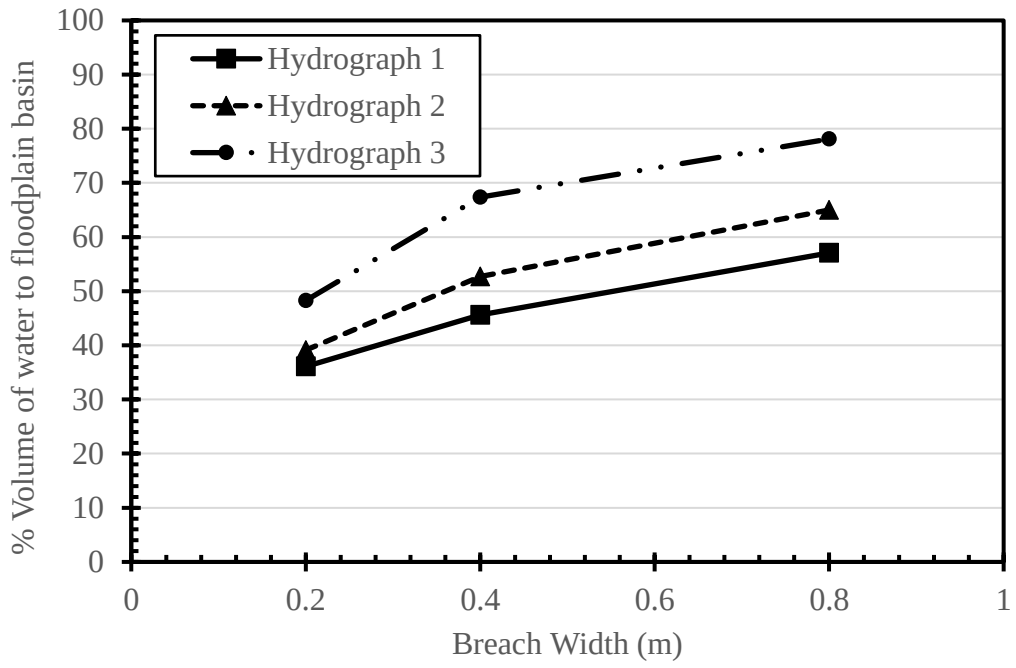

Figure 4.20 Percentage of increasing the volume of flood water passed to the floodplain basin fro different inflow hydrographs

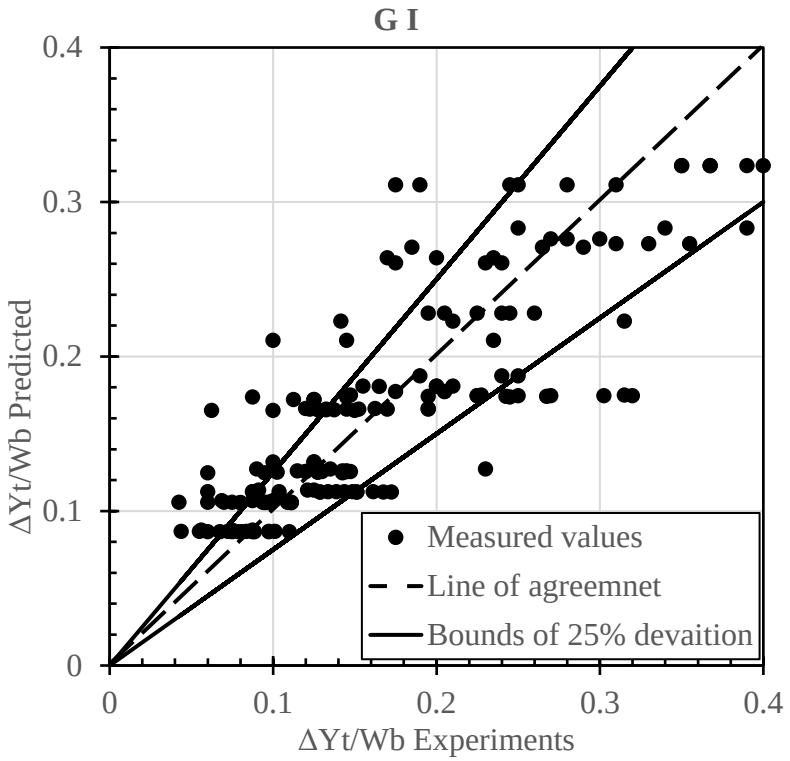

Figure 4.21 Predicted and measured $\Delta Y_t/W_b$ (active flood management tests)

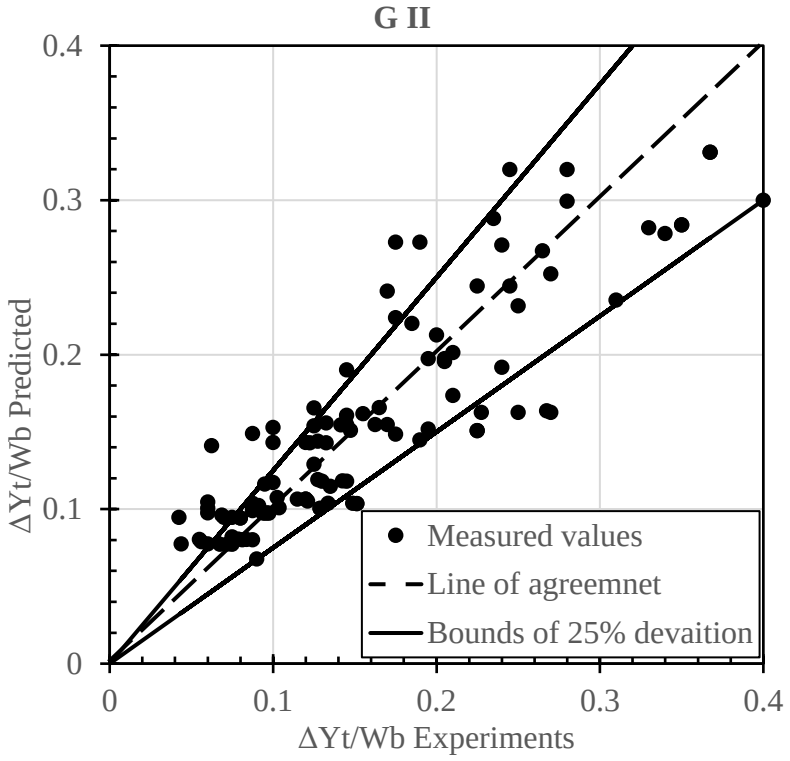

Figure 4.22 Predicted and measured $\Delta Y_t/W_b$ (fixed flood basin area)

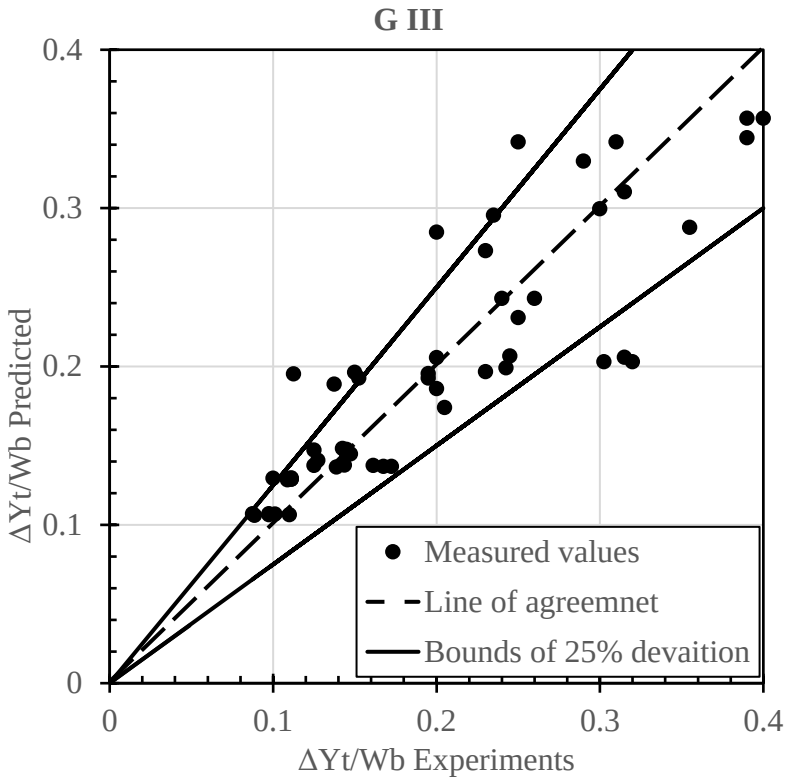

Figure 4.23 Predicted and measured $\Delta Y_t/W_b$ (flood basin with an outlet)

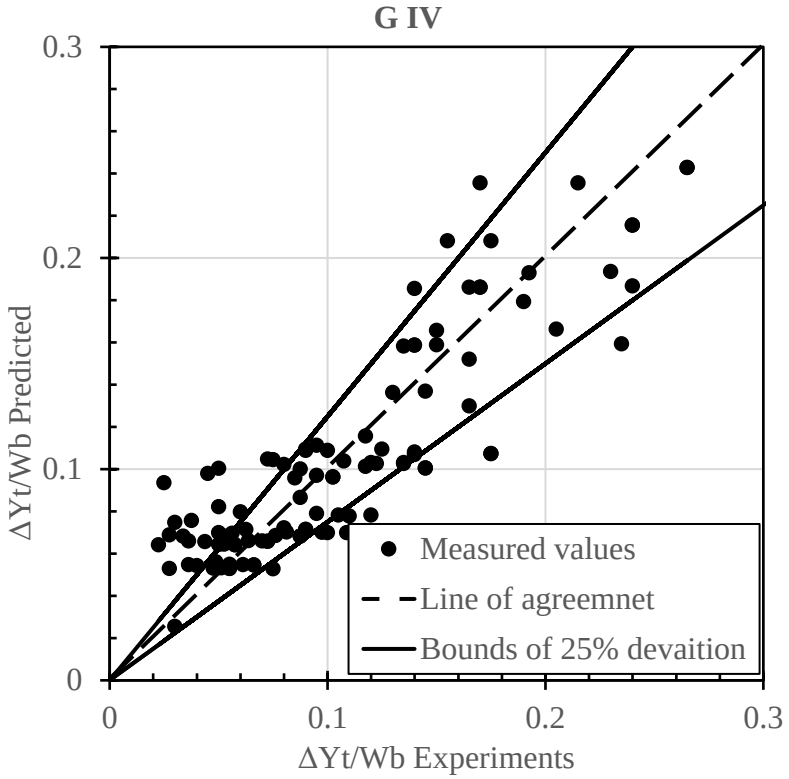

Figure 4.24 Predicted and measured $\Delta Y_t/W_b$ (passive flood management tests)

CHAPTER 5

CONCLUSION

Two experimental studies related to levee breach flow have been conducted in this work. Extensive sets of data were collected from laboratory experiments and analyzed. The first study involves levee breach flow through a fully developed breach. Experiments were conducted by considering different breach openings and downstream water levels. Surface velocity and water depth were measured using a PTV method and an ultrasonic distance measurement probe, respectively. The data were utilized to calibrate model coefficients of a 1D dynamic model of dividing flow. The predictive model was further validated using measurements from a set of additional experiments showing satisfactory agreement. The second study is focused on flood stage reduction by flow diversion using an active and a passive approach. In the active approach, a levee section is suddenly removed allowing diversion of part of the floodwater to an initially dry basin. This emulates the fuse plug method of an engineered levee breach. In the passive approach, the floodplain is already connected to the channel prior to the arrival of the flood. Different hydrograph shapes, breach width, and flood basin areas were considered.

The important conclusions from the first study are listed below:

1. Breach discharge increased due to an increase in breach width and an increase in the downstream water level.

2. The water depth in the channel decreased with an increase in breach width.
3. The water surface in the area adjacent to the breach entrance had a significant undulation.
4. A clear dip occurred in the water surface along the breach and it was more pronounced in case of large breach openings.
5. The surface velocity in both directions was measured by using the PIVLab Matlab tool. A large stagnation area that developed downstream of the breach close to the right-side channel wall was identified from the surface velocity measurements.
6. The stagnation zone area increased with an increase in the breach discharge and weir height.
7. A one-dimensional analytical model was developed for estimating the discharge and average water depth within the breach from known upstream discharge and downstream water depth.
8. Two model coefficients appear in the control volume analysis used to derive the 1D analytical model. These are the interfacial shear force coefficient, *Ki*, between the control volumes and the separation zone shear coefficient, *Ks*, for the stagnation force in the main channel downstream of the breach section. Both coefficeints can be expressed as functions of the relative breach to channel width and the upstream Froude number.
9. It was observed from the analysis that the value of the interfacial shear force coefficient, *Ki*, decreased with an increase of discharge ratio, ξ.

10. The separation zone shear coefficient, *Ks*, increased due to an increase in the downstream water depth or breach width both of which lead to an increase in discharge ratio.
11. Eight additional experiments were run to validate the analytical model by considering inlet discharge that was higher and lower than the constant discharge used in the first set of 28 experiments. A different breach width of 0.55m, not considered in the first set of experiments was used in these eight tests. The results show a good agreement between measurements and model prediction.

The important conclusions from the second study involving flood management by controlled levee breach are outlined below:

1. The water depth at upstream and downstream target locations decreased when the duration of the flood hydrograph increased for the same volume of water released.
2. The percentage of reduction in water depth at target locations was higher for short-duration high-peak floodwaves.
3. An increase in the breach width led to a decrease in the floodwater level at target locations in the main channel. The decrease was between 8.7-50 % and 2.6-28 % for water level drop at the upstream target location 3 under the active and passive management scenarios, respectively. The small percentage was for the case with a breach width of 0.2 m and a basin area of 6 m^2 and the large percentage was for the test with an open floodbasin area and breach width of 0.8 m.

4. The floodplain area had a strong effect on the main channel flood stage reduction. However, the amount of flood depth reduction was also related to other parameters e.g. the flood duration and the breach size.
5. A small breach size and a small basin area were less effective in flood depth reduction when the flood wave had a larger peak and shorter duration compared to equivalent cases with a smaller peak and longer duration flood wave.
6. The upstream target location was affected more by the engineered levee breach than the downstream location. The upstream location experienced flood reduction due to wave modification whereas the downstream location experienced depth reduction due to a reduction in flow volume.
7. The percentage volume of flood water that passed to the floodplain increased with an increase in the breach width. The volume of water entering the flood basin in case of the long duration flood wave, e.g., Hydrograph 3, was more than that in experiments involving Hydrograph 2 and 1.
8. Non-dimensional relationship between dependent the variable; i.e., the decrease in water depth at target locations (ΔY_t) and independent variables, i.e., peak discharge, time to peak, base time, floodplain basin area, width of the breach, width of the channel, water density, gravitational acceleration, and target location (Q_p, T_p, T_b, A_b, W_b, W_c, ρ, g, X_t), has been developed.
9. Multivariate analysis has been done to develop a prediction model for non-dimensional depth reduction as a function of the non-dimensional groups obtained from the dimensional analysis. The data were grouped according to experimental conditions i.e. active flood management scenario, passive flood management

scenario, closed flood basin, and open flood basin. It was found that except for the base flow duration, T_b, all other independent variables were significant in the developed relationships.

BILIOGRAPHY

(CDWR), California Department of Water Resources. 1984. “Non-Project Levee Hazard Mitigation.”

Abdo, Khaled Mamdouh Mohamed. 2014. “Numerical Modeling of Free Surface Flows Using Depth Averaged and 3D Models.” PhD Dissertation, Unviersity of South Carolina.

Alchetron. 2005. “17th Streer Canal.” 2005. https://alchetron.com/17th-Street-Canal.

Barkdoll, Brian D., Brad L. Hagen, and A. Jacob Odgaard. 1998. “Experimental Comparison of Dividing Open-Channel with Duct Flow in T-Junction.” *Journal of Hydraulic Engineering* 124 (1): 92–95. https://doi.org/10.1061/(ASCE)0733-9429(1998)124:1(92).

Best, James L., and Ian Reid. 1984. “Separation Zone at Open-Channel Junctions.” *Journal of Hydraulic Engineering* 110 (11): 1588–94. https://doi.org/10.1061/(ASCE)0733-9429(1984)110:11(1588).

Bitesize, BBC. n.d. “Flood Management.” https://www.bbc.co.uk/bitesize/guides/ztb78mn/revision/1.

Britannica, Encyclopadia. 2019. “Superdome.” Encyclopædia Britannica. 2019. https://www.britannica.com/event/Hurricane-Katrina#/media/1/1087226/229419.

California Water, Verbatim. n.d. “Yolo Bypass Symposium, Part 1: A Flood of Plans and

Possibilities." Accessed October 1, 2019. https://mavensnotebook.com/2015/02/18/yolo-bypass-symposium-part-1-a-flood-of-plans-and-possibilities/.

Chinnarasri, Chaiyuth, Tawatchai Tingsanchali, Sutat Weesakul, and Somchai Wongwises. 2003. "Flow Patterns and Damage of Dike Overtopping." *International Journal of Sediment Research* 18 (4): 301–9.

Coleman, Stephen E., Darryl P. Andrews, and M. Grant Webby. 2002. "Overtopping Breaching of Noncohesive Homogeneous Embankments." *Journal of Hydraulic Engineering* 128 (9): 829–38. https://doi.org/10.1061/(ASCE)0733-9429(2002)128:9(829).

Elalfy, Ezzat. 2015. "Numerical and Experimental Investigations of Dam and Levee Failure." PhD Dissertation, Unviersity of South Carolina.

Elalfy, Ezzat, Mohamed Elkholy, Cyrus K. Riahi-Nezhad, and M. Hanif Chaudhry. 2018. "Estimation of Discharge through a Levee Breach with Constant Cross Section." *Journal of Hydraulic Engineering* 144 (4): 6018005. https://doi.org/10.1061/(ASCE)HY.1943-7900.0001430.

Elalfy, Ezzat, Ali Asghari Tabrizi, and M. Hanif Chaudhry. 2017. "Numerical and Experimental Modeling of Levee Breach Including Slumping Failure of Breach Sides." *Journal of Hydraulic Engineering* 144 (2): 4017066.

Emelen, Sylvie Van, Sandra Soares-Frazão, Cyrus K Riahi-Nezhad, M. Hanif Chaudhry, Jasim Imran, and Yves Zech. 2012. "Simulations of the New Orleans 17th Street Canal Breach Flood." *Journal of Hydraulic Research* 50 (1): 70–81.

Encyclopædia Britannica, Inc. 2019. “Hurricane Katrina.” In . https://www.britannica.com/event/Hurricane-Katrina.

Engineers, US Army Corps of, and Mississippi Valley Division. 2019. “Birds Point-New Madrid Floodway.” https://www.mvd.usace.army.mil/Portals/52/docs/MRC/BirdsPoint_NewMadrid.pdf?ver=2017-07-27-143310-350.

Feliciano Cestero, Jose A., Jasim Imran, and M.Hanif Chaudhry. 2015. “Experimental Investigation of the Effects of Soil Properties on Levee Breach by Overtopping.” *Journal of Hydraulic Engineering* 141 (4): 4014085. https://doi.org/10.1061/(ASCE)HY.1943-7900.0000964.

Feyrer, F, T Sommer, and W Harrell. 2006. “Managing Floodplain Inundation for Native Fish: Production Dynamics of Age-0 Splittail (Pogonichthys Macrolepidotus) in California’s Yolo Bypass.” *Hydrobiologia* 573 (1): 213–26.

Franca, M J, and A B Almeida. 2002. “Experimental Tests on Rockfill Dam Breaching Process.” In *IAHR-International Symposium on Hydraulic and Hydrological Aspects of Reliability and Safety Assessment of Hydraulic Structures, St. Petersburg*, 29–31.

Giudice, Giuseppe Del, Rudy Gargano, Giacomo Rasulo, and Daniele Siciliano. 2014. “Preliminary Estimate of Detention Basin Efficiency at Watershed Scale.” *Water Resources Management* 28 (4): 897–913. https://doi.org/10.1007/s11269-014-0518-1.

Guo, James C.Y. 2012. “Off-Stream Detention Design for Storm-Water Management.” *Journal of Irrigation and Drainage Engineering* 138 (4): 371–76.

https://doi.org/10.1061/(ASCE)IR.1943-4774.0000406.

Guo, James C Y. 1999. “Detention Basin Sizing for Small Urban Catchments.” *Journal of Water Resources Planning and Management* 125 (6): 380–82.

Gurram, Sampath Kumar, Karam S. Karki, and Willi H. Hager. 1997. “Subcritical Junction Flow.” *Journal of Hydraulic Engineering* 123 (5): 447–55. https://doi.org/10.1061/(ASCE)0733-9429(1997)123:5(447).

Hsu, Chung-Chieh, Wen-Jung Lee, and Chang-Hsi Cheng. 1998. “Subcritical Open-Channel Junction Flow.” *Journal of Hydraulic Engineering* 124 (8): 847–55. https://doi.org/10.1061/(ASCE)0733-9429(1998)124:8(847).

Hsu, Chung-Chieh, Feng-Shuai Wu, and Wen-Jung Lee. 1998. “Flow at 90° Equal-Width Open-Channel Junction.” *Journal of Hydraulic Engineering* 124 (2): 186–91. https://doi.org/10.1061/(ASCE)0733-9429(1998)124:2(186).

Jaffe, David A., and Brett F. Sanders. 2001a. “Engineered Levee Breaches for Flood Mitigation.” *Journal of Hydraulic Engineering* 127 (6): 471–79. https://doi.org/10.1061/(ASCE)0733-9429(2001)127:6(471).

Jaffe, David A, and Brett F Sanders. 2001b. “Engineered Levee Breaches for Flood Mitigation.” *Journal of Hydraulic Engineering* 127 (6): 471–79.

Jianchun, Huang, Larry J. Weber, and Yong G. Lai. 2002. “Three-Dimensional Numerical Study of Flows in Open-Channel Junctions.” *Journal of Hydraulic Engineering* 128 (3): 268–80. https://doi.org/10.1061/(ASCE)0733-9429(2002)128:3(268).

Jongman, B., H. Kreibich, H. Apel, J. I. Barredo, P. D. Bates, L. Feyen, A. Gericke, J. Neal, J.C.J.H. Aerts, and P. J. Ward. 2012. "Comparative Flood Damage Model Assessment: Towards a European Approach."

Kakinuma, Takaharu, and Yasuyuki Shimizu. 2014. "Large-Scale Experiment and Numerical Modeling of a Riverine Levee Breach." *Journal of Hydraulic Engineering* 140 (9): 4014039. https://doi.org/10.1061/(ASCE)HY.1943-7900.0000902.

Kunreuther, Howard. 2006. "Disaster Mitigation and Insurance: Learning from Katrina." *The Annals of the American Academy of Political and Social Science* 604 (1): 208–27.

Larocque, Lindsey Ann. 2012. "Experimental and Numerical Modeling of Dam-Break and Levee-Breach Flows." PhD Dissertation, Unviersity of South Carolina.

LaRocque, Lindsey Ann, Mohamed Elkholy, M.Hanif Chaudhry, and Jasim Imran. 2013. "Experiments on Urban Flooding Caused by a Levee Breach." *Journal of Hydraulic Engineering* 139 (9): 960–73. https://doi.org/10.1061/(ASCE)HY.1943-7900.0000754.

LaRocque, Lindsey Ann, Jasim Imran, and M. Hanif Chaudhry. 2013. "Experimental and Numerical Investigations of Two-Dimensional Dam-Break Flows." *Journal of Hydraulic Engineering* 139 (6): 569–79. https://doi.org/10.1061/(ASCE)HY.1943-7900.0000705.

Martino, F. De, and F. De Paola. 2010. "Experimental Survey on Off-Stream Floodplain Storages: First Results." *WIT Transactions on Information and Communication*

Technologies 43: 645–54.

McEnroe, Bruce M. 1992. “Preliminary Sizing of Detention Reservoirs to Reduce Peak Discharges.” *Journal of Hydraulic Engineering* 118 (11): 1540–49. https://doi.org/10.1061/(ASCE)0733-9429(1992)118:11(1540).

Miller, Sky, and M. Hanif Chaudhry. 1989. “Dam-Break Flows in Curved Channel.” *Journal of Hydraulic Engineering* 115 (11): 1465–78.

Paola, Francesco De, and Gustavo Marini. 2011. “Experimental Research on Floodplain Storage Inundation: Preliminary Results.” *Energy and Environment Research* 1 (1): 53.

Pirzadeh, BAHAREH, and HAMID Shamloo. 2007. “Numerical Investigation of Velocity Field in Dividing Open-Channel Flow.” In *Proceedings of the 12th WSEAS International Conference on APPLIED*.

Ramamurthy, Amruthur S., Luis b. Carballada, and Due Minn Tran. 1988. “Combining Open Channel Flow at Right Angled Junctions.” *Journal of Hydraulic Engineering* 114 (12): 1449–60. https://doi.org/10.1061/(ASCE)0733-9429(1988)114:12(1449).

Ramamurthy, Amruthur S., Junying QU, and Diep Vo. 2007. “Numerical and Experimental Study of Dividing Open-Channel Flows.” *Journal of Hydraulic Engineering* 133 (10): 1135–44. https://doi.org/10.1061/(ASCE)0733-9429(2007)133:10(1135).

Ramamurthy, Amruthur S., Due Minh Tran, and Luis b. Carballada. 1990. “Dividing Flow in Open Channels.” *Journal of Hydraulic Engineering* 116 (3): 449–55.

https://doi.org/10.1061/(ASCE)0733-9429(1990)116:3(449).

Riahi-Nezhad, Cyrus K. 2013. “Experimental Investigation of Steady Flows At A Breached Levee.”

Rifai, Ismail, Kamal El Kadi Abderrezzak, Sebastien Erpicum, Pierre Archambeau, Damien Violeau, Michel Pirotton, and Benjamin Dewals. 2018. “Floodplain Backwater Effect on Overtopping Induced Fluvial Dike Failure.” *Water Resources Research* 54 (11): 9060–73.

Rozov, Andrey L. 2003. “Modeling of Washout of Dams.” *Journal of Hydraulic Research* 41 (6): 565–77.

Sanders, Brett F., and Nikolaos D. Katopodes. 1999. “Active Flood Hazard Mitigation. I: Bidirectional Wave Control.” *Journal of Hydraulic Engineering* 125 (10): 1057–70.

Sattar, Ahmed M, Ahmed A Kassem, and M. Hanif Chaudhry. 2008. “Case Study: 17th Street Canal Breach Closure Procedures.” *Journal of Hydraulic Engineering* 134 (11): 1547–58.

Savant, Gaurav, Charlie Berger, Tate O. McAlpin, and Jennifer N. Tate. 2011. “Efficient Implicit Finite-Element Hydrodynamic Model for Dam and Levee Breach.” *Journal of Hydraulic Engineering* 137 (9): 1005–18. https://doi.org/10.1061/(ASCE)HY.1943-7900.0000372.

Seed, R. B., R. G. Bea, A. Athanasopoulos-Zekkos, G. P. Boutwell, J. D. Bray, C. Cheung, D. Cobos-Roa, et al. 2008. “New Orleans and Hurricane Katrina. III: The 17th Street Drainage Canal.” *Journal of Geotechnical and Geoenvironmental*

Engineering 134 (5): 740–61. https://doi.org/10.1061/(ASCE)1090-0241(2008)134:5(740).

Shabayek, Shazy, Peter Steffler, and Faye Hicks. 1999. "Dividing Flows in Open Channel Junctions." In *Annual Conference of the Canadian Society for Civil Engineering*, 11–20. Regina, Saskatchewan.

———. 2002. "Dynamic Model for Subcritical Combining Flows in Channel Junctions." *Journal of Hydraulic Engineering* 128 (9): 821–28. https://doi.org/10.1061/(ASCE)0733-9429(2002)128:9(821).

Sharp, Jeb. n.d. "Ten Years Later, the Lessons of Hurricane Katrina Apply to All of Us." PRI's The World. https://www.pri.org/stories/2015-08-14/ten-years-later-lessons-hurricane-katrina-apply-all-us.

Shome, M.L., and P.M. Steffler. 2006. "Flood Plain Filling by a Monoclinal Flood Wave." *Journal of Hydraulic Engineering* 132 (5): 529–32. https://doi.org/10.1061/(ASCE)0733-9429(2006)132:5(529).

Sommer, Ted, Bill Harrell, Matt Nobriga, Randall Brown, Peter Moyle, Wim Kimmerer, and Larry Schemel. 2001. "California's Yolo Bypass: Evidence That Flood Control Can Be Compatible with Fisheries, Wetlands, Wildlife, and Agriculture." *Fisheries* 26 (8): 6–16. https://doi.org/10.1577/1548-8446(2001)026<0006:CYB>2.0.CO;2.

Tabrizi, Ali Asghari, Lindsey Ann LaRocque, M. Hanif Chaudhry, Enrica Viparelli, and Jasim Imran. 2017. "Embankment Failures during the Historic October 2015 Flood in South Carolina: Case Study." *Journal of Hydraulic Engineering* 143 (8): 5017001. https://doi.org/10.1061/(ASCE)HY.1943-7900.0001315.

Taylor, Edward H. 1944. “Flow Characteristics at Open-Channel Junctions.” *American Society of Civil Engineers Transactions* 109: 893–902.

Thielicke, William, and Eize Stamhuis. 2014. “PIVlab–towards User-Friendly, Affordable and Accurate Digital Particle Image Velocimetry in MATLAB.” *Journal of Open Research Software* 2 (1).

ToDAY, USA. n.d. “What Are the Worst Floods in American History? A Rundown of the Top 30.” https://www.usatoday.com/story/money/economy/2018/07/24/worst-floods-in-american-history/37070093/.

Topa, M. E., M. Giugni, and F. De Paola. 2015. “Off-Stream Floodplain Storage: Numerical Modeling and Experimental Analysis.” *Journal of Irrigation and Drainage Engineering* 141 (1): 4014040. https://doi.org/10.1061/(ASCE)IR.1943-4774.0000746.

USGS. 2011. “Ohio and Mississippi River Flooding May 2011 Landsat Comparison.Jpg.” 2011. https://commons.wikimedia.org/wiki/File:Ohio_and_Mississippi_River_Flooding_May_2011_Landsat_comparison.jpg.

Walker, Brad. 2016. “Comparison of the Birds Point-New Madrid Floodway, Mississippi River and the Yolo Bypass, Sacramento River.” *Journal of Earth Science* 27 (1): 47–54.

Webber, Norman Bruton, and C A Greated. 1966. “An Investigation of Flow Behaviour at the Junction of Rectangular Channels.” *Proceedings of the Institution of Civil Engineers* 34 (3): 321–34.

Weber, Larry J., Eric D. Schumate, and Nicola Mawer. 2001. "Experiments on Flow at a 90° Open-Channel Junction." *Journal of Hydraulic Engineering* 127 (5): 340–50. https://doi.org/10.1061/(ASCE)0733-9429(2001)127:5(340).

Yang, Qing-Yuan, Xian-Ye Wang, Wei-Zhen Lu, and Xie-Kang Wang. 2009. "Experimental Study on Characteristics of Separation Zone in Confluence Zones in Rivers." *Journal of Hydrologic Engineering* 14 (2): 166–71. https://doi.org/10.1061/(ASCE)1084-0699(2009)14:2(166).

Yu, Ming-hui, Yin-ling Deng, Lian-chao Qin, Dang-wei Wang, and Ya-ling Chen. 2009. "Numerical Simulation of Levee Breach Flows under Complex Boundary Conditions." *Journal of Hydrodynamics, Ser. B* 21 (5): 633–39.